Solid State Chemical Exchange in Some Sodium Salts as Studied By 2D Nutation NMR

By
Hiroshi Ohki

SOLID STATE CHEMICAL EXCHANGE IN SOME SODIUM SALTS AS STUDIED BY 2D NUTATION NMR

BY

HIROSHI OHKI

DEPARTMENT OF CHEMISTRY

FACULTY OF SCIENCE

OSAKA UNIVERSITY

1990

Contents

Abstract

A new theoretical method which is based on the Liouville representation was established to describe the evolution of the quadrupolar spin system under the influence of strong rf field, which has been termed 'nutation'. The Liouville formalism was introduced to handle time development of the spin system and to construct the theoretical expression for the complex interactions between the rf field and the multilevel spin system. Although the dimension of the matrix to be determined becomes far larger than that based on standard density matrix or fictitious spin methods, the formalism with the Liouvillian can easily be coded for computation and therefore is much suitable for the calculation by big computers. Also the Liouville representation has a form which can incorporate effects other than spin interaction in a straightforward manner. This property makes it possible to apply the nutation method to chemically exchanging system.

The new method was coded by FORTRAN to prepare the general simulation program which is necessary for analyzing the experimental 2D nutation spectra. The program can be applied to quadrupolar nuclei with spin numbers $3/2 \sim 9/2$ and to systems with and without chemical exchange.

The 2D nutation NMR experiments were conducted for ^{23}Na in several compounds. The ^{23}Na resonance in $NaNO_2$ and in $NaHgCl_3.2H_2O$ was used to examine the optimal experimental conditions for the 2D nutation spectra and to evaluate the sensitivity of the spectra to the quadrupole coupling constant, e^2Qq/h, and the asymmetry parameter, η, of the electric field gradient at the site of the resonant nucleus.

The ^{23}Na 2D nutation NMR was applied to Na_2SeO_3 to distinguish the three crystallographically nonequivalent Na sites in this compound. The quadrupole coupling constants at the individual sites could be determined and also η was estimated for two of the three sites in this material.

$Na_{1+x}Zr_2Si_xP_{3-x}O_{12}$ has been known as a typical sodium ion conductor. The ^{23}Na 2D nutation NMR was used to obtain the direct information on the sodium transport in this material. The spectrum was remarkably temperature dependent and indicated unambiguously that the sodium ions are exchanging between the two nonequivalent sites. The spectrum was analyzed by the new theoretical method developed here and the rate of the Na ion exchange was estimated at each temperature. It was found that the activation energy deduced from the nutation spectra differs significantly from that determined by a previous conductivity measurement. The large discrepancy between the two values was interpreted qualitatively by the following model. In the 2D nutation NMR, the spectra are governed by the local exchange of the Na ion between two sites, whereas the net ionic conduction must accompany the long-range ion transport through the formation of vacancy in addition to the fluctuational exchange.

1. Introduction

Solid state nuclear magnetic resonance (NMR) can provide the information on the local static structure of the solid phase and molecular or ionic motions in the solid. The line splitting in single crystal and the line shape in powdered or polycrystalline material can now be routinely analyzed to determine the local structure of solid. Very often the line shape varies with temperature reflecting the onset of some molecular or ionic motion in solid. The measurements of line characteristics as well as the relaxation behavior of the spin system as a function of temperature (or pressure in some cases) give fruitful information on the molecular motion excited in the solid.

In the (solid) powdered samples, the spectra are broadened by several interactions such as dipole-dipole interaction, chemical shifts, and so on. For the quadrupolar nuclei which have the spins I greater than 1/2, the structure of the spectrum is often determined by strong quadrupole interaction that is caused by the coupling between the nuclear electric quadrupole moment and the electric field gradient (EFG). The quadrupole interaction can be used to examine the local site symmetry of the resonant nucleus and the electronic structure of molecular and ionic species in the crystalline solid. The quadrupolar nuclei are also used as a powerful probe for the "slow" molecular motion in solid. In the case where the quadrupole interaction is sufficiently large, the usual pure nuclear quadrupole resonance can apply to determine the quadrupole coupling constant (e^2Qq/h) and the asymmetry parameter of the electric field gradient (η). If the e^2Qq/h is consider-

ably small, one observes the quadrupole interaction as a perturbation to the NMR. Sometimes the strength of the quadrupole interaction is comparable with those of other interactions. In such case the usual NMR on powdered specimen cannot separate the individual interactions.

Two- or multi-dimensional NMR methods evolve different interactions along different coordinate axes and examine the different interactions independently. 2D nutation NMR recently proposed is one of such methods. It separates the quadrupole interaction from chemical shift interaction and others by evolving these different interactions onto two directions. In this method one measures the central component of the spectrum which is perturbed by the second order quadrupole interaction for the half-integer spin system but, by evolving the spectrum onto different directions under a specific condition, one can pick up the quadrupole interaction in the form free from other interactions. An important character of the nutation NMR lies in that crystallographically nonequivalent sites can be distinguished and the quadrupole interaction parameters as well as the magnitude of the chemical shift at each site can be determined.

It seems promising to utilize the nutation NMR by making use of the most of its specific characters to examine the dynamic process, in other words, chemical exchange process between nonequivalent sites. Although the quadrupole interaction of deuterium has been widely used to trace the chemical exchange in solid state, there has not been developed any direct method to study the motion of the quadrupolar nuclei with half-integer spins in the solid state. Since in solid electrolytes and fast ionic conduc-

tors various ions play the main role and as many of these ions have half-integer spins, number of valuable information about the ionic motion can be obtained if the nutation NMR can be used to examine the motional process in solid.

In the present work, a theoretical formulation of the 2D nutation NMR method using a new technique based on the Liouville representation is given. Next a method to incorporate the chemical exchange into the theory of the nutation NMR will be developed. Then $NaNO_2$ and $NaHgCl_3.2H_2O$ will be used to test the efficiency of this method for determination of the quadrupole interaction parameters. Na_2SeO_3 is chosen to demonstrate how to separate and distinguish any crystallographically nonequivalent sites in crystal. Finally a model ionic conductor, $Na_{1+x}Zr_2Si_xP_{3-x}O_{12}$, is chosen to examine the effect of the chemical exchange on 2D nutation NMR spectrum, and the data were analyzed by the simulation method. The applicability of the 2D nutation NMR for chemically exchanging system will be discussed.

2. Theory

2.1. Liouville Representation in NMR

General treatment of pulsed NMR spectroscopy has been done using time dependent density matrix formalism. Throughout the text in this thesis, however, the Liouville (superoperator) formalism [1] will be used to describe the time evolution of the spin system. Since the Liouville representation is not familiar to the most of chemists, it seems to be the due course to give brief introduction of this special formalism. The Liouville representation is suitable for handling complicated time development of the density matrix and is well adopted to computer implementation, because it has a transparent presentation of the commutator which is by all means needed in the calculation of the evolution of density matrix. Hereafter, several important properties of the Liouville formalism are summarized in comparison with the usual Schrödinger representation.

a) In the Schrödinger representation, the density matrix ρ obeys the von Neumann equation of motion [2]

$$d\rho/dt = -i[H,\rho] \ , \qquad (2.1.1)$$

where H is the total Hamiltonian of the system in the frequency units. In the Liouville formalism, the elements of the density matrix form density superkets (basis sets) and the time dependence of the density superkets is determined by the Liouvillian L :

$$d\boldsymbol{\rho}/dt = -iL\boldsymbol{\rho} \ , \qquad (2.1.2)$$

where $\boldsymbol{\rho}$ is the density superkets in the column form, i.e.,

$$\rho = {}^t(\rho_{11}\ \rho_{12}\ \rho_{13}\ \ldots\ \rho_{1n}\ \rho_{21}\ \ldots\ \ldots\ \rho_{nn})\ , \tag{2.1.3}$$

where n = 2I+1 and I is the spin. L is defined through the relation

$$L = H \otimes E - E \otimes {}^tH\ , \tag{2.1.4}$$

where E is the unit operator which has the same dimension as H, and ${}^tH$ represents the transposed matrix of H and $\otimes$ stands for the direct product [3] of two matrices. (See appendix.)

When the Hamiltonian can be diagonalized by a Unitary matrix U through the similarity transformation :

$$H^d = U^{-1}HU\ , \tag{2.1.5}$$

(H^d means diagonalized Hamiltonian,) then the Liouvillian can be diagonalized by the use of the same Unitary matrix :

$$\begin{aligned} L^d &= U^{-1}LU \\ &= (U^{-1} \otimes U^{-1})(H \otimes E - E \otimes {}^tH)(U \otimes U) \\ &= H^d \otimes E - E \otimes H^d\ , \end{aligned} \tag{2.1.6}$$

It should be noted that while the Hamiltonian plays the role of the operator characterizing the time evolution as well as that of operator specifying the energy of the system, the Liouvillian plays the former role only. This can be seen by the fact that, according to (2.1.6), the eigenvalues of Liouvillian consist of the differences of eigenvalues of the corresponding Hamiltonian.

b) When the Hamiltonian can be separated into a large time-independent interaction H_0 and a much smaller term H_1, one often writes the equation of motion of the spin system

in the interaction representation which removes unnecessary term H_0 from the Hamiltonian. In this case, the Liouvillian can be written

$$L = L_0 + L_1 \ , \tag{2.1.7}$$

where

$$L_0 = H_0 \otimes E - E \otimes {}^tH_0 \ , \tag{2.1.8a}$$

$$L_1 = H_1 \otimes E - E \otimes {}^tH_1 \ . \tag{2.1.8b}$$

Then the Liouville description of the interaction representation is expressed by

$$\boldsymbol{\rho}^* = \exp(+iL_0 t)\boldsymbol{\rho} \ , \tag{2.1.9}$$

$$L^* = \exp(+iL_0 t)L_1 \exp(-iL_0 t) \ , \tag{2.1.10}$$

where $\boldsymbol{\rho}^*$ and L^* are density superkets and Liouvillian in the interaction representation, respectively. Accordingly the equation of motion of the density superkets becomes

$$d\boldsymbol{\rho}^*/dt = -iL^*\boldsymbol{\rho} \ . \tag{2.1.11}$$

If the Liouvillian L^* is explicitly time-independent, Eq. (2.1.11) can be solved formally :

$$\boldsymbol{\rho}^*(t) = \exp(-iL^* t)\boldsymbol{\rho}(0) \ . \tag{2.1.12}$$

c) Another feature of the Liouville formalism is in its convenience in calculating the observables. For example, the magnetization along the x-axis is described in the Schrödinger representation as

$$M_x = \mathrm{Tr}(I_x \rho) \ , \tag{2.1.13}$$

while in the Liouville formalism,

$$M_x = I_x \rho \ , \qquad (2.1.14)$$

where I_x is the operator in the row form.

Thus one can write physical quantities simply as a product of matrices and vectors.

Appendix

The properties of direct product are summarized as follows. Direct product of two matrices A and B of n dimensions is defined by

$$A \times B = \begin{pmatrix} a_{11}B & a_{12}B & \cdots & a_{1n}B \\ a_{21}B & a_{22}B & \cdots & a_{2n}B \\ \cdot & \cdot & \cdots & \cdot \\ \cdot & \cdot & \cdots & \cdot \\ a_{n1}B & a_{n2}B & \cdots & a_{nn}B \end{pmatrix}$$

Thus the resultant matrix has n^2 dimension. And

$$(A + B) \otimes C = A \otimes C + B \otimes C \ ,$$

$$(A \otimes B)(C \otimes D) = AC \otimes BD \ ,$$

where + has usual meaning of matrix sum.

2.2. 2D Nutation NMR

In the high magnetic field, the NMR spectra of quadrupolar nuclei that have the spins $I \geq 1$ consist generally of $2I+1$ lines due to quadrupole interaction. In the powdered or polycrystalline samples the angles between the external magnetic field and the principal axes of the electric field gradient (EFG) are distributed at random in each microcrystal and therefore the spectra show characteristic powder patterns as exemplified in Fig. 2.1. The powder patterns shown in Fig. 2.1 are ideal ones and if such spectral patterns are observed one can analyze the spectra to determine the quadrupole interaction parameters. In many cases, however, powder spectrum gives indistinct structure owing to strong quadrupole interaction and/or dipolar interaction; sometimes the former makes the spectrum spread over several hundred kHz and as a result causes the signal to be buried under the noise.

For half-integer spins, the central peak, that corresponds to the transition between the spin states $|+1/2\rangle \leftrightarrow |-1/2\rangle$, can be almost always observed because it is not affected by quadrupole interaction in the first order perturbation. Therefore it is meaningful to search for a method or methods to determine the quadrupole interaction parameters from observed central transition only. One method widely used is the line shape analysis of the normal one dimensional (1D) spectrum, which is governed by the second order quadrupole interaction. But one weak point of this method lies in the fact that the interactions other than the quadrupole interaction cause the line broadening and/or line shift and it becomes difficult to determine the

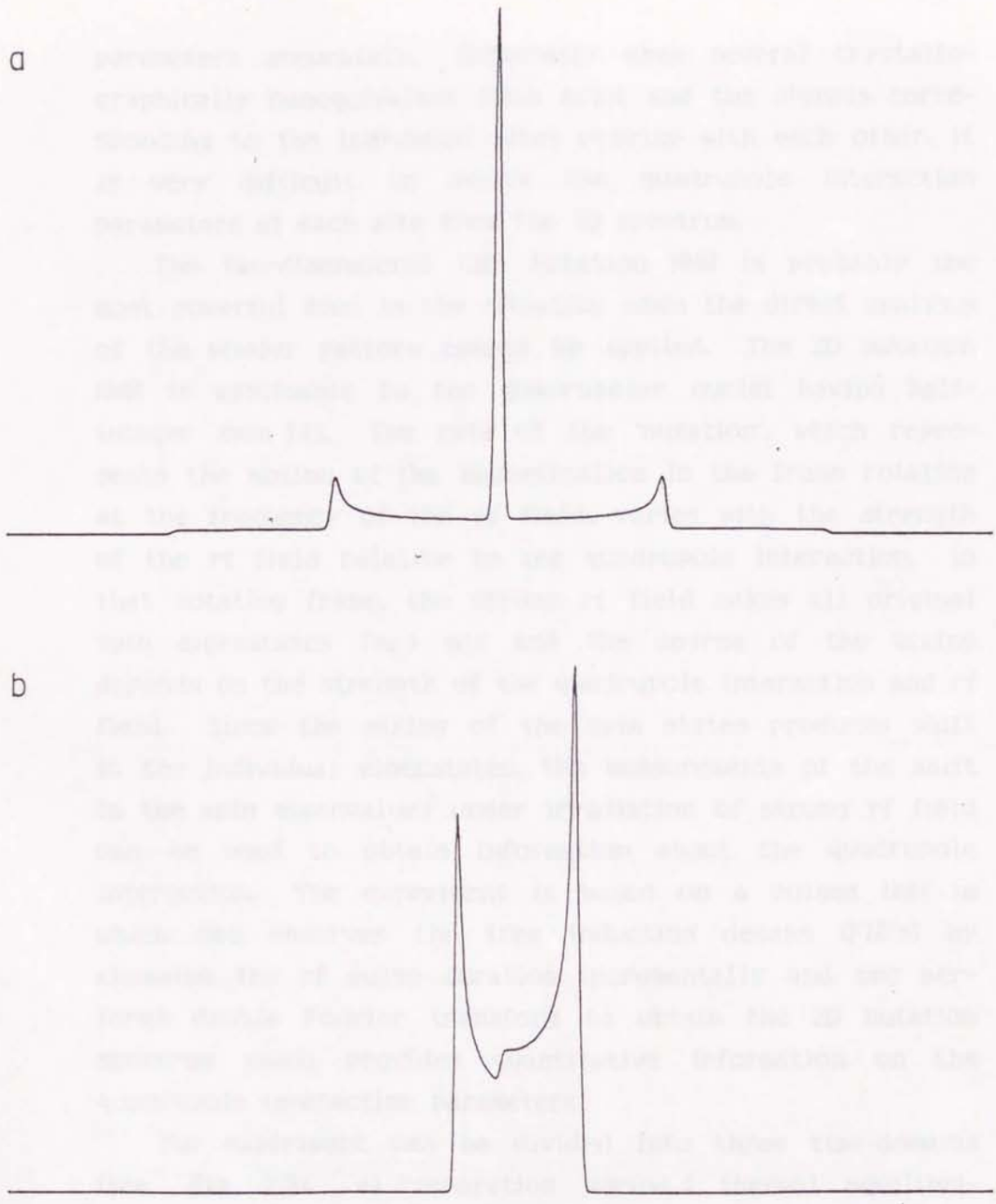

Figure 2.1

Simulated a) the first order and b) the second order powder lineshapes for I = 3/2 (η = 0).

parameters accurately. Especially when several crystallographically nonequivalent sites exist and the signals corresponding to the individual sites overlap with each other, it is very difficult to derive the quadrupole interaction parameters at each site from the 1D spectrum.

The two-dimensional (2D) nutation NMR is probably the most powerful tool in the situation when the direct analysis of the powder pattern cannot be applied. The 2D nutation NMR is applicable to the quadrupolar nuclei having half-integer spin [4]. The rate of the 'nutation', which represents the motion of the magnetization in the frame rotating at the frequency of the rf field, varies with the strength of the rf field relative to the quadrupole interaction. In that rotating frame, the strong rf field makes all original spin eigenstates $|m_z\rangle$ mix and the degree of the mixing depends on the strength of the quadrupole interaction and rf field. Since the mixing of the spin states produces shift in the individual eigenstates, the measurements of the shift in the spin eigenvalues under irradiation of strong rf field can be used to obtain information about the quadrupole interaction. The experiment is based on a pulsed NMR in which one observes the free induction decays (FID's) by changing the rf pulse duration incrementally and one performs double Fourier transform to obtain the 2D nutation spectrum which provides quantitative information on the quadrupole interaction parameters.

The experiment can be divided into three time-domains (see Fig. 2.2). a) Preparation period : thermal equilibrium magnetization is established, b) Evolution period : the magnetization nutates around the rf field under the influ-

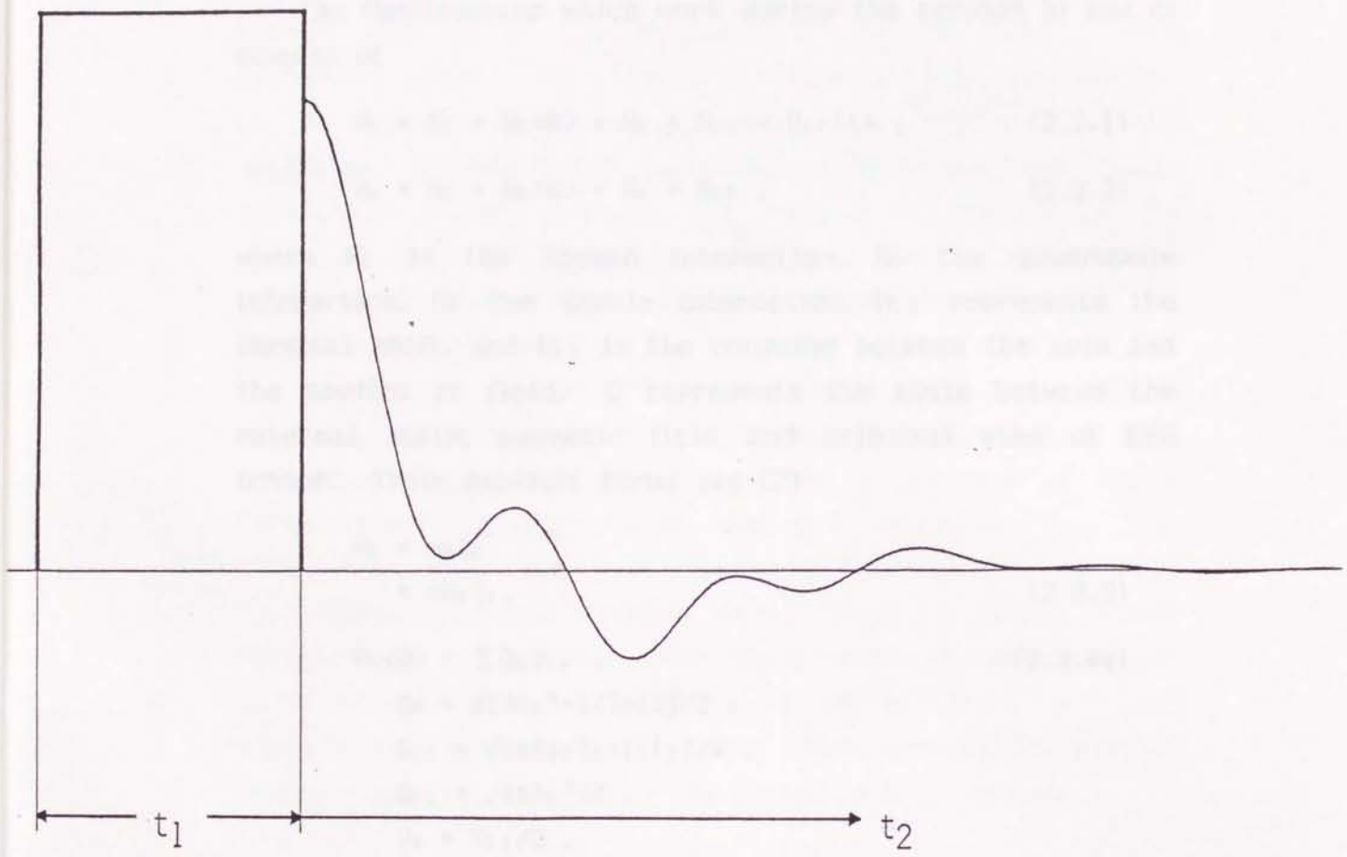

Figure 2.2

Schematic representation of 2D nutation NMR experiment.

ence of an interaction Hamiltonian, H_1, during t_1, and c) Detection period : the magnetization along x-y plane in the laboratory frame is detected under the influence of another interaction, H_2, in the duration t_2.

The Hamiltonians which work during the periods b) and c) consist of

$$H_1 = H_Z + H_Q(\Omega) + H_D + H_{CS} + H_{rf}(t) , \qquad (2.2.1)$$

$$H_2 = H_Z + H_Q(\Omega) + H_D + H_{CS} , \qquad (2.2.2)$$

where H_Z is the Zeeman interaction, H_Q the quadrupole interaction, H_D the dipole interaction, H_{CS} represents the chemical shift, and H_{rf} is the coupling between the spin and the applied rf field. Ω represents the angle between the external static magnetic field and principal axes of EFG tensor. Their explicit forms are [2]

$$H_Z = \omega_0 I_Z = \gamma H_0 I_Z , \qquad (2.2.3)$$

$$H_Q(\Omega) = \sum Q_m V_{-m} , \qquad (2.2.4a)$$

$$Q_0 = a[3I_Z^2 - I(I+1)]/2 ,$$

$$Q_{\pm 1} = \sqrt{6}a[I_Z I_\pm + I_\pm I_Z]/4 ,$$

$$Q_{\pm 2} = \sqrt{6}aI_\pm^2/4 ,$$

$$V_0 = V_{ZZ}/2 ,$$

$$V_{\pm 1} = (V_{ZX} \pm iV_{ZY})/\sqrt{6} ,$$

$$V_{\pm 2} = (V_{XX} - V_{YY} \pm 2iV_{XY})/2\sqrt{6} ,$$

$$a = eQ/[I(2I-1)] , \qquad (2.2.4b)$$

$$H_D = \Sigma I_i D I_j , \qquad (2.2.5)$$

$$H_{CS} = H\sigma I , \qquad (2.2.6)$$

and

$$H_{rf} = \omega_1 [I_x \cos(\omega_0 t) + i I_y \sin(\omega_0 t)] , \qquad (2.2.7)$$

where ω_0 is the nuclear Larmor frequency, D and σ are the dipole interaction and the chemical shift tensors, respectively, and ω_1 is the strength of the rf field in the frequency units. Note that the Liouvillians in the absence of the chemical shift does not produce any net shift of the spectrum. (Although the quadrupole interaction leads to an asymmetric powder pattern, the center of gravity of its spectrum does not change. Also, the dipolar interaction makes the spectrum split but the center of gravity of the spectrum does not move.)

Henceforth, we will always assume that the relative strength of the different interactions is $H_Z \gg H_Q \simeq H_{rf} \gg H_D, H_{CS}$. This situation is realized in the case of nuclei with fairly large quadrupole interaction such as ^{23}Na, ^{39}K, ^{59}Co, ^{93}Nb etc. The most important condition is that the pulse apparatus can provide very strong rf field. Under above conditions one can treat the quadrupole interaction as well as the chemical shift as a perturbation and can neglect weaker dipole interaction. Then quadrupole interaction can be expanded up to the second order terms as

$$H_Q' = H_Q^{(1)} + H_Q^{(2)} , \qquad (2.2.8)$$

where

$$H_Q^{(1)} = e^2qQ/8I(2I-1)(3\cos^2\theta - 1 + \eta \sin^2\theta \cos 2\phi) \times [3I_Z^2 - I(I+1)]$$
$$= \omega_Q [I_Z^2 - I(I+1)/3] , \qquad (2.2.9)$$

and

$$H_Q^{(2)} = (3e^2qQ/2I(2I-1))^2 I_z/32\omega_0$$
$$\times[\{9(1-\cos^2\theta)^2-6\eta(1-\cos^4\theta)\cos2\phi$$
$$+\eta^2(1+\cos^2\theta)^2\cos2\phi+4\eta^2\cos^2\theta(1-\cos^2 2\phi)\}$$
$$\times[2I_z^2-2I(I+1)+1]$$
$$-\{9(1-\cos^2\theta)\cos^2\theta+6\eta(1-\cos^2\theta)\cos^2\theta\cos2\phi$$
$$+\eta^2(1-\cos^2\theta)\cos^2\theta\cos^2 2\phi$$
$$+\eta^2(1-\cos^2\theta)(1-\cos^2 2\phi)\}$$
$$\times4[8I_z^2-4I(I+1)+1]] \quad , \quad (2.2.10)$$

where, θ and ϕ are the polar and the azimuthal angles of the direction of the static magnetic field with respect to the principal axes of the EFG, respectively, and others have usual meanings. The chemical shift interaction is represented by

$$H_{CS}' = \sigma I_z \quad . \quad (2.2.11)$$

Usually one can assume that the second order quadrupole interaction is negligible in the presence of a strong rf pulse, and the chemical shift term can be included in the Zeeman term, the Hamiltonians in Eqs. (2.2.1-2) can be redefined to be

$$H_1 = H_Q^{(1)} + H_{rf} \quad , \quad (2.2.12)$$

and

$$H_2 = H_Q^{(1)} + H_Q^{(2)} \quad . \quad (2.2.13)$$

The density superkets (Eq. (2.1.10)) at a time t_1+t_2 becomes in the frame rotating at ω_0 (interaction representa-

tion),

$$\rho^{\bullet}(t_1+t_2)=\exp(-iL_2^{\bullet}t_2)\exp(-iL_1^{\bullet}t_1)\rho(0) \ , \qquad (2.2.14)$$

and

$$L_1^{\bullet} = H_1^{\bullet} \otimes E - E \otimes {}^{t}H_1^{\bullet} \ , \qquad (2.2.15)$$

$$L_2^{\bullet} = H_2^{\bullet} \otimes E - E \otimes {}^{t}H_2^{\bullet} \ , \qquad (2.2.16)$$

where

$$H_1^{\bullet} = H_0^{\bullet} + H_{rf}^{\bullet} \ , \qquad (2.2.17)$$

$$H_2^{\bullet} = H_0^{\bullet} \ , \qquad (2.2.18)$$

and

$$H_0^{\bullet} = H_0{}' = H_0^{(1)} + H_0^{(2)} \ , \qquad (2.2.19)$$

$$H_{rf}^{\bullet} = \omega_1 I_x \ , \qquad (2.2.20)$$

In Eq. (2.2.14) $\rho(0)$ is the density superkets at thermal equilibrium. In the high temperature approximation, it yields

$$\rho(0) = (1 - \hbar\omega_0 I_z/kT)/(2I+1) \ , \qquad (2.2.21)$$

assuming that the Zeeman coupling dominates other interactions. The unit ket 1 in Eq. (2.2.21) can be always disregarded in the calculation since it does not contribute to signal.

Hereafter, Eq. (2.2.14) is solved for I = 3/2 as an example with respect to each period, i.e., evolution and detection periods.

a) Evolution period

Before examining the general feature of the nutation

NMR, two limiting cases will be studied as an illustration.

In the evolution period an rf pulse, $H_1 = \omega_1/\gamma$, is applied on the spin system. If the rf strength is much stronger than the quadrupole interaction, the spin system can be treated as if the quadrupole interaction is absent while the rf field is applied. Then the Hamiltonian becomes

$$H_1 = \begin{pmatrix} 0 & \sqrt{3}\omega_1/2 & 0 & 0 \\ \sqrt{3}\omega_1/2 & 0 & \omega_1 & 0 \\ 0 & \omega_1 & 0 & \sqrt{3}\omega_1/2 \\ 0 & 0 & \sqrt{3}\omega_1/2 & 0 \end{pmatrix} . \qquad (2.2.22)$$

This Hamiltonian can be diagonalized through a similarity transformation by the orthogonal matrix :

$$R = \begin{pmatrix} \sqrt{3} & 1 & -1 & \sqrt{3} \\ -1 & \sqrt{3} & \sqrt{3} & 1 \\ -1 & \sqrt{3} & -\sqrt{3} & -1 \\ \sqrt{3} & 1 & 1 & -\sqrt{3} \end{pmatrix} / 2\sqrt{2} , \qquad (2.2.23)$$

and the corresponding eigenvalues are $-\omega_1/2$, $3\omega_1/2$, $\omega_1/2$, and $3\omega_1/2$. Then one can immediately show that the magnetization nutates around the rf field at the characteristic frequency ω_1.

In the opposite case when the rf pulse strength is much smaller than the quadrupole interaction, the rf pulse can merely excites the central transition when the rf frequency satisfies nearly the resonance condition, and so no effective mixing of the eigenstates occurs. This is because the energy difference of the adjacent levels is quite different from each other. Hence one can pick up the components concerning with the central transition from the Hamiltonian

$$H' = \begin{pmatrix} 0 & \omega_1 \\ \omega_1 & 0 \end{pmatrix}, \qquad (2.2.24)$$

and this has the eigenvalues $\pm\omega_1$. Therefore the motion of the magnetization is represented by the rotation at frequency of $2\omega_1$. In general, it can be shown that the magnetization corresponding to the central transition rotates at $(I+1/2)\omega_1$ [2].

In summary, when quadrupole interaction is weak enough compared with the strength of the rf field, then the magnetization nutates at ω_1, and in the opposite case the magnetization nutates at $(I+1/2)\omega_1$.

If the quadrupole interaction and the rf field are comparable in magnitude, the nutational motion becomes complex. The equation of motion of the spin system in such complex cases has been solved using several different techniques [5]. In the present work a new technique based on the Liouville representation is introduced to solve the problem.

The matrix representation of the Hamiltonian in the period t_1 can be written as

$$H_1 = \begin{pmatrix} \omega_Q & \sqrt{3}\omega_1/2 & 0 & 0 \\ \sqrt{3}\omega_1/2 & -\omega_Q & \omega_1 & 0 \\ 0 & \omega_1 & -\omega_Q & \sqrt{3}\omega_1/2 \\ 0 & 0 & \sqrt{3}\omega_1/2 & \omega_Q \end{pmatrix}, \qquad (2.2.25)$$

where ω_Q is defined in Eq. (2.2.9). This Hamiltonian can be diagonalized through the similarity transformation by the orthogonal matrix [6]

$$Q = \begin{pmatrix} \cos\theta_- & -\sin\theta_- & -\sin\theta_+ & \cos\theta_+ \\ \sin\theta_- & \cos\theta_- & \cos\theta_+ & \sin\theta_+ \\ \sin\theta_- & \cos\theta_- & -\cos\theta_+ & -\sin\theta_+ \\ \cos\theta_- & -\sin\theta_- & \sin\theta_+ & -\cos\theta_+ \end{pmatrix} / \sqrt{2} \ , \qquad (2.2.26a)$$

$$\tan 2\theta_\pm = (\sqrt{3}/2)\omega_1 / (\omega_Q \pm \omega_1/2) \ , \qquad (2.2.26b)$$

and the corresponding eigenvalues are

$$\begin{aligned} \lambda_1 &= \omega_1/2 + (\omega_1^2+\omega_Q^2-\omega_1\omega_Q)^{1/2} \ , \\ \lambda_2 &= \omega_1/2 - (\omega_1^2+\omega_Q^2-\omega_1\omega_Q)^{1/2} \ , \\ \lambda_3 &= -\omega_1/2 - (\omega_1^2+\omega_Q^2+\omega_1\omega_Q)^{1/2} \ , \\ \lambda_4 &= -\omega_1/2 + (\omega_1^2+\omega_Q^2+\omega_1\omega_Q)^{1/2} \ . \end{aligned} \qquad (2.2.27)$$

The Liouvillian can be diagonalized by taking account of Eq. (2.1.6) and it leads to the density superkets at the end of the pulse as

$$\boldsymbol{\rho}^*(t_1) = R\exp(-iL^d{}_1 t_1)R^{-1}\boldsymbol{\rho}(0) \ , \qquad (2.2.28a)$$

or

$$\boldsymbol{\rho}^*{}_j(t_1) = \Sigma\, [R_{jk}R_{k1}\boldsymbol{\rho}_1(0)]\exp(-i\lambda_1 t_1) \ , \qquad (2.2.28b)$$

where λ_1 is the 1-th eigenvalue of the Liouvillian. In the above Eq. (2.2.28b), $A_{j1} = \Sigma\, [R_{jk}R_{k1}\boldsymbol{\rho}_1(0)]$ is called the 'transition amplitude' which represents the intensity of the component with the frequency λ_1.

b) Detection period

After the rf pulse field is switched off, the Hamiltonian (also the Liouvillian) is diagonal and the density superkets at a time t_1+t_2 is given by

$$\boldsymbol{\rho}^*(t_1+t_2) = \exp(-iL_2 t_2)\boldsymbol{\rho}^*(t_1) \ . \qquad (2.2.29)$$

A lengthy manipulation yields the result that the signal corresponding to the central transition at a given orientation of the principal axes of the EFG with respect to H_0 is proportional to

$$\begin{aligned} S(t_1+t_2) \propto & \\ & \{[3\sin 2\theta_- \sin 2\theta_+ -(1-\cos 2\theta_-)(1+\cos 2\theta_+)]\sin(\lambda_3-\lambda_1)t_1 \\ & -[3\sin 2\theta_- \sin 2\theta_+ +(1-\cos 2\theta_-)(1-\cos 2\theta_+)]\sin(\lambda_4-\lambda_1)t_1 \\ & -[3\sin 2\theta_- \sin 2\theta_+ +(1+\cos 2\theta_-)(1+\cos 2\theta_+)]\sin(\lambda_3-\lambda_2)t_1 \\ & +[3\sin 2\theta_- \sin 2\theta_+ -(1+\cos 2\theta_-)(1-\cos 2\theta_+)]\sin(\lambda_4-\lambda_2)t_1\} \\ & \times \exp(-i\omega_Q^{(2)} t_2) , \end{aligned} \tag{2.2.30}$$

where $\omega_Q^{(2)}$ is the second order quadrupole shift of the central transition expressed by [7]

$$\begin{aligned} \omega_Q^{(2)} = & (e^2qQ/h)^2/192\omega_0 \\ & \times\{9(1-\cos^2\theta)^2-6\eta(1-\cos^4\theta)\cos 2\phi \\ & +\eta^2(1+\cos^2\theta)^2\cos^2 2\phi+4\eta^2\cos^2\theta(1-\cos^2 2\phi) \\ & -72(1-\cos^2\theta)\cos^2\theta-48\eta(1-\cos^2\theta)\cos^2\theta\cos 2\phi \\ & -8\eta^2(1-\cos^2\theta)\cos^2\theta\cos^2 2\phi \\ & -8\eta^2(1-\cos^2\theta)(1-\cos^2 2\phi)\} . \end{aligned} \tag{2.2.31}$$

Eq. (2.2.30) indicates that four of six transitions between the four eigenvalues contribute to the spectrum and their transition frequencies can be determined by numerical analysis of the spectrum. It should be noted that Eq. (2.2.30) consists of two parts; one is the nutation which is merely a superposition of sine functions of t_1, and the other depends on t_2 and is governed by the second order quadrupole interaction.

2.3. Chemical Exchange Effect

Chemical exchange means that the nucleus jumps between the 'sites' whose environments are different from each other, i.e., crystallographically nonequivalent sites in solids.

The basic assumption of the chemical exchange is that the principle of detailed balance between the sites is satisfied, i.e.,

$$p_j k_{ji} = p_i k_{ij} \ , \qquad (2.3.1)$$

where p_j stands for the thermal equilibrium population of the j-th site and k_{ji} represents the exchange rate from the j-th to i-th site. Then one can write the exchange matrix for m sites :

$$K = \begin{pmatrix} k_{11} & k_{12} & \dots & k_{1m} \\ k_{21} & k_{22} & \dots & k_{2m} \\ \cdot & \cdot & \dots & \cdot \\ k_{m1} & k_{m2} & \dots & k_{mm} \end{pmatrix} , \qquad (2.3.2)$$

where the diagonal component k_{ii} is the rate of jump from i-th site to another, i.e., the reciprocal of the average life time at the i-th site. The sign of k_{ii} is taken to be negative (or zero). Each column must satisfy the following relation

$$k_{j1}+k_{j2}+ \dots +k_{jm} = 0 \ . \qquad (2.3.3)$$

Another assumption adopted here is that the spin-spin interaction between the sites is extremely small and can be neglected. This assumption makes possible to describe the Liouvillian and the density superkets in a simple form.

In principle, in the case where the chemical exchangae occurs among the m sites, the density superkets ρ is defined by [8]

$$\rho = \rho^{(1)} \otimes \rho^{(2)} \otimes \ldots \otimes \rho^{(m)} \quad , \qquad (2.3.4)$$

where $\rho^{(j)}$ represents the density superkets at the j-th site and × means the direct product of the kets. Eq. (2.3.4) tells that the cross terms between the density superkets at different sites should be calculated in order to describe the time evolution of the system. Since such cross terms appear mainly as a result of the interaction between spins at different sites, and fortunately, the spin-spin interaction between quadrupolar nuclei is usually very weak, one can ignore this type of interaction. Then, the total density superkets can be reduced as follows :

$$\rho = \rho^{(1)} \oplus \rho^{(2)} \oplus \ldots \oplus \rho^{(m)} \quad , \qquad (2.3.5)$$

where $\oplus$ means the direct sum of the density superkets. Similarly, the Liouvillian consists in principle of complex components if we take account of the interaction between the different sites. However, if we disregard the spin-spin interaction as mentioned above, the Liouvillian can be written in a simple form as

$$L = \begin{pmatrix} L^{(1)} & 0 & 0 & \ldots & 0 \\ 0 & L^{(2)} & 0 & \ldots & 0 \\ 0 & 0 & L^{(3)} & \ldots & 0 \\ . & . & . & \ldots & . \\ 0 & 0 & 0 & \ldots & L^{(m)} \end{pmatrix} , \qquad (2.3.6)$$

where $L^{(j)}$ is the Liouvillian corresponding to the j-th

site.

When the chemical exchange occurs, under the assumption that the exchange between the sites is instantaneous, the spin does not change its state during the jump. In other words no relaxation occurs in the course of the exchange process. Then

$$d\rho/dt = -(iL+K)\rho \ , \tag{2.3.7}$$

and

$$K = \begin{pmatrix} k_{11} & k_{12} & k_{13} & \dots & k_{1m} \\ k_{21} & k_{22} & k_{23} & \dots & k_{2m} \\ . & . & . & \dots & . \\ k_{m1} & k_{m2} & k_{m3} & \dots & k_{mm} \end{pmatrix} \otimes E_K \ , \tag{2.3.8}$$

where E_K is $(2I+1)^2$ dimensional unit matrix.

2.4. Chemical Exchange Effect on the Nutation Spectrum

In this section, two-site exchange is examined for simplicity but the extension to the general multisite case is straightforward.

In usual treatment of the chemical exchange, the effect of chemical exchange on the spin system is neglected during the short rf pulse so as to simplify the problem. But in this work, the exchange of spins should be taken into account because it has severe effect on the nutation spectrum.

The Liouvillians corresponding to the j-th site are

$$L^{(j)}{}_1 = L_Q{}^{(j)} + L_{CS}{}^{(j)} , \qquad (2.4.1a)$$

$$L^{(j)}{}_2 = L_Q{}^{(j)} + L_{CS}{}^{(j)} + L_{rf} , \qquad (2.4.1b)$$

where $L_Q{}^{(j)}$ and $L_{CS}{}^{(j)}$ stand for quadrupole interaction and chemical shift at the j-th site, respectively. The exchange matrix becomes

$$K = \begin{pmatrix} k_1 & -k_2 \\ -k_1 & k_2 \end{pmatrix} \otimes E_K \quad . \qquad (2.4.2)$$

Thus the density superkets at a time t_1+t_2 becomes

$$\rho(t_1+t_2) = \exp\{-(iL_2+K)t_2\}\exp\{-(iL_1+K)t_1\}\rho(0) , \qquad (2.4.3)$$

where L_1 and L_2 are the Liouvillians in the presence and absence of the rf pulse, respectively.

Now two limiting cases are examined.

i) Slow motion regime : $k_1, k_2 \ll H_Q, H_{rf}$

In this case the chemical exchange effect can be treated as a perturbation because the effect on the spectrum from

the chemical exchange is small compared with that from the quadrupole and rf couplings. Then one can diagonalize the Liouvillian alone by means of the orthogonal matrix Eq. (2.2.26) :

$$L^d = \begin{pmatrix} Q^{-1(1)} & 0 \\ 0 & Q^{-1(2)} \end{pmatrix} \begin{pmatrix} L^{(1)} & 0 \\ 0 & L^{(2)} \end{pmatrix} \begin{pmatrix} Q^{(1)} & 0 \\ 0 & Q^{(2)} \end{pmatrix}$$

$$= \begin{pmatrix} L^{d(1)} & 0 \\ 0 & L^{d(2)} \end{pmatrix} . \qquad (2.4.4)$$

And the exchange matrix becomes

$$K^s = \begin{pmatrix} k_1 E_K & -Q^{(1)-1} k_2 Q^{(2)} \\ -Q^{(2)-1} k_1 Q^{(1)} & k_2 E_K \end{pmatrix} . \qquad (2.4.5)$$

According to the perturbation theory, the diagonal terms of the exchange matrix should cause the change of the spectrum in the first order. Hence the line width of the peak corresponding to each site is determined by the exchange rate k_1 and k_2, respectively.

ii) Fast Motion Regime : $k_1, k_2 \gg H_0, H_{rf}$

In the opposite case, one must diagonalize the exchange matrix and treat the quadrupole and rf pulse as the perturbation. To diagonalize the exchange matrix, one must symmetrize the exchange matrix if it is not symmetric. This symmetrization can be done by the matrix P,

$$P_{ij} = \sqrt{p_i}\,\delta_{ij} \qquad (2.4.6)$$

through the similarity transformation, where δ_{ij} stands for the Kronecker's delta. The Liouvillian is not altered and the exchange matrix becomes

$$K^s = \begin{pmatrix} 1/\sqrt{p_1} & 0 \\ 0 & 1/\sqrt{p_2} \end{pmatrix} \begin{pmatrix} -k_1 & k_2 \\ k_1 & -k_2 \end{pmatrix} \begin{pmatrix} \sqrt{p_1} & 0 \\ 0 & \sqrt{p_2} \end{pmatrix} \otimes E_K ,$$

$$= \begin{pmatrix} -k_1 & k' \\ k' & -k_2 \end{pmatrix} \otimes E_K . \qquad (2.4.7)$$

This can be diagonalized by

$$K^d = \begin{pmatrix} \cos\Phi & -\sin\Phi \\ \sin\Phi & \cos\Phi \end{pmatrix} \begin{pmatrix} -k_1 & k' \\ k' & -k_2 \end{pmatrix} \begin{pmatrix} \cos\Phi & \sin\Phi \\ -\sin\Phi & \cos\Phi \end{pmatrix} \otimes E_K ,$$

$$= \begin{pmatrix} -(k_1+k_2) & 0 \\ 0 & 0 \end{pmatrix} \otimes E_K , \qquad (2.4.8a)$$

$$\tan 2\Phi = 2k'/(k_1-k_2) , \qquad (2.4.8b)$$

and so the Liouvillian is expressed as

$$L^f = \begin{pmatrix} L^{(1)}+L^{(2)} & 0 \\ 0 & L^{(1)}+L^{(2)} \end{pmatrix}$$

$$+ (L^{(1)}-L^{(2)}) \begin{pmatrix} \cos 2\Phi & \sin 2\Phi \\ \sin 2\Phi & -\cos 2\Phi \end{pmatrix} . \qquad (2.4.9)$$

Here the diagonal blocks of the Liouvillian determine predominantly the spectral appearance. However the components of the Liouvillian corresponding to $-(k_1+k_2)$ decrease so fast that these can be neglected. Then the spectrum is characterized by :

$$(1-\cos 2\Phi)L^{(1)} + (1+\cos 2\Phi)L^{(2)}$$
$$= p_1 L^{(1)} + p_2 L^{(2)} . \qquad (2.4.10)$$

Thus the spectrum is described by the use of the weight-averaged Liouvillian. In the case of the two-site jump the time-averaged spectrum shows a characteristic pattern de-

pending on the relative orientation of the principal axes of the EFG tensor at the two sites. Hence the analysis of the spectrum at fast motion regime can determine the angle between the EFG principal axes at the two sites.

iii) Intermediate cases

The spectrum will change its appearance drastically if the rate of chemical exchange becomes comparable to the difference of the nutation frequencies at different sites. Therefore the 2D nutation spectrum can be applied to chemically exchanging systems to determine the rate of exchange when it is of the comparable order with e^2Qq/h (and also with ω_1). For the analysis of the complicated spectrum in the above region one must simulate the nutation spectrum with the exchange rate as a variable parameter.

References

[1] See, for example,
R.R. Ernst, G. Bodenhausen, and A. Wokaun,
Principles of Nuclear Magnetic Resonance in One and Two Dimensions, Oxford Press, 1987.

J. Jeener,
Superoperators in Magnetic Resonance,
Adv. Magn. Reson., Vol. 10, Academic Press, 1982.

[2] A. Abragam,
Principle of Magnetic Resonance,
Oxford University Press, 1961.

[3] G. Arfken,
Mathmatical Methods for Physicists,
Academic Press, 1970.

[4] A. Samoson and E. Lippmaa,
Chem. Phys. Lett., **100**(3), 205 (1983).

A. Samoson and E. Lippmaa,
Phys. Rev., B **28**, 6567 (1983).

[5] H. Ohki, N. Nakamura, and H. Chihara,
27th NMR touronkai yokousyuu, Sapporo, 1988.

R. Janssen, and W.S. Veeman,
J. Chem. Soc., Faraday Trans. I, **84**, 3747 (1988).

P.P. Man,
J. Magn. Reson., **67**, 78 (1986).

[6] L. Pandey, S. Towta, and D.G. Hughes,
J. Chem. Phys., **85**, 6923 (1986).

[7] D.R. Torgeson and R.G. Barnes,
J. Chem. Phys., **62**(10), 3968 (1975).

[8] J. Sandström,
Dynamic NMR Spectroscopy, Academic Press, 1982

[9] T.E. Bull,
J. Magn. Reson., **8**, 344 (1972).

3. Simulation

3.1. Principle

3.1.1. Diagonalization of the Liouvillians

In the case when only one kind of site exists, the calculation is straightforward since the analytical expression given in Sec. 2.2 can be applied. Even when several nonequivalent sites exist in the crystal and when no chemical exchange occurs, the whole spectrum can be represented by the superposition of the spectrum corresponding to each site. In the case where the chemical exchange occurs, one should calculate the Eq. (2.4.3), or equivalent to say, one must diagonalize the matrices in each period numerically. Because the matrices L_1+K and L_2+K in Eq. (2.4.3) are complex and non-Hermitian and have very large dimension of $(2I+1)^2\times$(number of site), they cannot be diagonalized directly by the usual methods. Then several modifications on the matrices must be made.

At first, the exchange matrix should be transformed by the matrix P so as to symmetrize the whole matrix. Then,

$$L^S{}_1 = (P^{-1} \otimes E_K)(L_1 + K)(P \otimes E_K)$$
$$= L_1 + K^S \ , \qquad (3.1.1a)$$
$$L^S{}_2 = (P^{-1} \otimes E_K)(L_2 + K)(P \otimes E_K)$$
$$= L_2 + K^S \ , \qquad (3.1.1b)$$

where

$$K^S = (P^{-1} \otimes E_K)K(P \otimes E_K) \ , \qquad (3.1.1c)$$

and P is defined by Eq. (2.4.6). Then it is proved that the matrix $L^S{}_1$ (and also $L^S{}_2$) can be diagonalized by a complex orthogonal matrix. (The complex orthogonal matrix means

that the multiplication of its transposed matrix and itself yields the unit matrix.) It should be noted that the exchange matrix is symmetrized by the above transformation which is however independent of the Liouvillian at each site.

In the evolution period when rf pulse is applied, another transformation is needed to reduce the dimension of the matrix to be diagonalized. This can be achieved by transforming the I_z basis* to I_x basis [1]. When the rows and the columns are suitably interchanged, the Liouvillian at the j-th site L_j can be factorized so as to have a block-diagonal structure whose blocks have the dimension $(2I+1)^2/4 = 4$.

$$L^x{}_j = (RT)^{-1} L_j (RT)$$
$$= \begin{pmatrix} A_j & & & 0 \\ & B_j & & \\ & & B'_j & \\ 0 & & & A'_j \end{pmatrix}, \qquad (3.1.2)$$

and density superket at the site j becomes

$$\boldsymbol{\rho}^x{}_j = (RT)^{-1} \boldsymbol{\rho}_j \ , \qquad (3.1.3)$$

where $R = R \otimes R$ (R is defined in Eq. (2.2.23)) is an

---

* 'I_z basis' means that the axis parallel to the static external magnetic field is the quantization axis. Thus I_z becomes good quantum number. Also, 'I_x basis' means that the axis parallel to the rf field is the quantization axis and in this choice of the basis, I_x is good quantum number.

orthogonal matrix which operates to transform the basis from I_z to I_x, and T the matrix to interchange the rows and the columns. By this transformation, the exchange matrix remains unchanged. The explicit matrix forms of the block matrices A, A', B, and B' for I = 3/2 are :

$$A_j = \begin{pmatrix} 0 & \sqrt{3}\omega_{Q\,j} & -\sqrt{3}\omega_{Q\,j} & 0 \\ \sqrt{3}\omega_{Q\,j} & -2\omega_{Q\,j}+4\omega_1 & 0 & -\sqrt{3}\omega_{Q\,j} \\ -\sqrt{3}\omega_{Q\,j} & 0 & 2\omega_{Q\,j}-4\omega_1 & \sqrt{3}\omega_{Q\,j} \\ 0 & -\sqrt{3}\omega_{Q\,j} & \sqrt{3}\omega_{Q\,j} & 0 \end{pmatrix} / 2 \,, \tag{3.1.4a}$$

$$B_j = \begin{pmatrix} 2\omega_{Q\,j}+2\omega_1 & \sqrt{3}\omega_{Q\,j} & \sqrt{3}\omega_{Q\,j} & 0 \\ \sqrt{3}\omega_{Q\,j} & 6\omega_1 & 0 & \sqrt{3}\omega_{Q\,j} \\ \sqrt{3}\omega_{Q\,j} & 0 & -2\omega_1 & \sqrt{3}\omega_{Q\,j} \\ 0 & \sqrt{3}\omega_{Q\,j} & \sqrt{3}\omega_{Q\,j} & -2\omega_{Q\,j}+2\omega_1 \end{pmatrix} / 2 \,, \tag{3.1.4b}$$

$$B'_j = \begin{pmatrix} -2\omega_{Q\,j}-2\omega_1 & -\sqrt{3}\omega_{Q\,j} & -\sqrt{3}\omega_{Q\,j} & 0 \\ -\sqrt{3}\omega_{Q\,j} & -6\omega_1 & 0 & -\sqrt{3}\omega_{Q\,j} \\ \sqrt{3}\omega_{Q\,j} & 0 & -2\omega_1 & -\sqrt{3}\omega_{Q\,j} \\ 0 & -\sqrt{3}\omega_{Q\,j} & -\sqrt{3}\omega_{Q\,j} & 2\omega_{Q\,j}-2\omega_1 \end{pmatrix} / 2 \,, \tag{3.1.4c}$$

$$A'_j = \begin{pmatrix} 0 & -\sqrt{3}\omega_{Q\,j} & \sqrt{3}\omega_{Q\,j} & 0 \\ -\sqrt{3}\omega_{Q\,j} & 2\omega_{Q\,j}+4\omega_1 & 0 & \sqrt{3}\omega_{Q\,j} \\ \sqrt{3}\omega_{Q\,j} & 0 & -2\omega_{Q\,j}-4\omega_1 & -\sqrt{3}\omega_{Q\,j} \\ 0 & \sqrt{3}\omega_{Q\,j} & -\sqrt{3}\omega_{Q\,j} & 0 \end{pmatrix} / 2 \,, \tag{3.1.4d}$$

where $\omega_{Q\,j}$ represents the first order quadrupole interaction at the site j. The corresponding density superkets at j-th

site transformed as the Liouvillian are given by :

$$\rho^{x}{}_{j} = p_j{}^{t}(0\ 0\ 0\ 0\ \sqrt{3}\ 3\ 0\ -\sqrt{3}\ \sqrt{3}\ 3\ 0\ -\sqrt{3}\ 0\ 0\ 0\ 0). \qquad (3.1.5)$$

Because the elements of the density superkets corresponding to the matrices A and A' on the basis I_x are zero at thermal equilibrium, these can be disregarded. Because the matrices B and B' are complex conjugates with each other and the density superkets corresponding to B and B' are identical at time zero, the matrix to be diagonalized is reduced to

$$L^{s}{}_{1}' = \begin{pmatrix} iB_1 - k_1 E_8 & k' E_8 \\ k' E_8 & iB_2 - k_2 E_8 \end{pmatrix}, \qquad (3.1.6)$$

where B_j is given in Eq. (3.1.4b) and E_8 is the unit matrix which has the same dimension as B_j's.

Although the I_x basis is very convenient for diagonalizing the Liouvillian, it is not suitable for calculation of the FID's since the transition observed in the detection period is labelled by the transition between the quantum number m_z, which is the eigenvalues of I_z. Then it has to be put back to the I_z basis.

In the detection period, the Liouvillian is diagonal and exchange matrix merely couples the density superkets with the same labels belonging to different sites. Then one calculates a matrix which consists of the elements concerning only with the central transition. Because the dimension of its matrix, $L^{s}{}_{2}'$, is the number of the sites, this matrix can be easily diagonalized compared with that in the evolution period.

Then the FID signal at a time t_1+t_2 becomes

$$S(t_2,t_1) \propto I_x \rho(t_2,t_1)$$
$$= \sum P_{i\,i} Q_{2\,i\,j} \exp[-iL_2{}^d{}_j t_2] Q_2{}^{-1}{}_{j\,k}$$
$$\times R_{k\,l} Q_{1\,l\,m} \exp[-iL_1{}^d{}_m t_1] Q_1{}^{-1}{}_{m\,n} \rho_x(0)_n \ , \tag{3.1.7}$$

where Q_1 and Q_2 are complex orthogonal matrices which diagonalize $L^S{}_1'$ and $L^S{}_2'$, respectively.

The Liouvillians $L^S{}_1'$ and $L^S{}_2'$ have special properties : It is symmetric (or can be symmetrized by the method described in Sec. 3.1), and all their elements distant from the diagonal element by a certain fixed number, which denotes a band width, are zero. These properties can be fully utilized to perform the numerical diagonalization. There are many possible methods to do this but the present work adopts a method which consists of two stages [2]. First is to find a transformation which reduces the band width and gives the symmetric tridiagonal matrix but keeps the symmetric and bandform characters of the Liouvillians unchanged. This is accomplished by the successive Jacobi rotation in the plane of i and j = i+1 which is the orthogonal transformation

$$J(i,j,\chi) = \begin{pmatrix} \cdots & \cdot & \cdot & \cdot & \cdot & \cdots \\ \cdots & \cdot & \cdot & \cdot & \cdot & \cdots \\ \cdots & 1 & 0 & 0 & 0 & \cdots \\ \cdots & 0 & \cos\chi & \sin\chi & 0 & \cdots \\ \cdots & 0 & -\sin\chi & \cos\chi & 0 & \cdots \\ \cdots & 0 & 0 & 0 & 1 & \cdots \\ \cdots & \cdot & \cdot & \cdot & \cdot & \cdots \\ \cdots & \cdot & \cdot & \cdot & \cdot & \cdots \end{pmatrix} \begin{matrix} \\ \\ \\ i) \\ j) \\ \\ \\ \\ \end{matrix} . \qquad (3.1.8)$$

This procedure is for eliminating the matrix element at (i,i+1). Although the Jacobi rotation creates a new non-zero element at (i+b,j+b), where b is the band width of the matrix, a series of rotations gives rise to result that i+b or j+b is greater than the dimension of the matrix. Thus one can eliminate the element without creating another one. These transformations are continued until the matrix is tridiagonalized. Then the Liouvillian becomes

$$L^T = \Pi(J^{-1}{}_i) L^S \Pi J_i \ , \qquad (3.1.9)$$

where L^T has zero off-diagonal elements except those immediately adjacent to the diagonal one.

Secondly, the matrix is diagonalized by the QR method. Let A_0 be a general symmetric n-dimensional matrix to be diagonalized. An origin-shift parameter s_j is suitably selected so as to realize the factorization $A_j - s_j E = Q_j R_j$ where Q_j is a complex orthogonal matrix and R_j is an upper triangular matrix, then $A_{j+1} = Q_j^{-1} A_j Q_j$ can be obtained. When this procedure is iterated it can be shown that this series of matrices similar to A_0 generally tends to an upper

triangular matrix. Since A_θ is a tridiagonal matrix, the resultant matrix is diagonal and its diagonal elements give the eigenvalues in this case.

In each step of iteration, the origin shift is chosen to be one of the two eigenvalues of 2×2 submatrix at the bottom right-hand corner that has smaller modulus. The Jacobi rotations to effect the decomposition $A_j - s_j E = Q_j R_j$ is used to triangularize A_j, i.e., in the rotations in the planes (i,r+1) where i=1,2,···r, rotation angle is determined such that the element (r+1,i) becomes zero.

The actual diagonalization subprogram is the modification of the one in the NUMPAC routine in the Nagoya University. First stage of the tridiagonalization is referred to [2]. And second stage is QR method modified by the use of complex orthogonal matrix instead of Unitary matrix.

3.1.2 Powder Averaging

In the powdered samples, the crystals are oriented at random with respect to the magnetic field. Thus one must designate the orientation of the principal axes of the EFG tensor with respect to the static magnetic field so as to perform the powder averaging [3] :

$$f(t_2, t_1) = \int d\phi \int \sin\theta d\theta \; S(t_2, t_1) \; . \qquad (3.1.10)$$

The coordinate transformation from the laboratory frame to the crystalline frame (a coordinate fixed in the crystalline specimen) is represented by the rotation :

$$R_c = \begin{pmatrix} \cos\theta\cos\phi & \cos\theta\sin\phi & -\sin\theta \\ -\sin\phi & \cos\phi & 0 \\ \sin\theta\cos\phi & \sin\theta\sin\phi & \cos\theta \end{pmatrix}, \qquad (3.1.11)$$

where θ and ϕ are the polar and the azimuthal angles of the crystalline frame referred to the direction of the static magnetic field, respectively. When the EFG principal axes at the site j are indicated by the Euler angles α, β, and γ in the crystalline frame by :

$$R_j = \begin{pmatrix} \cos\alpha & \sin\alpha & 0 \\ -\sin\alpha & \cos\alpha & 0 \\ 0 & 0 & 1 \end{pmatrix} \begin{pmatrix} \cos\beta & 0 & -\sin\beta \\ 0 & 1 & 0 \\ \sin\beta & 0 & \cos\beta \end{pmatrix} \begin{pmatrix} \cos\gamma & \sin\gamma & 0 \\ -\sin\gamma & \cos\gamma & 0 \\ 0 & 0 & 1 \end{pmatrix}, \qquad (3.1.12)$$

then the matrix representing the rotation from the orientation of the magnetic field to the EFG principal axes is given by

$$R_j'(\theta_j, \phi_j) = R_j R_c \ . \qquad (3.1.13)$$

Here, the terms needed in the actual calculation are

$$z_j^2 = \cos^2\theta_j \ ,$$
$$x_j^2 - y_j^2 = \sin^2\theta_j \cos 2\phi_j \ , \qquad (3.1.14)$$

where

$$\begin{aligned} x_j &= [\cos\alpha\cos\beta\cos\gamma - \sin\alpha\sin\gamma]x_c \\ &\quad + [\cos\alpha\cos\beta\sin\gamma + \sin\alpha\cos\gamma]y_c - \cos\alpha\sin\beta z_c \ , \\ y_j &= -[\sin\alpha\cos\beta\cos\gamma + \cos\alpha\sin\gamma]x_c \\ &\quad - [\sin\alpha\cos\beta\sin\gamma - \cos\alpha\cos\gamma]y_c + \sin\alpha\sin\beta z_c \ , \\ z_j &= \sin\beta\cos\gamma x_c + \sin\beta\sin\gamma y_c + \cos\beta z_c \ , \end{aligned} \qquad (3.1.15)$$

and

$$x_c = \sin\theta\cos\phi \ ,$$
$$y_c = \sin\theta\cos\phi \ ,$$
$$z_c = \cos\theta \ , \qquad (3.1.16)$$

where θ_j and ϕ_j are the polar angles of the EFG principal axes with respect to the magnetic field at the site j. By the use of z_j^2 and $x_j^2-y_j^2$, the first and the second order quadrupole interactions are expressed by

$$\omega_Q^{(1)}{}_j = e^2qQ/8I(2I-1)\{3z_j^2-1+\eta(x_j^2-y_j^2)\} \ , \qquad (3.1.17)$$

$$\omega_Q^{(2)}{}_j = (e^2qQ/h)^2/192\omega_0 \{9(1-z_j^2)^2-6\eta(1+z_j^2)(x_j^2-y_j^2) +4\eta^2z_j^2+\eta^2(x_j^2-y_j^2)^2 -72z_j^2(1-z_j^2)-48\eta z_j^2(x_j^2-y_j^2) -8\eta^2(1-z_j^2)+8\eta^2(x_j^2-y_j^2)^2\} \ . \qquad (3.1.18)$$

Then the calculation must be performed over the ranges $0 < \theta < \pi$, and $-\pi < \phi \leq \pi$ in order to accomplish the powder averaging.

In the actual calculation, $\cos\theta$ is used instead of θ because the powder averaging (3.1.10) can be rewritten as

$$f(t_2,t_1) = \int d\phi \int d(\cos\theta)\ S(t_2,t_1) \ . \qquad (3.1.19)$$

Thus the region of the integration is divided into N with respect to $\cos\theta$ ($-1 < \cos\theta < +1$) and ϕ ($-\pi < \phi \leq \pi$).

In the case where only one kind of site exists, one can tentatively coincide the crystalline frame with the EFG

principal axes. Since $S(t_2,t_1)$ is symmetric with respect to $\cos\theta$ and ϕ, the number of calculation can be reduced by a factor of 4 of the total division.

3.1.3 Line Broadening

The line broadening effect should be incorporated as the multiplication of the FID's Eq. (3.1.19) by the Gaussian (or Lorentzian) function. Since the origin of the line broadening is mainly due to dipole interaction in the detection period but the distribution of (static) quadrupole interaction and/or dipole interaction cause the line broadening in the evolution period, the broadening factors in each period may be different, and in practice they are used as adjustable parameters. Other reasons which bring about the line broadening are discussed later.

3.1.4 2D Fourier transformation

The FID's obtained by the above procedure should be Fourier-transformed to deduce the 2-dimensional spectrum.

$$g(\omega_2,\omega_1) = \int \exp(-i\omega_2 t_2)dt_2 \int \exp(-i\omega_1 t_1)dt_1 \; f(t_2,t_1) , \tag{3.1.20}$$

where $f(t_2,t_1)$ is given in Eq. (3.1.19).

3.2 Computational Procedure

Two simulation programs were constructed, one for the simulation of 2D nutation spectrum without chemical exchange and the other with chemical exchange.

Brief explanation of the former is given in the following. Although the analytical expression has been given, the diagonalization is performed numerically so as to be able to treat the general case in which spin $I \geq 3/2$.

1) Parameter Input

Input the parameters necessary to simulate the spectrum.

- spin number
- Larmor frequency
- quadrupole coupling constant and asymmetry parameter
- rf pulse strength in the frequency unit
- number of experiments and increment of the pulse length
- number of sampling points and sampling interval
- number of division over the sphere for numerical integration

2) Quadrupole Interaction

The first and the second order quadrupole interactions are determined at a given angle θ and ϕ with respect to the external magnetic field.

3) Calculation of the FID

Diagonalize the Hamiltonian and calculate the evolution of the density matrix to evaluate the FID signal. These are accumulated in the range $0 \leq \cos\theta < 1$, and $0 \leq \phi < \pi$.

Short explanation of the simulation program with chemical exchange is given below.

1) Parameter Input

Input the parameters necessary to calculate the FID's.

Larmor frequency

number of site for exchange

e^2qQ/h, η and the Euler angles which relate the crystalline frame and the principal axes of the EFG at each site

relative population of each site

chemical exchange rate between any pair of the sites

rf pulse strength in the frequency unit

number of experiments and increment of the pulse length

number of sampling points and sampling interval

number of division over the sphere for numerical integration

2) Quadrupole interaction at a given orientation

The first and the second order quadrupole interactions are calculated at a given angle θ and ϕ with respect to the external magnetic field.

3) Calculation of FID

Diagonalize the Liouvillians corresponding to each dimension and calculate the FID.

These are summed over the sphere in the range $-1 < \cos\theta < 1$ and $-\pi < \phi \leq \pi$.

In each case, the number of divisions over the sphere is chosen to be sufficient to produce the powder spectrum, i.e., 3000-10000. A set of data points 128×256 are used to calculate the FID's. The program lists are given in

Appendix. The program is coded in FORTRAN and calculated by the ACOS-6 of the computer center of Osaka University and/or NEC PC-9801E/VM personal computer.

The Fourier transformation (Eq. (3.1.20)) was done by the use of the ASPECT-3000 minicomputer incorporated in the BRUKER MSL-200 NMR system. The ASPECT-3000 is equipped with an array processor which can execute the 2D Fourier transformation very efficiently and with the plotting routine to draw up the spectrum. The data conversion program provided by BRUKER Co. Ltd. was modified to convert the data format between the MS-DOS operating system on NEC PC-9801 personal computer and the ASPECT-3000 system. The line broadening parameters can also be defined in the ASPECT-3000 system.

References

[1] R. Janssen and W.S. Veeman,
J. Chem. Soc., Faraday Trans., I, **84**, 3747 (1988).

[2] R.G. Gordon and T. Messenger,
in *Electron Spin Relaxation in Liquids*,
Ed. by L.T. Muus and P.W. Atkins, Plenum Press, 1972.

[3] See, for example,
U. Haeberlen,
High Resolution NMR in Solids,
Adv. Magn. Reson., suppl. 1, Academic Press, 1976.

4. Sample

4.1. $NaNO_2$ and $NaHgCl_3.2H_2O$

$NaNO_2$ crystallizes in an orthorhombic (space group Im2m) crystal system with the unit cell dimension of a = 3.569 Å, b = 5.563 Å, and c = 5.384 Å, Z = 2. [1]

Crystal of $NaHgCl_3.2H_2O$ is orthorhombic (space group Pnma) with four molecules in the unit cell [2]. The lattice parameters are : a = 9.372 Å, b = 4.037 Å, and c = 18.71 Å. Sodium atoms are coordinated by two H_2O molecules and four chlorine atoms.

Both of the above compounds have only one kind of sodium site and can be used to preliminary test of 2D nutation NMR method.

4.2 Na_2SeO_3

This crystal has three nonequivalent sodium sites [3]. This sample can be used to examine whether 2D nutation NMR method can be applied to determine the quadrupole interaction parameters at each site.

4.3. $Na_{1+x}Zr_2Si_xP_{3-x}O_{12}$

The system $Na_{1+x}Zr_2Si_xP_{3-x}O_{12}$ has been known to be a fast alkali-ion conductor. [4] The crystal structure is shown in Fig. 4.1. [5] Complete solid solution exists for the composition between x = 0 and 3 and the crystal structure varies between R3 ($0.0 \leq x < 1.8$, $2.2 < x \leq 3.0$) and C2/c ($1.8 \leq x \leq 2.2$). The latter is a slightly deformed structure of the former. The structure consists of a three-dimensional skeletal network of PO_4 (and/or SiO_4) tetrahedra which are corner-shared with ZrO_6 octahedra. The ZrO_6 octahedron is linked by three PO_4 tetrahedra so as to form a ribbon along the hexagonal c-axis and also linked by six PO_4

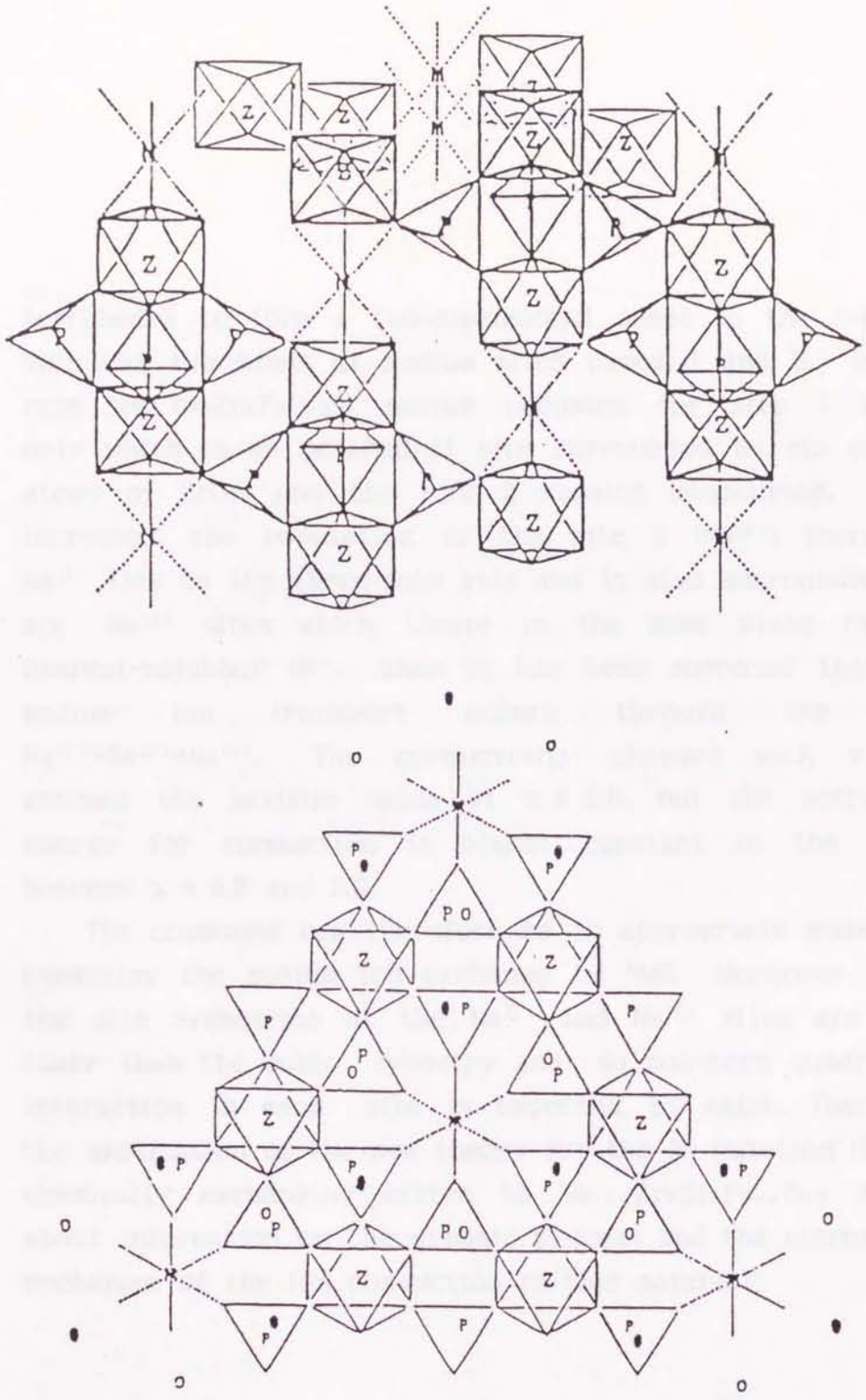

Figure 4.1

Crystal structure of $Na_{1+x}Zr_2Si_xP_{3-x}O_{12}$.

tetrahedra to form a two-dimensional sheet in the c-plane. This has two kinds of sodium sites named 1 and 2. In the case x=0 ($NaZr_2P_3O_{12}$), sodium occupies the site 1 ($Na^{(1)}$) only which is an octahedral site surrounded by six oxygen atoms of ZrO_6, and the site 2 remains unoccupied. As x increases, the population of the site 2 ($Na^{(2)}$) increases. $Na^{(1)}$ lies on the three-fold axis and is also surrounded by six $Na^{(2)}$ sites which locate in the same plane of the nearest-neighbor O^{2-}. Thus it has been supposed that the sodium ion transport occurs through the path $Na^{(1)} \rightarrow Na^{(2)} \rightarrow Na^{(1)}$. The conductivity changes with x and assumes the maximum value at x = 2.0, but the activation energy for conduction is almost constant in the range between x = 0.0 and 3.0.

The compound can therefore be an appropriate model for examining the sodium ion exchange by NMR. Moreover, since the site symmetries at the $Na^{(1)}$ and $Na^{(2)}$ sites are both lower than the cubic symmetry and so non-zero quadrupole interaction in each site is expected to exist. Therefore the application of the new theory for the 2D nutation NMR on chemically exchanging system to $Na_{1+x}Zr_2Si_xP_{3-x}O_{12}$ brings about information on the dynamic process and the microscopic mechanism of the ion conduction in this material.

References

[1] R.W.G. Wyckoff,
Crystal Structures, 2nd Ed., Vol. 2,
John Wiley & Sons, 1964

[2] R.W.G. Wyckoff,
Crystal Structures, 2nd Ed., Vol. 3,
John Wiley & Sons, 1965

[3] G. Perinet, P. Bianco, and R. Sabbah,
Bull. Soc. Fr. Mineral. Cristallogr., **91**(4), 396(1968).

[4] J.B. Goodenough, H.Y-P. Hong, and J.A. Kafalas,
Mat. Res. Bull., **11**, 203 (1976).

[5] H.Y-P. Hong,
Mat. Res. Bull., **11**, 173 (1976).

5. Experiment

5.1. Sample Preparation

5.1.1. $NaNO_2$ and $NaHgCl_2.2H_2O$

$NaNO_2$ is of commercial source (Nacalai Tesque, guaranteed reagent grade, purity 98.0%) and used without further purification.

$NaHgCl_3.2H_2O$ was prepared from aqueous solution of the appropriate mixture of NaCl (Tomita Seiyaku) and $HgCl_2$ (Nacalai Tesque, guaranteed reagent grade, purity 99.5%). Colorless polycrystals were grown by slow evaporation of water. The X-ray powder diffraction pattern of this product (Fig. 5.1) was compared with that calculated with the lattice parameters given in the literature [1]. The result identified $NaHgCl_3.2H_2O$ but indicated at once the existence of small amount of $HgCl_2$. However, this $HgCl_2$ impurity is supposed to have little influence on the NMR of ^{23}Na.

5.1.2. Na_2SeO_3

Na_2SeO_3 was prepared from aqueous solution of a stoichiometric mixture of NaOH (Nacalai Tesque, reagent grade, purity 93%) and selenius acid H_2SeO_3. [2] H_2SeO_3 is prepared by dissolving SeO_2 (Nacalai Tesque, guaranteed reagent grade, purity 98%) in water. Slow evaporation of the solution gave the white powder.

5.1.3. $Na_{1+x}Zr_2Si_xP_{3-x}O_{12}$

The powdered specimen was synthesized from the stoichiometric mixture of Na_2CO_3 : ZrO_2 : SiO_2 : $NH_4H_2PO_4$ = 1+x : 4 : 2x : 2(3-x), x=0.0, 1.0, and 2.0. [2] The reagents used here were : Na_2CO_3, Nacalai Tesque, guaranteed reagent grade, purity 99.5%; ZrO_2, Nacalai Tesque, reagent grade;

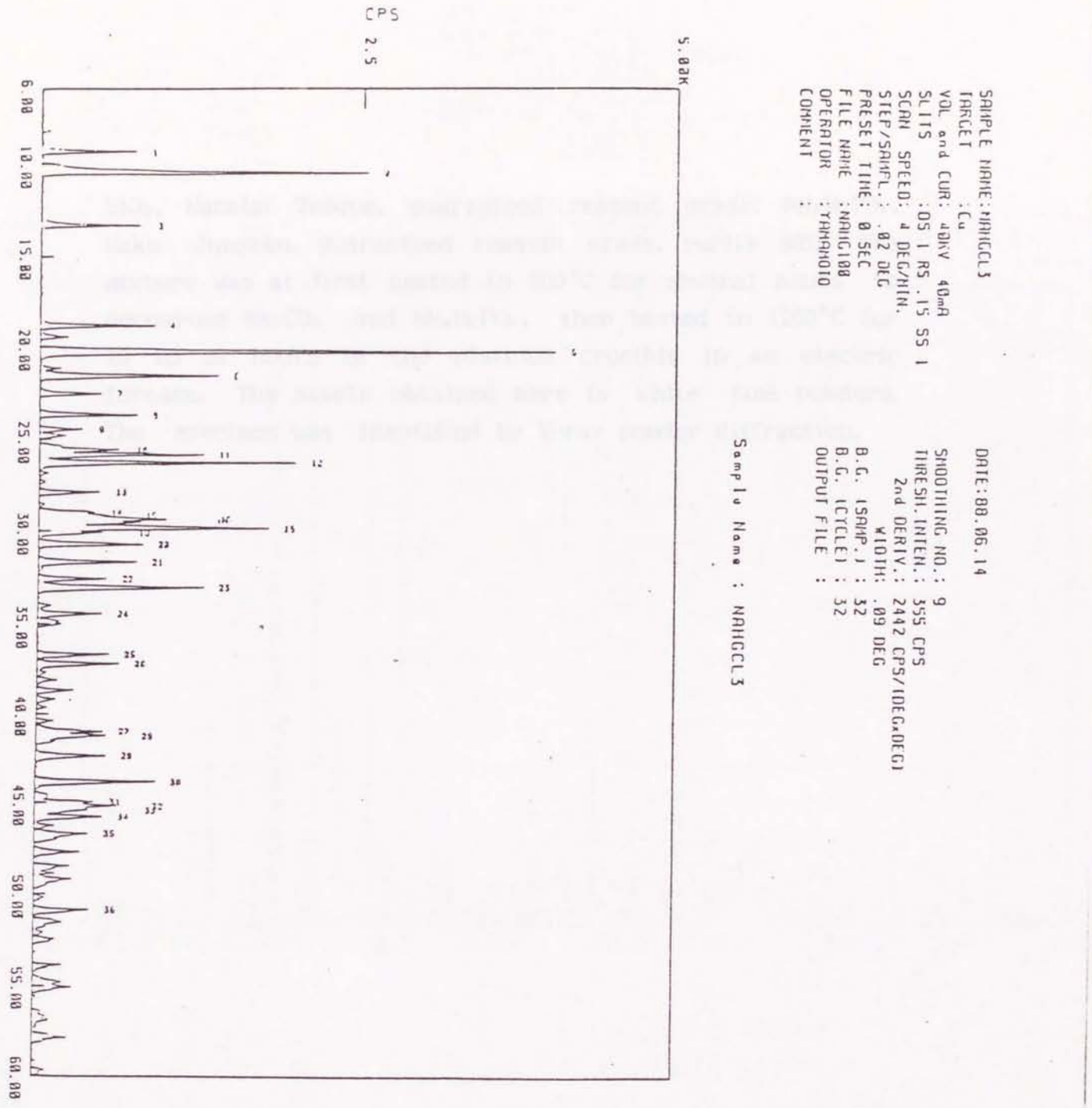

Figure 5.1

The X-ray powder diffraction pattern of $NaHgCl_3.2H_2O$.

SiO_2, Nacalai Tesque, guaranteed reagent grade; $NH_4H_2PO_4$, Wako Junyaku, guaranteed reagent grade, purity 98%. The mixture was at first heated to 900°C for several hours to decompose Na_2CO_3 and $NH_4H_2PO_4$, then heated to 1200°C for 10 to 20 hours in the platinum crucible in an electric furnace. The sample obtained here is white fine powders. The specimen was identified by X-ray powder diffraction.

SAMPLE NAME:NaZr2P3012
TARGET :Cu
VOL and CUR: 40KV 40mA
SLITS :DS 1 RS .3 SS 1
SCAN SPEED: 3 DEG/MIN.
STEP/SAMPL.: .02 DEG
PRESET TIME: 0 SEC
FILE NAME :01100
OPERATOR :YAMAMOTO
COMMENT :

DATE:89.10.20

SMOOTHING NO.: 11
THRESH.INTEN.: 157 CPS
2nd DERIV.: 263 CPS/(DEGxDEG)
WIDTH: .09 DEG
B.G.REDUCTION:NO EXECUTION
OUTPUT FILE :

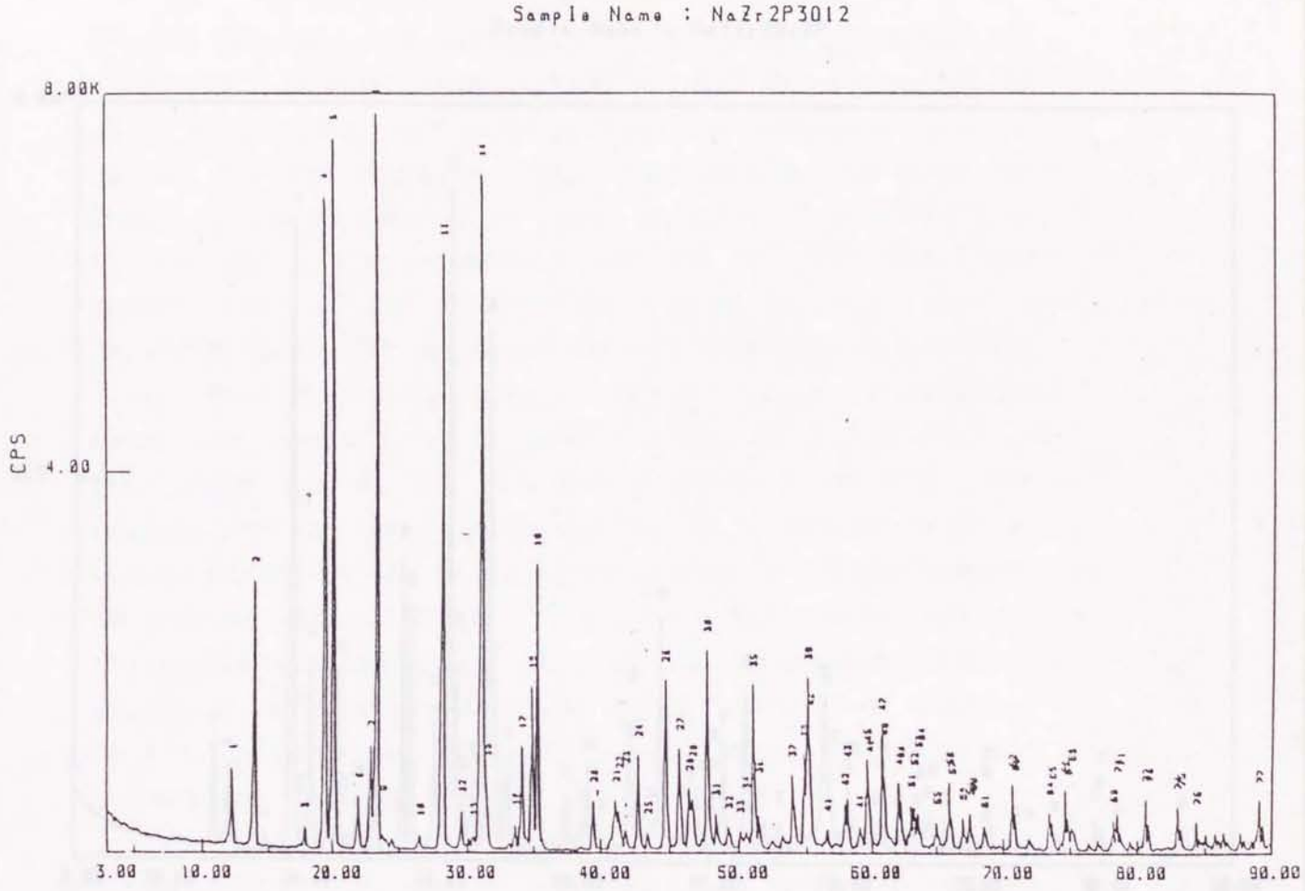

Figure 5.2
The X-ray powder diffraction pattern of $NaZr_2Si_3O_{12}$.

SAMPLE NAME:Na3Zr2Si2P
TARGET :Cu
VOL and CUR: 40KV 40mA
SLITS :DS 1 RS .3 SS 1
SCAN SPEED: 3 DEG/MIN.
STEP/SAMPL.: .02 DEG
PRESET TIME: 0 SEC
FILE NAME :03100
OPERATOR :YAMAMOTO
COMMENT :

DATE:89.10.27

SMOOTHING NO.: 11
THRESH. INTEN.: 137 CPS
2nd DERIV.: 263 CPS/(DEGxDEG)
WIDTH: .09 DEG
B.G.REDUCTION:NO EXECUTION
OUTPUT FILE :

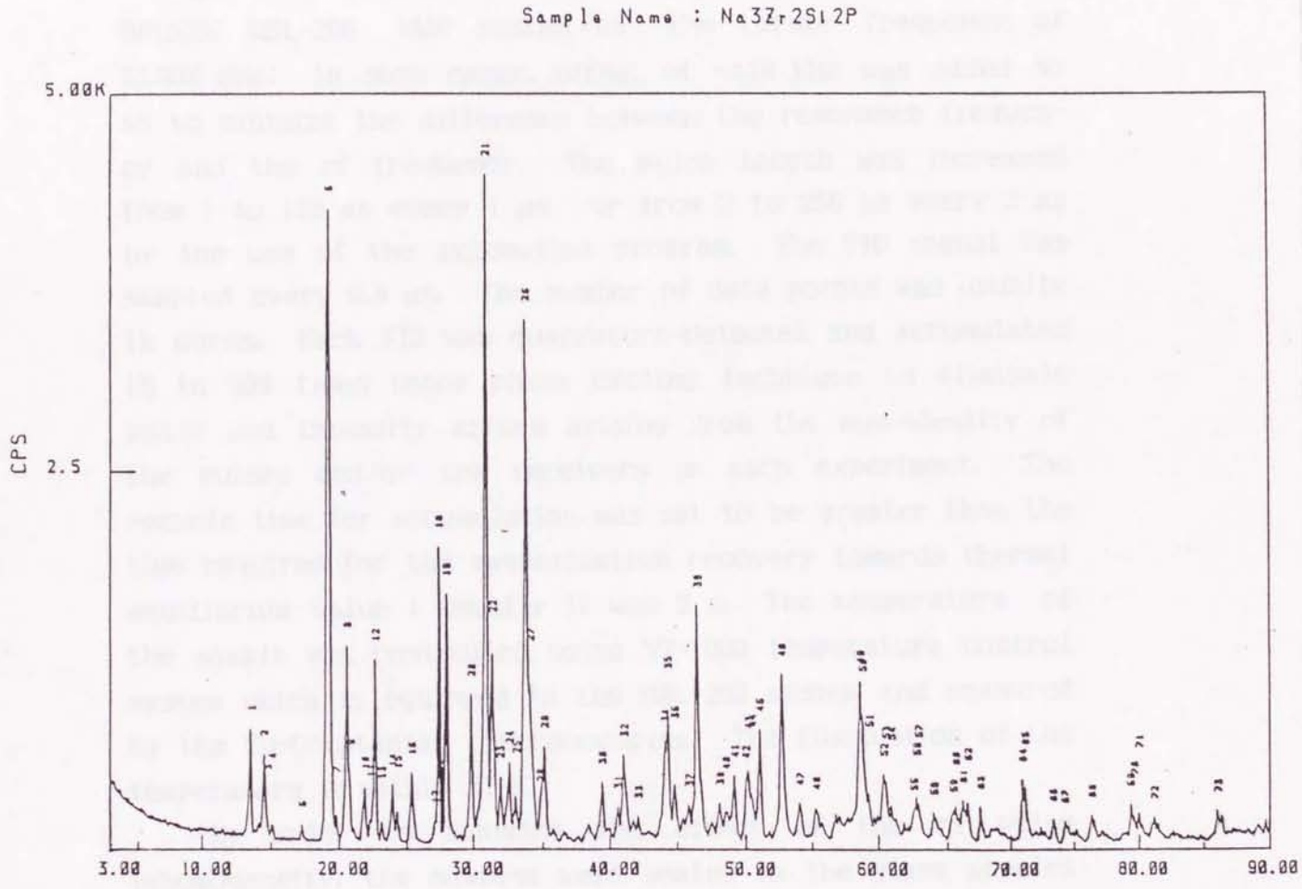

Figure 5.3
The X-ray powder diffraction pattern of $Na_3Zr_2SiP_2O_{12}$.

5.2 Nutation NMR

The ^{23}Na NMR spectrum was measured by the use of the BRUKER MSL-200 NMR system at the Larmor frequency of 52.938 MHz. In some cases, offset of ~±10 kHz was added so as to minimize the difference between the resonance frequency and the rf frequency. The pulse length was increased from 1 to 128 μs every 1 μs, or from 2 to 256 μs every 2 μs by the use of the automation program. The FID signal was sampled every 0.8 μs. The number of data points was usually 1k words. Each FID was quadrature-detected and accumulated 16 to 500 times using phase cycling technique to eliminate phase and intensity errors arising from the non-ideality of the pulses and/or the receivers in each experiment. The recycle time for accumulation was set to be greater than the time required for the magnetization recovery towards thermal equilibrium value : Usually it was 5 s. The temperature of the sample was controlled using VT-1000 temperature control system which is equipped in the MSL-200 system and measured by the Cu-Constantan thermocouples. The fluctuation of the temperature is within ±1 K.

In order to minimize the effect of the rf pulse inhomogeneity, the samples were sealed in the glass ampules with 10mmφ in ca. 10mm long. The signal of sodium from the ampule was negligible since the glass ampule used here was very thin and the amount of sodium in it was negligibly small compared with that in the sample.

The data acquired were 2D Fourier transformed by the use of ASPECT-3000 computer. Before 2D FT, zero filling up to 1k or 2k words in the F_1 dimension was made in order to increase the digital resolution of the spectrum. In some

cases, the trapezoidal function was multiplied to the F_1 data to avoid the effect of cut-off of the tail that causes auxiliary wiggles on either side of the spectrum [4].

References

[1] R.W.G. Wyckoff,
Crystal Structures, 2nd Ed., Vol. 3,
John Wiley & Sons, 1965

[2] The Merck Index, 8th Ed.,
Merck & Co., Inc., 1968.

[2] J.B. Goodenough, H.Y-P. Hong, and J.A. Kafalas,
Mat. Res. Bull., **11**, 203 (1976).

[3] L-O. Hagman and P. Kierkegaard,
Acta Chem. Scand., **22**, 1822 (1968).

[4] T.C. Farrar and E.D. Becker,
Pulse and Fourier Transform NMR, Academic Press, 1971.

A.G. Marshall and F.R. Verdun,
Fourier Transforms in NMR, Optical,
and Mass Spectrometry, Elsevier, 1990.

6. Data Analysis

6.1 Nutation Spectrum

Figs. 6.1 and 6.2 show stacked and contour plots of typical 2D nutation spectrum simulated with parameters e^2Qq/h = 0.2 MHz, η = 0, and $\omega_1/2\pi$ = 50 kHz. The horizontal axis, which will be called F_2 for brevity, is the conventional 1D NMR spectrum axis and the projection onto this axis gives the powder spectrum characterized by the second order quadrupole interaction. (See Fig. 6.2a.) The vertical axis, F_1, shows the nutation spectrum whose pattern varies with strength of the quadrupole interaction relative to the rf strength.

If the Hamiltonian in the evolution period, H_2, does not contain any useful information other than quadrupole interaction, an FT over t_1 gives nutation spectrum which gives rise directly to the ratio $\Omega_Q/\omega_1 = [3e^2Qq/2I(2I-1)\hbar]/\omega_1$, where Ω_Q is the lowest pure quadrupole resonance frequency.

Fig. 6.3 illustrates the simulated dependence of the nutation spectrum on the strength of the quadrupole interaction for I = 3/2 (η = 0 and $\omega_1/2\pi$ = 50 kHz). The numbers on the right-hand side of the spectrum represent e^2Qq/h. The bottom spectrum corresponds to the case when the quadrupole interaction is absent; only one sharp peak appears at around ω_1 as mentioned in Sec. 2.3. As the strength of the quadrupole interaction is increased, the spectrum splits into several peaks and they move away from ω_1. In the topmost spectrum, the quadrupole interaction is so strong that only one peak is found at around $2\omega_1$. In this case, the intensity of the peak at $2\omega_1$ is reduced to 1/4 of that of the peak at ω_1 in the case of e^2Qq/h = 0, indicating that

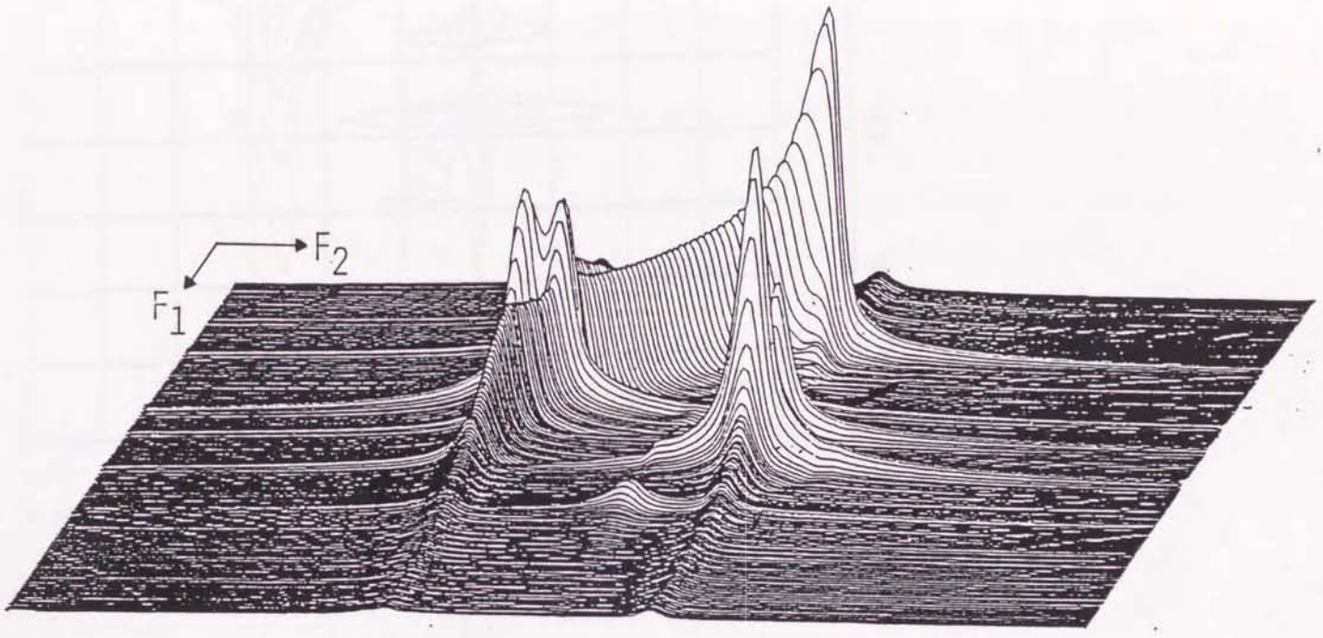

Figure 6.1

Stacked plot of 2D nutation spectrum simulated with parameters e^2Qq/h = 0.2 MHz, η = 0, $\omega_1/2\pi$ = 50 kHz.

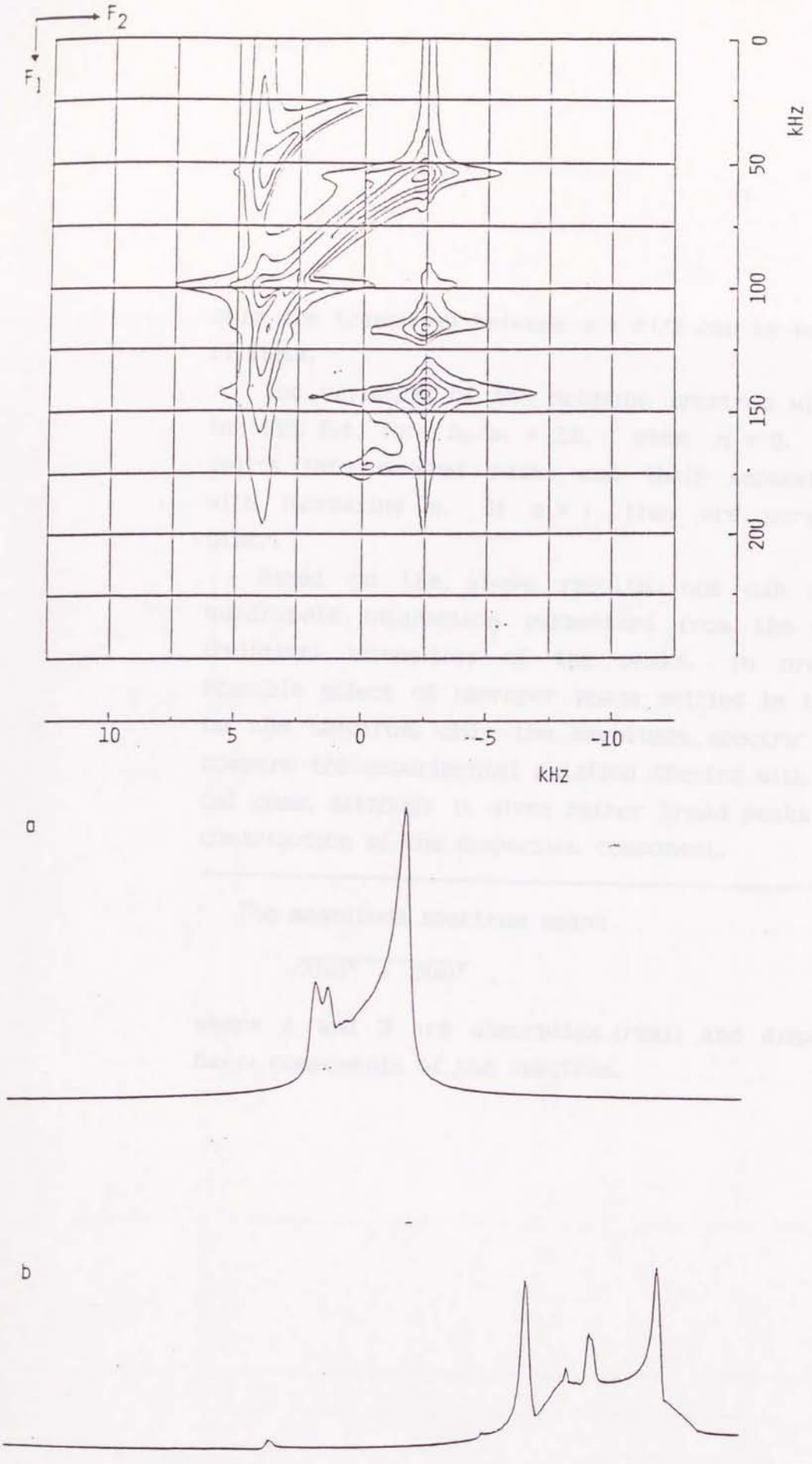

Figure 6.2

Contour plot of simulated 2D nutation spectrum. Calculated parameters are as in Fig. 6.1. a) Projections onto F_1 and b) F_2 axis, respectively.

only the transition between m = ±1/2 can be excited by weak rf field.

The variation of the nutation spectrum with η is shown in Fig. 6.4 for $\Omega_0/\omega_1 = 2.0$. When $\eta \neq 0$, the spectrum splits into several peaks and their separations increase with increasing η. If $\eta = 1$, they are merged with each other.

Based on the above results, one can determine the quadrupole interaction parameters from the positions and (relative) intensities of the peaks. In order to avoid possible effect of improper phase setting in the experiment on the spectrum, only the magnitude spectra* are used to compare the experimental nutation spectra with the theoretical ones, although it gives rather broad peaks owing to the contribution of the dispersion component.

---

* The magnitude spectrum means

$$\sqrt{A(\omega)^2 + D(\omega)^2} \ ,$$

where A and D are absorption (real) and dispersion (imaginary) components of the spectrum.

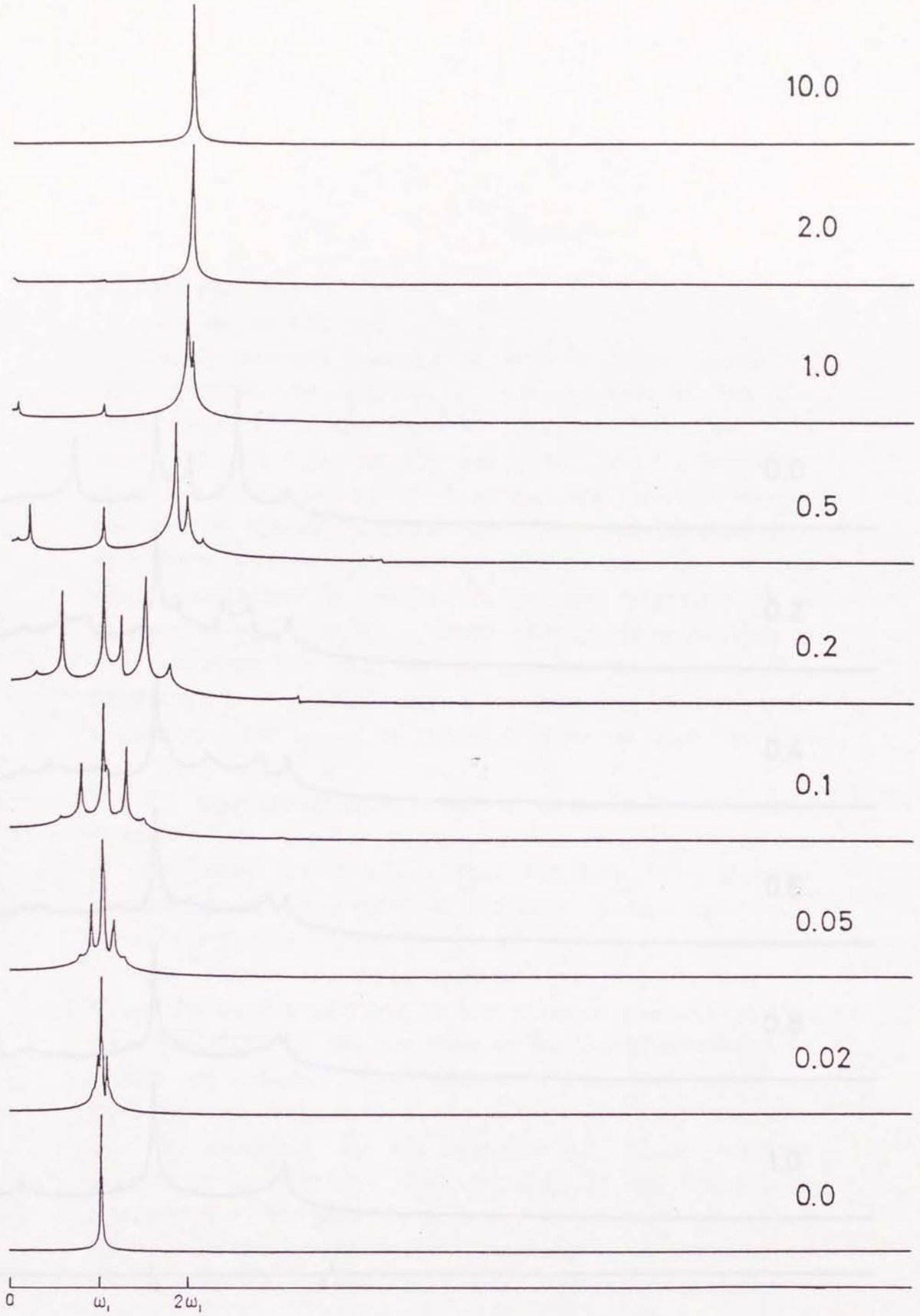

Figure 6.3

Dependence of nutation spectrum on the strength of quadrupole interaction.

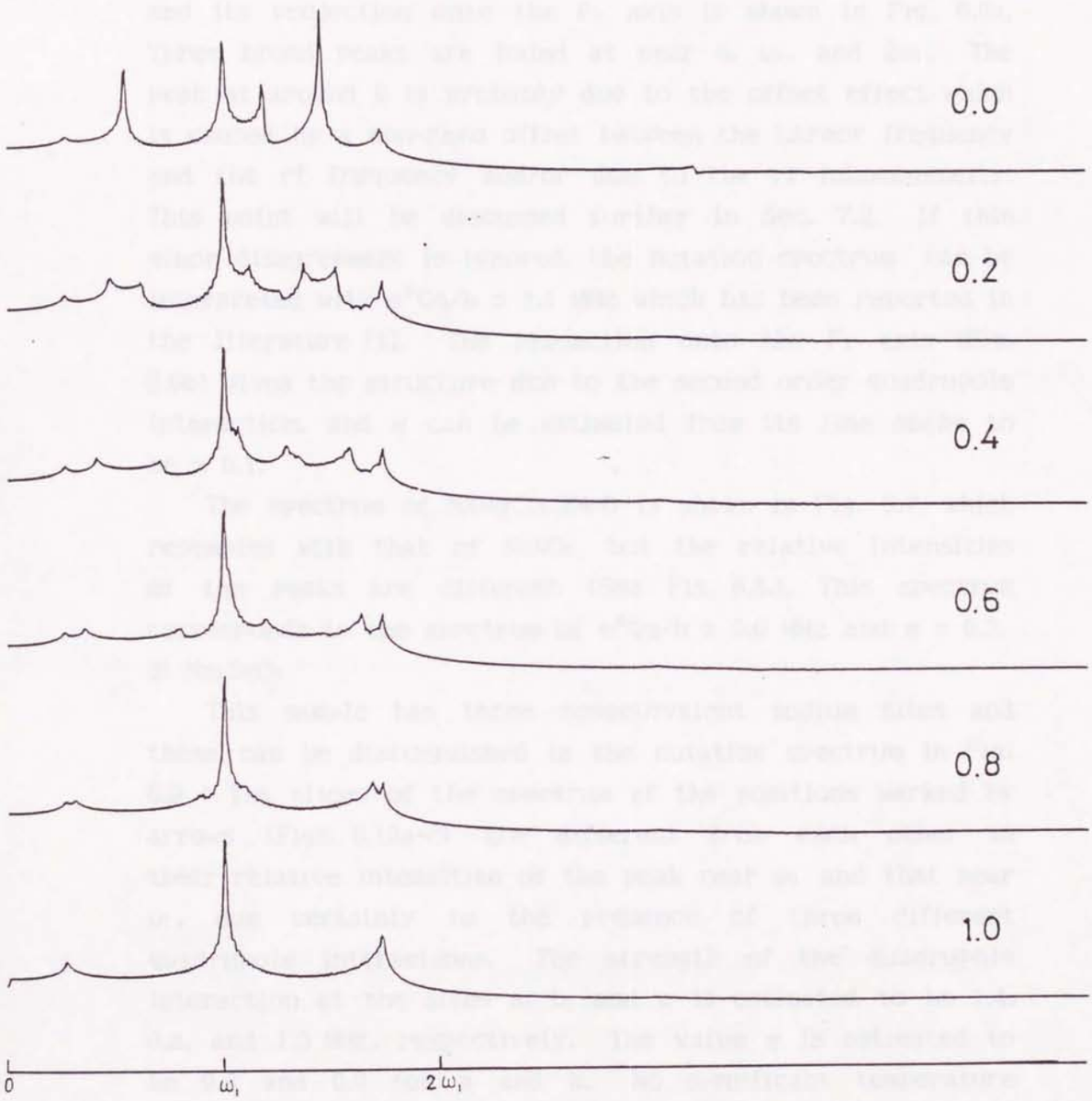

Figure 6.4

η dependence of nutation spectrum. $\Omega_0/\omega_1 = 2$.

6.2 Data Analysis

1) $NaNO_2$ and $NaHgCl_3.2H_2O$

The 2D nutation spectrum of $NaNO_2$ is shown in Fig. 6.5, and its projection onto the F_1 axis is shown in Fig. 6.6a. Three broad peaks are found at near 0, ω_1, and $2\omega_1$. The peak at around 0 is probably due to the offset effect which is caused by a non-zero offset between the Larmor frequency and the rf frequency and/or due to the rf inhomogeneity. This point will be discussed further in Sec. 7.2. If this minor disagreement is ignored, the nutation spectrum can be interpreted with $e^2Qq/h \simeq 1.1$ MHz which has been reported in the literature [1]. The projection onto the F_2 axis (Fig. 6.6b) gives the structure due to the second order quadrupole interaction, and η can be estimated from its line shape to be $\simeq 0.1$.

The spectrum of $NaHgCl_3.2H_2O$ is shown in Fig. 6.7, which resembles with that of $NaNO_2$, but the relative intensities of the peaks are different (See Fig. 6.8.). This spectrum corresponds to the spectrum of $e^2Qq/h \simeq 0.6$ MHz and $\eta \simeq 0.2$.

3) Na_2SeO_3

This sample has three nonequivalent sodium sites and these can be distinguished in the nutation spectrum in Fig. 6.9 : The slices of the spectrum at the positions marked by arrows (Figs. 6.10a-c) are different from each other in their relative intensities of the peak near ω_1 and that near ω_1, due certainly to the presence of three different quadrupole interactions. The strength of the quadrupole interaction at the sites a, b, and c is estimated to be 1.4, 0.8, and 1.3 MHz, respectively. The value η is estimated to be 0.8 and 0.0 for a and b. No significant temperature

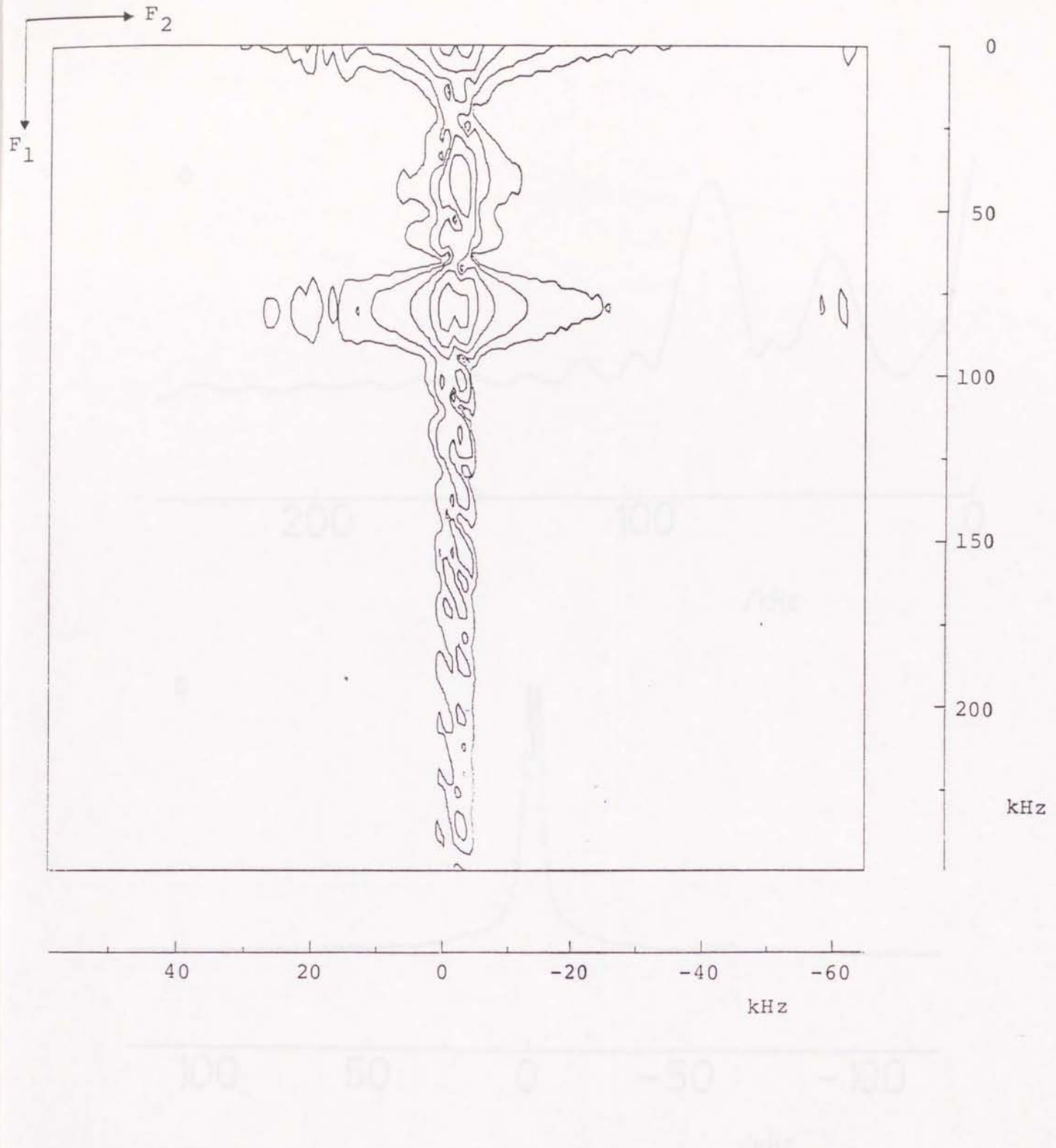

Figure 6.5

Contour plot of 2D nutation spectrum of $NaNO_2$ at room temperature.

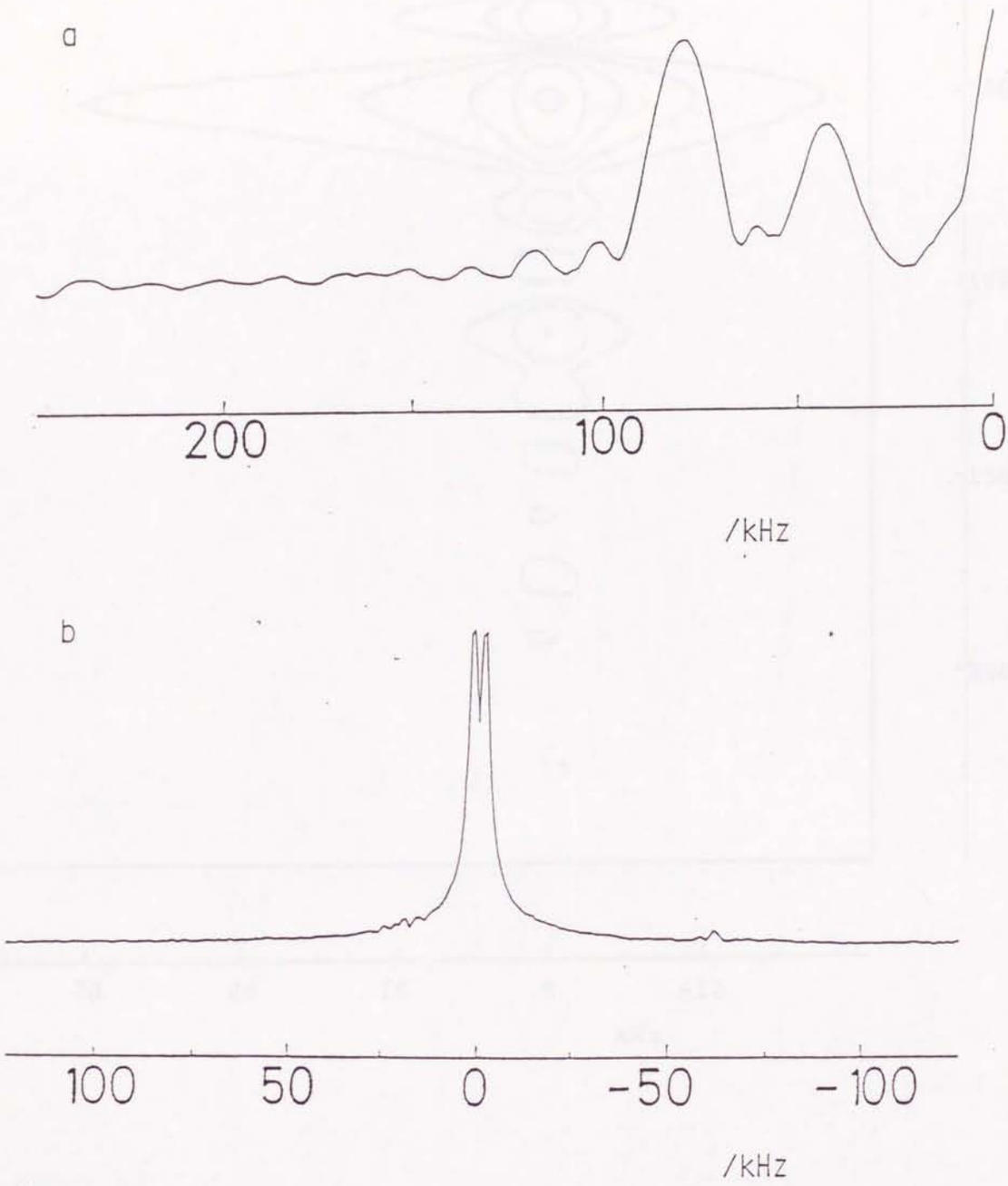

Figure 6.6

2D nutation spectrum of $NaNO_2$ at room temperature.
a) Projection onto F_1 axis. b) Projection onto F_2 axis.

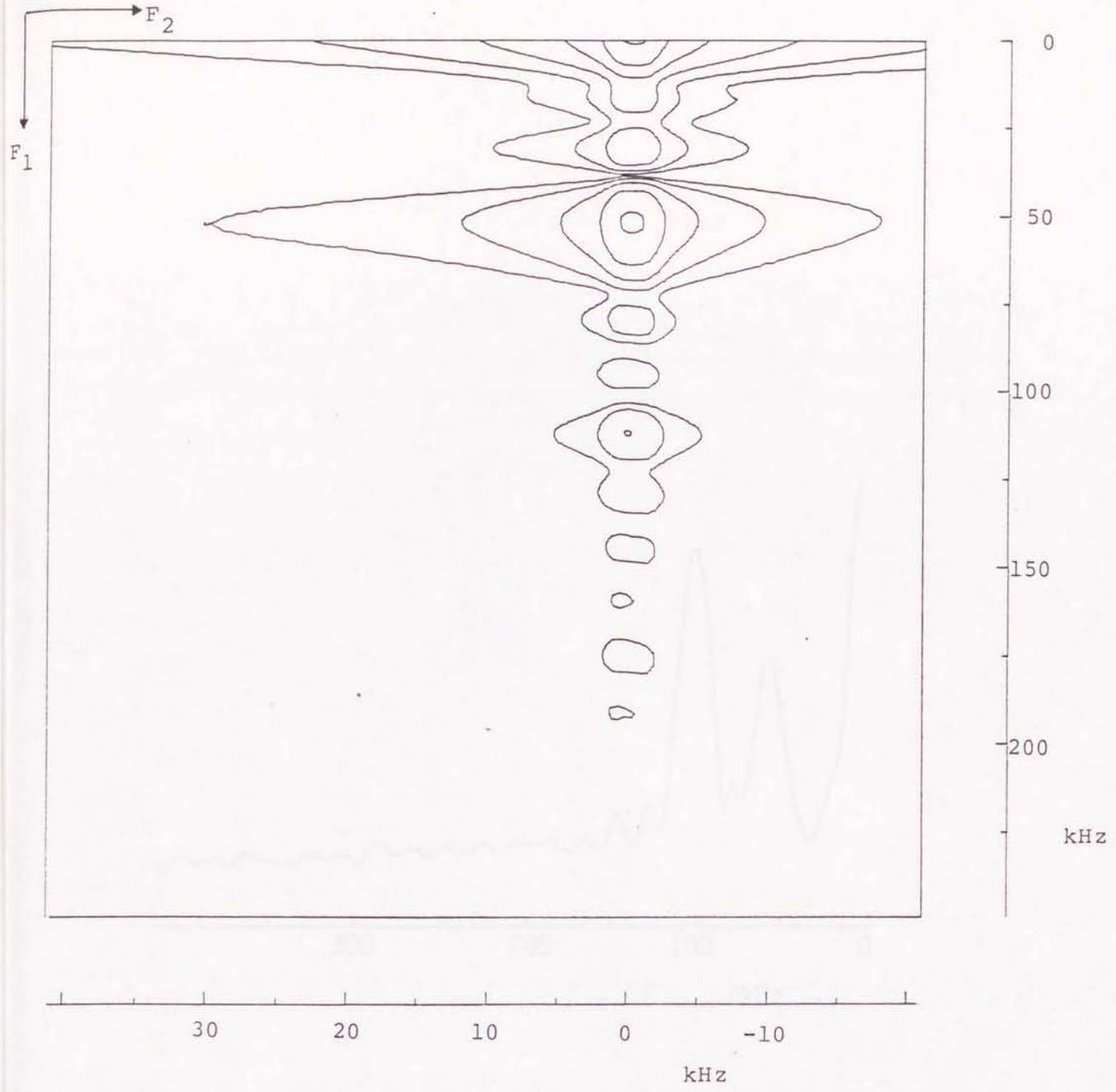

Figure 6.7

Contour plot of 2D nutation spectrum of $NaHgCl_3.2H_2O$ at room temperature.

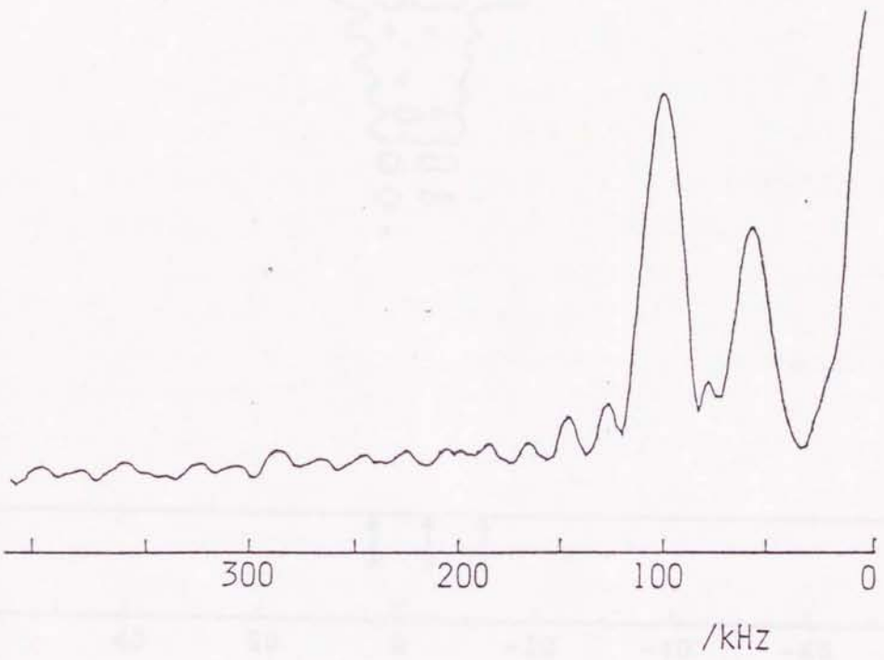

Figure 6.8

2D nutation spectrum of $NaHgCl_3.2H_2O$. Projection onto F_1 axis.

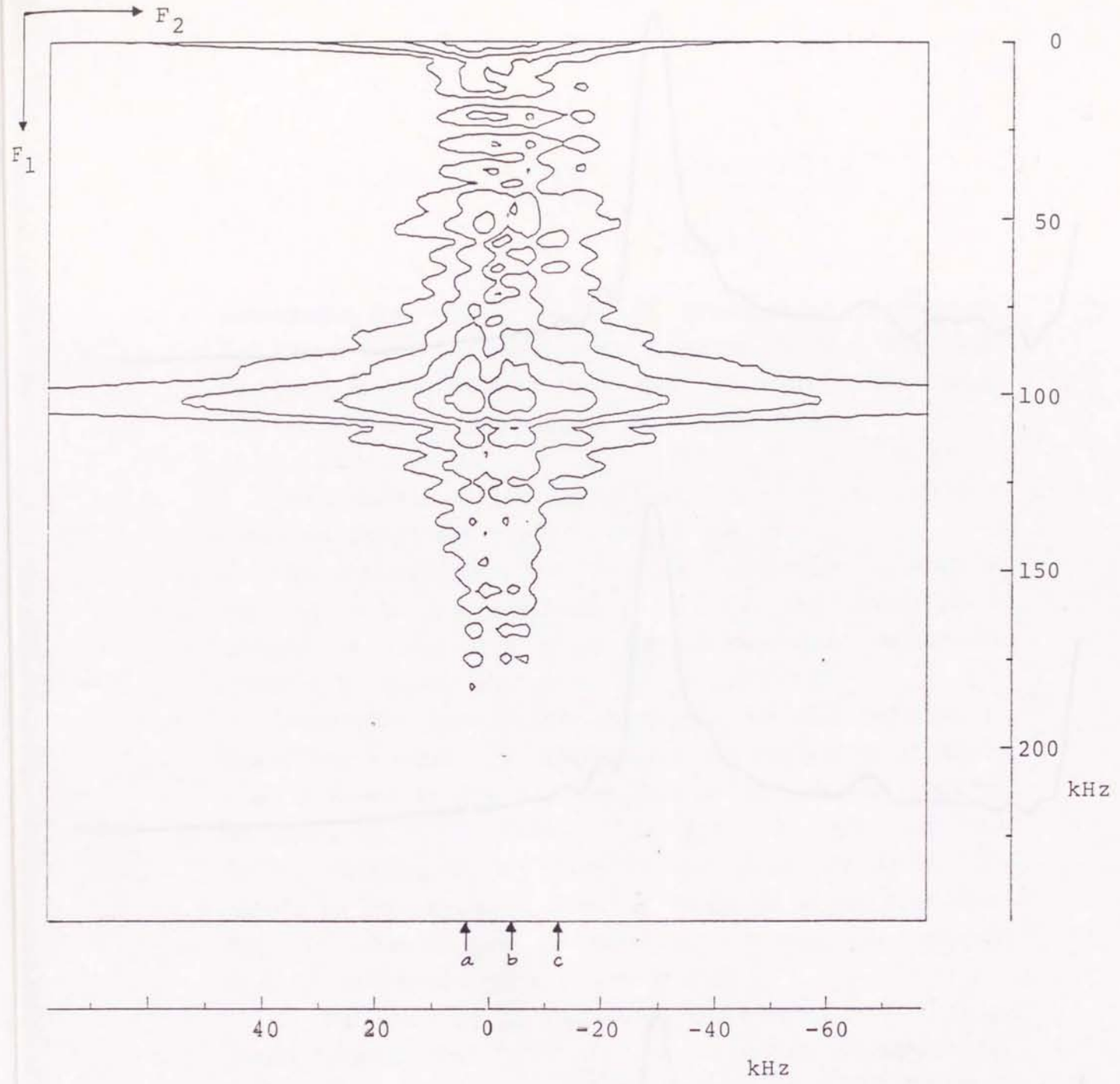

Figure 6.9

Contour plot of 2D nutation spectrum of Na_2SeO_3 at room temperature.

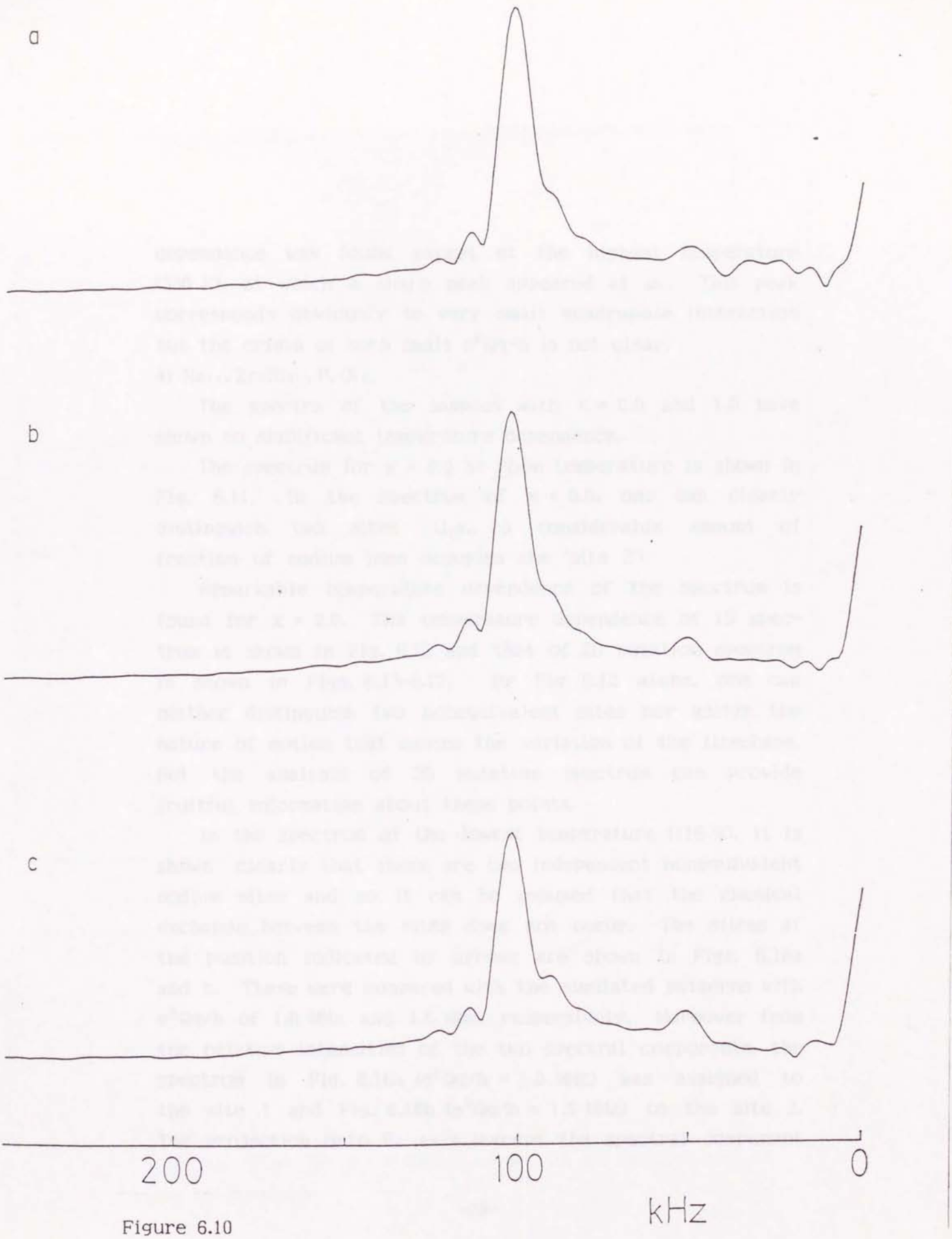

Figure 6.10

The slices of the spectrum at the positions marked by arrows in Fig. 6.9.

dependence was found except at the highest temperature (330 K), at which a sharp peak appeared at ω_1. This peak corresponds obviously to very small quadrupole interaction but the origin of such small e^2Qq/h is not clear.

4) $Na_{1+x}Zr_2Si_{3-x}P_xO_{12}$

The spectra of the samples with x = 0.0 and 1.0 have shown no significant temperature dependence.

The spectrum for x = 0.0 at room temperature is shown in Fig. 6.11. In the spectrum of x = 0.0, one can clearly distinguish two sites (i.e., a considerable amount of fraction of sodium ions occupies the 'site 2').

Remarkable temperature dependence of the spectrum is found for x = 2.0. The temperature dependence of 1D spectrum is shown in Fig. 6.12 and that of 2D nutation spectrum is shown in Figs. 6.13-6.17. By Fig. 6.12 alone, one can neither distinguish two nonequivalent sites nor assign the nature of motion that causes the variation of the lineshape. But the analysis of 2D nutation spectrum can provide fruitful information about these points.

In the spectrum of the lowest temperature (116 K), it is shown clearly that there are two independent nonequivalent sodium sites and so it can be assumed that the chemical exchange between the sites does not occur. The slices at the position indicated by arrows are shown in Figs. 6.18a and b. These were compared with the simulated patterns with e^2Qq/h of 1.0 MHz and 1.5 MHz, respectively. Moreover from the relative intensities of the two spectral components, the spectrum in Fig. 6.18a (e^2Qq/h = 1.0 MHz) was assigned to the site 1 and Fig. 6.18b (e^2Qq/h = 1.5 MHz) to the site 2. The projection onto F_2 axis (except the spectral component

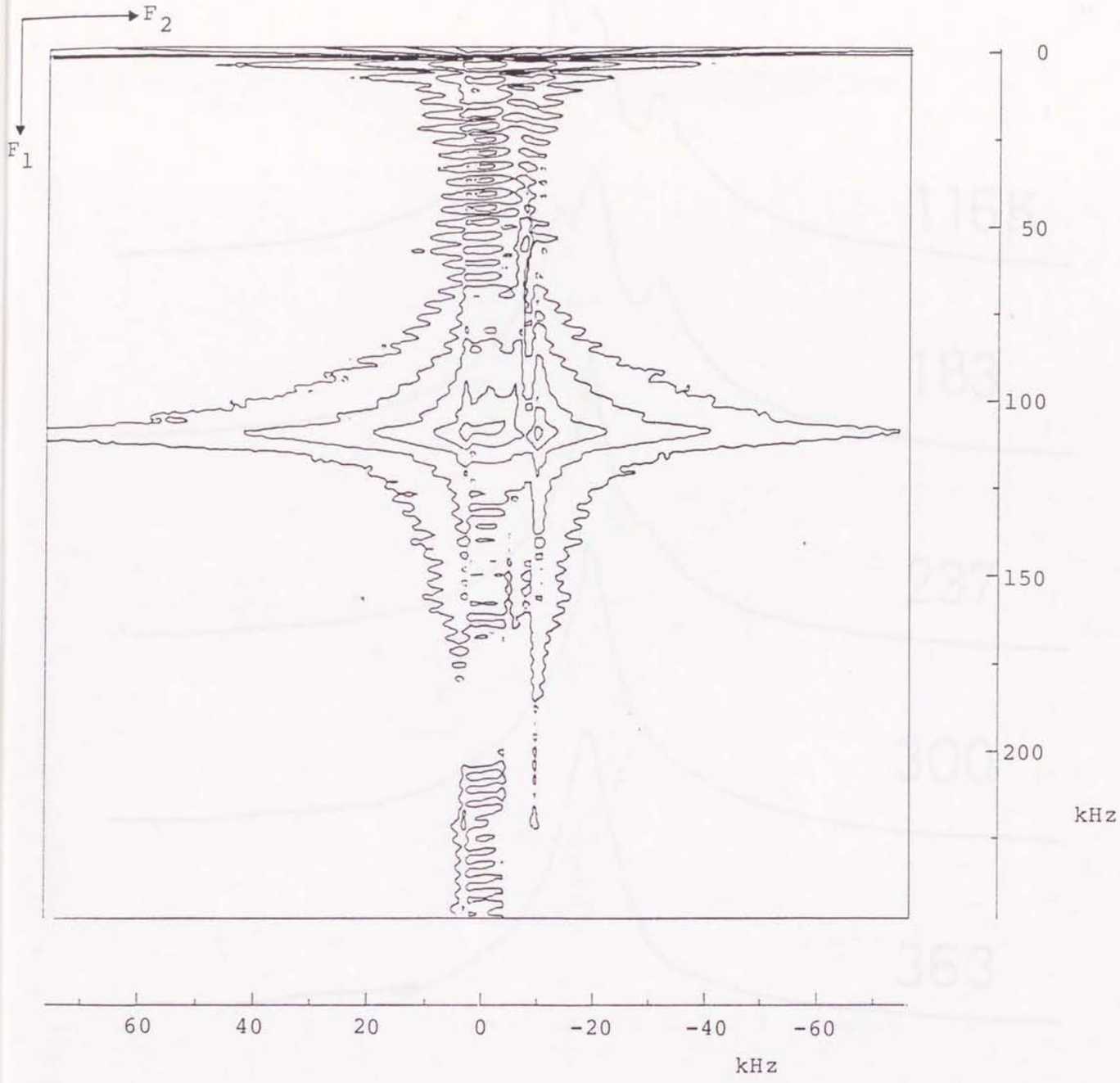

Figure 6.11

Contour plot of 2D nutation spectrum of $NaZr_2Si_3O_{12}$ at room temperature.

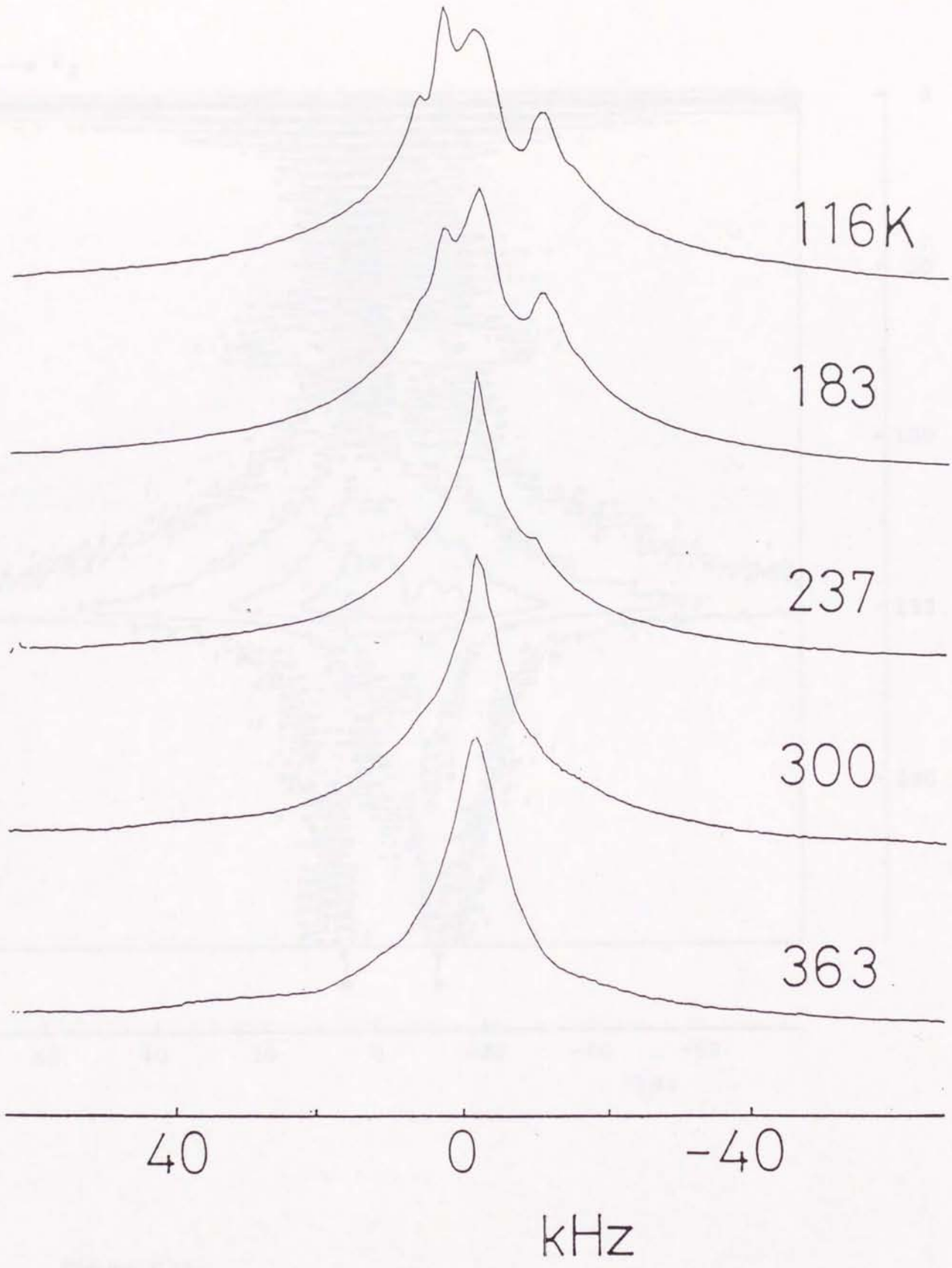

Figure 6.12

Temperature dependence of 1D spectrum of $Na_3Zr_2SiP_2O_{12}$.

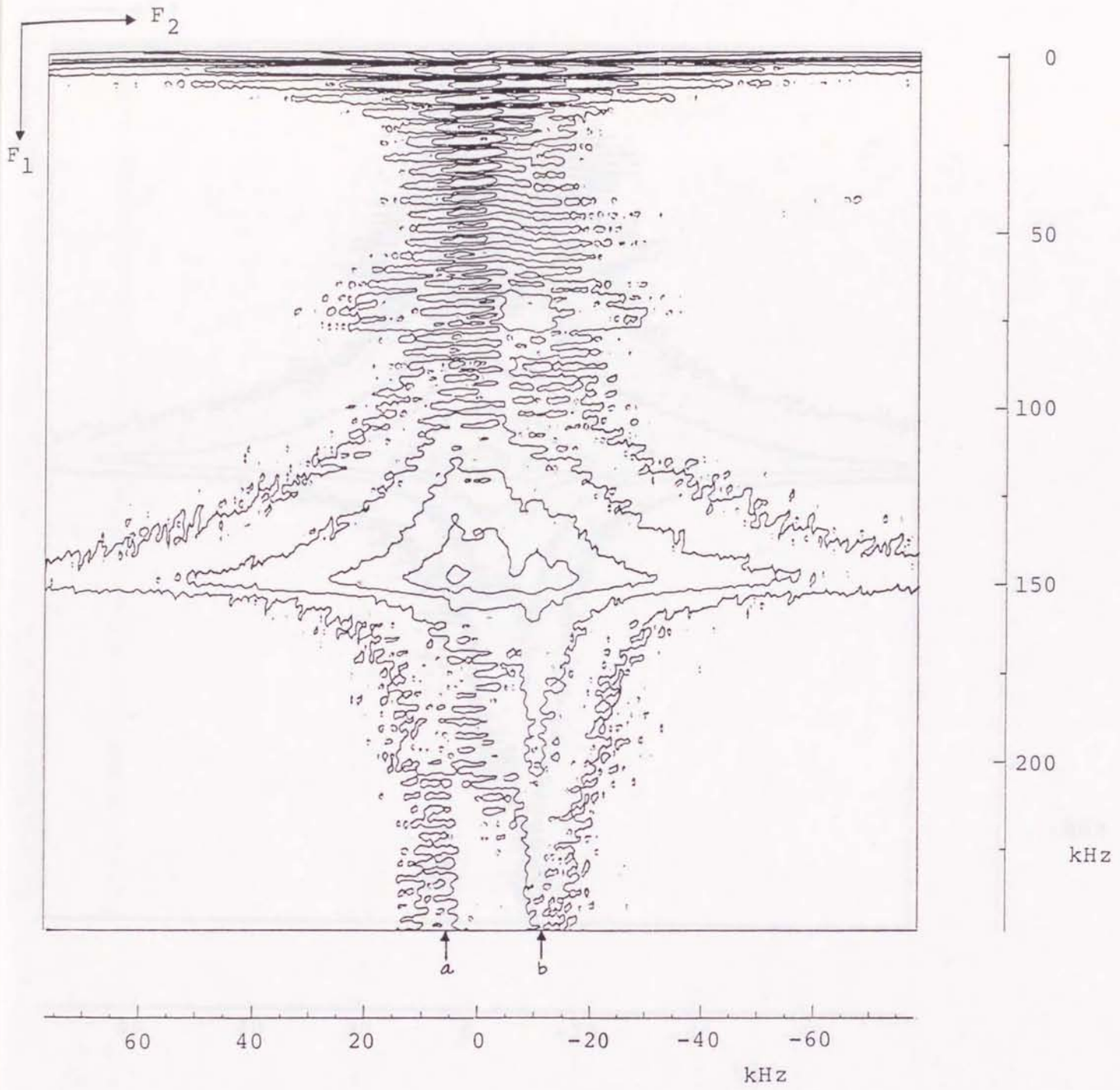

Figure 6.13

Contour plot of 2D nutation spectrum of $Na_3Zr_2SiP_2O_{12}$ at 116 K.

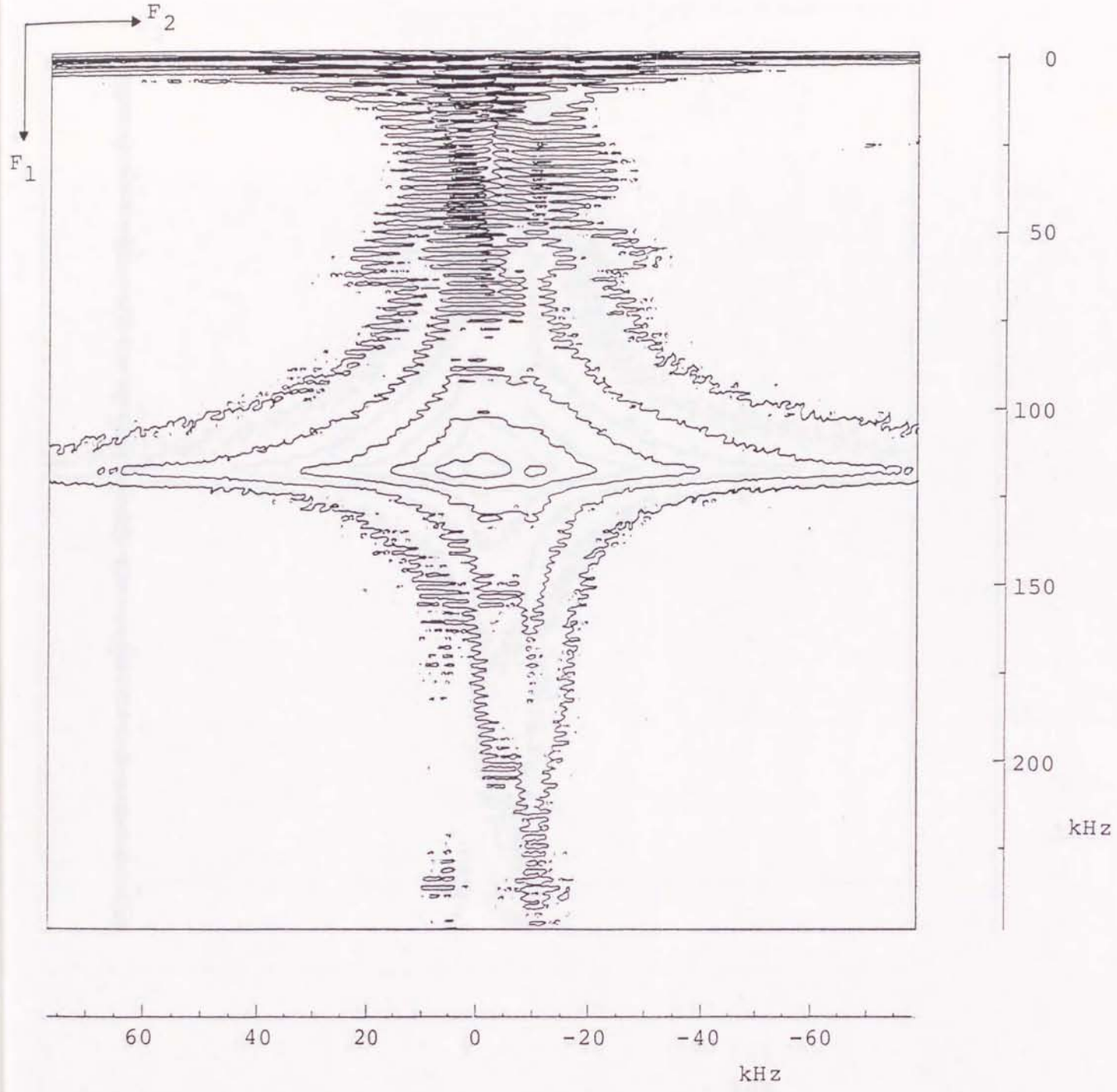

Figure 6.14

Contour plot of 2D nutation spectrum of $Na_3Zr_2SiP_2O_{12}$ at 186 K.

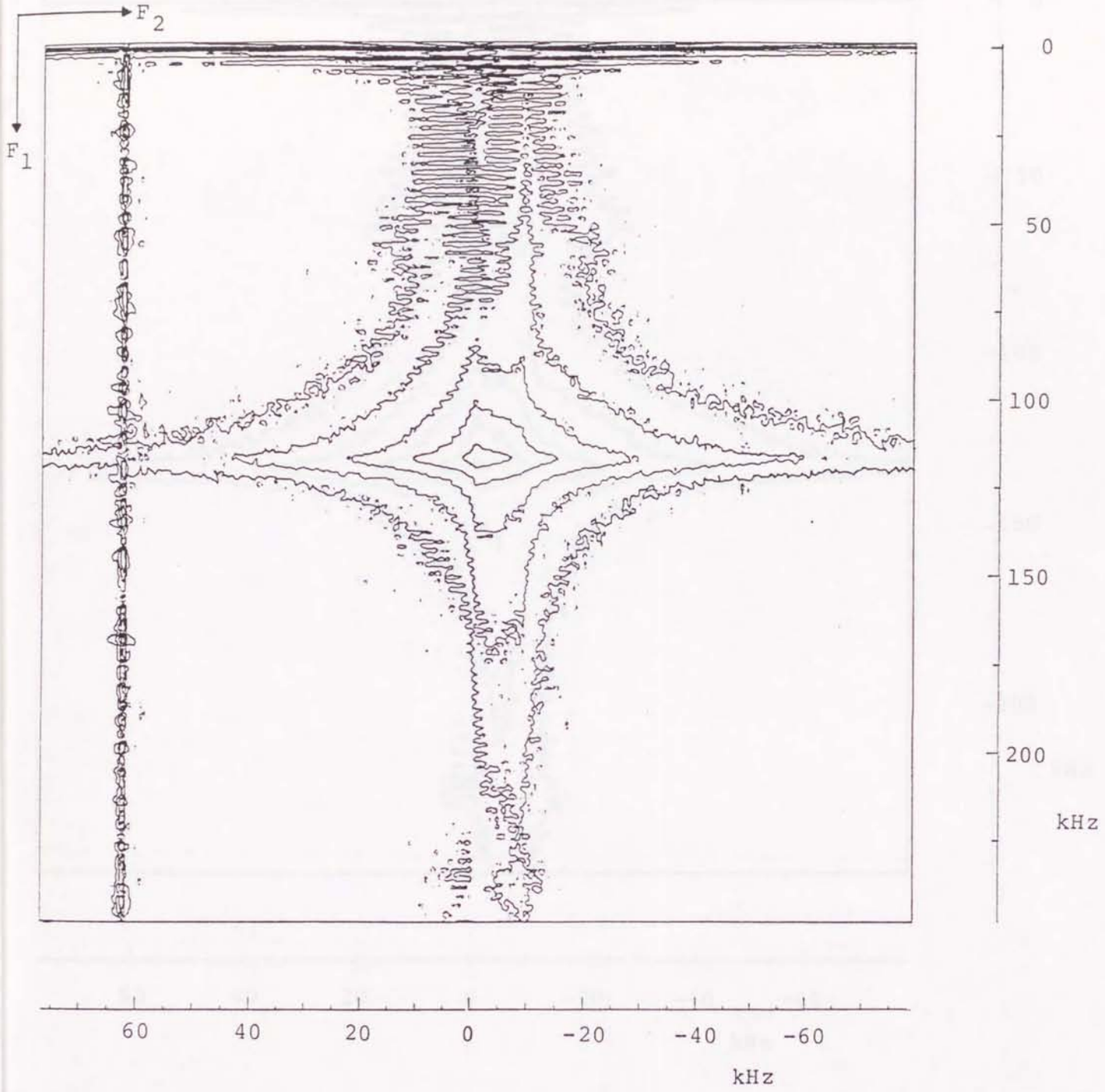

Figure 6.15

Contour plot of 2D nutation spectrum of $Na_3Zr_2SiP_2O_{12}$ at 237 K.

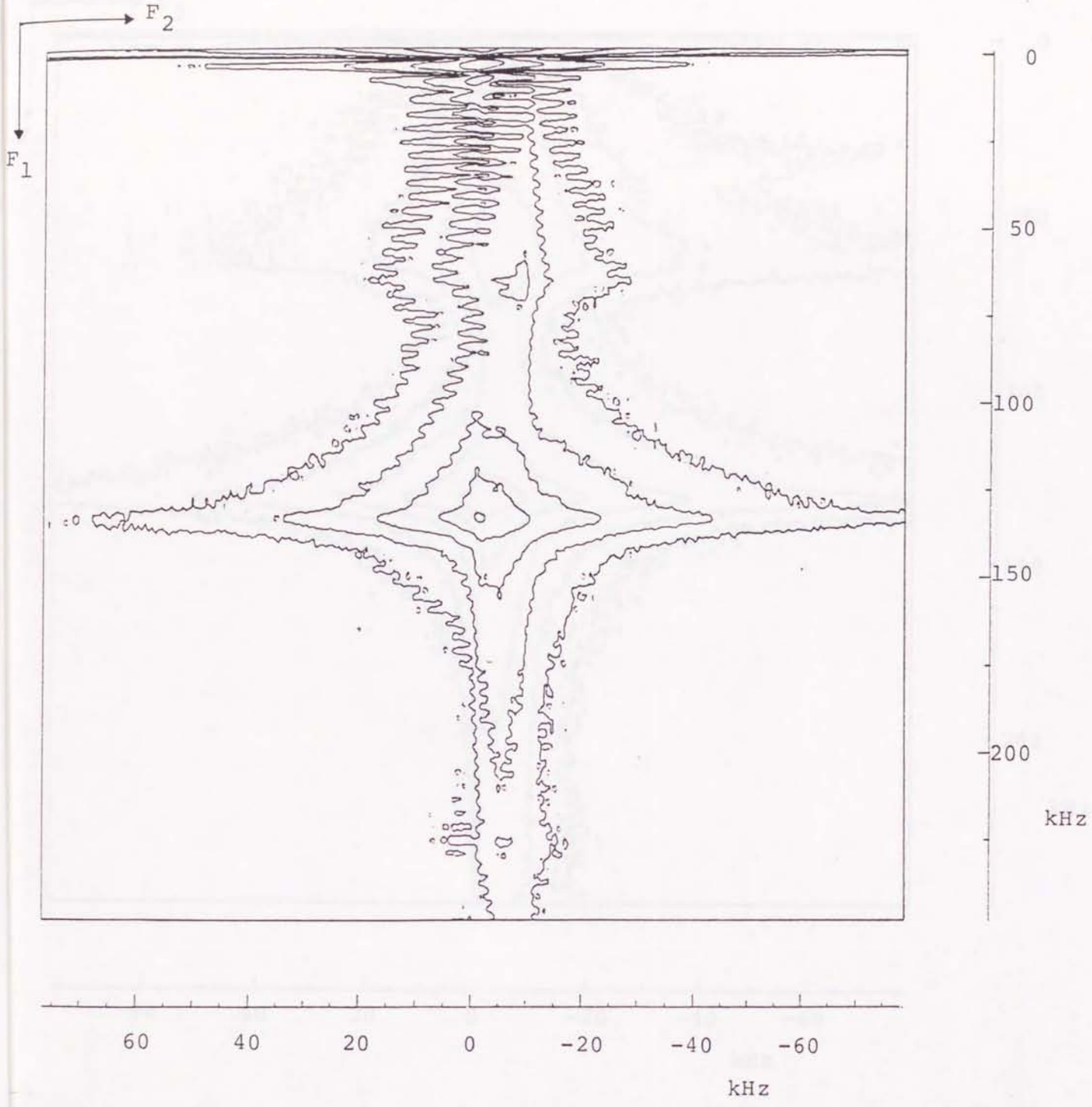

Figure 6.16

Contour plot of 2D nutation spectrum of $Na_3Zr_2SiP_2O_{12}$ at 300 K.

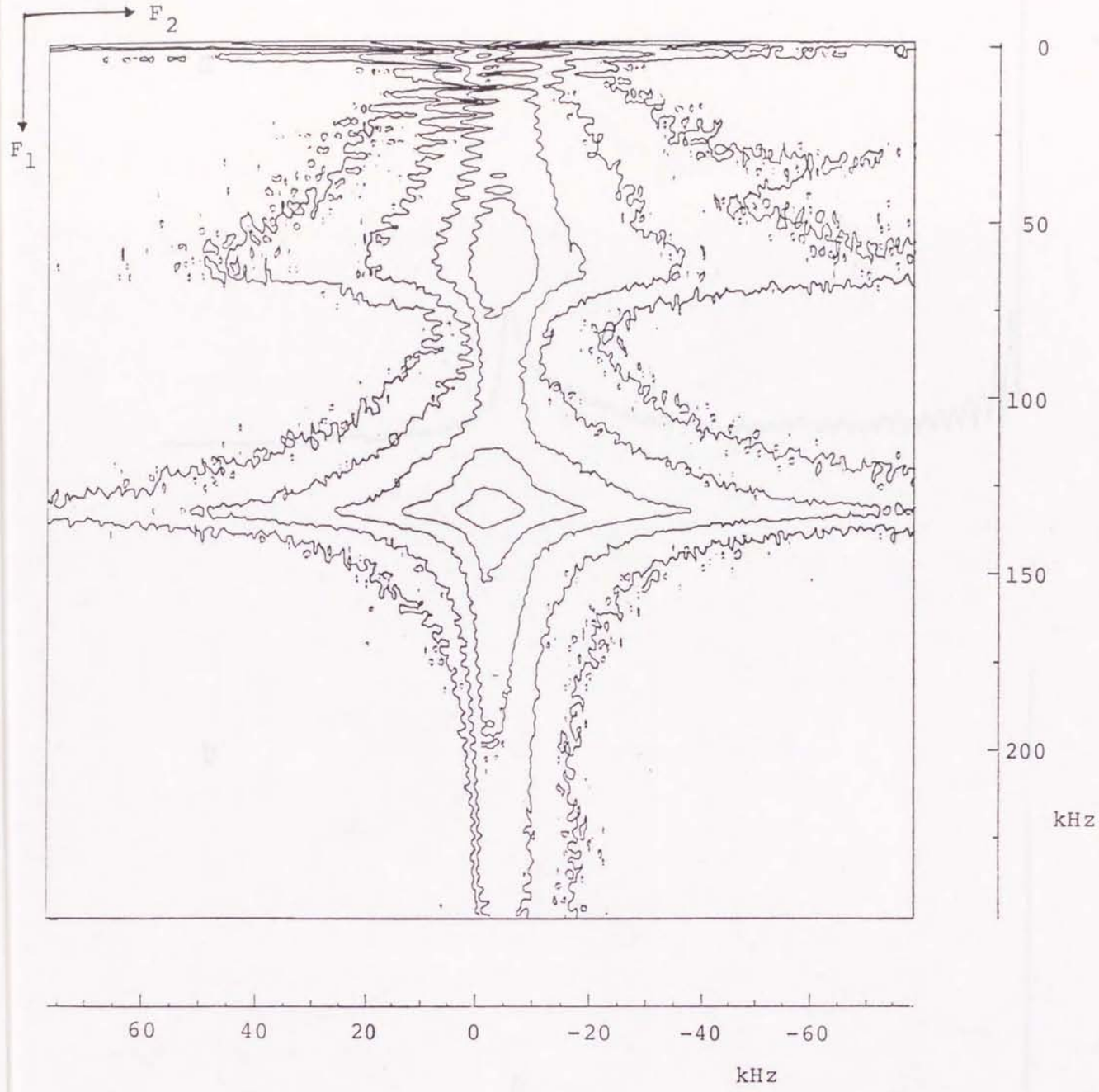

Figure 6.17

Contour plot of 2D nutation spectrum of $Na_3Zr_2SiP_2O_{12}$ at 363 K.

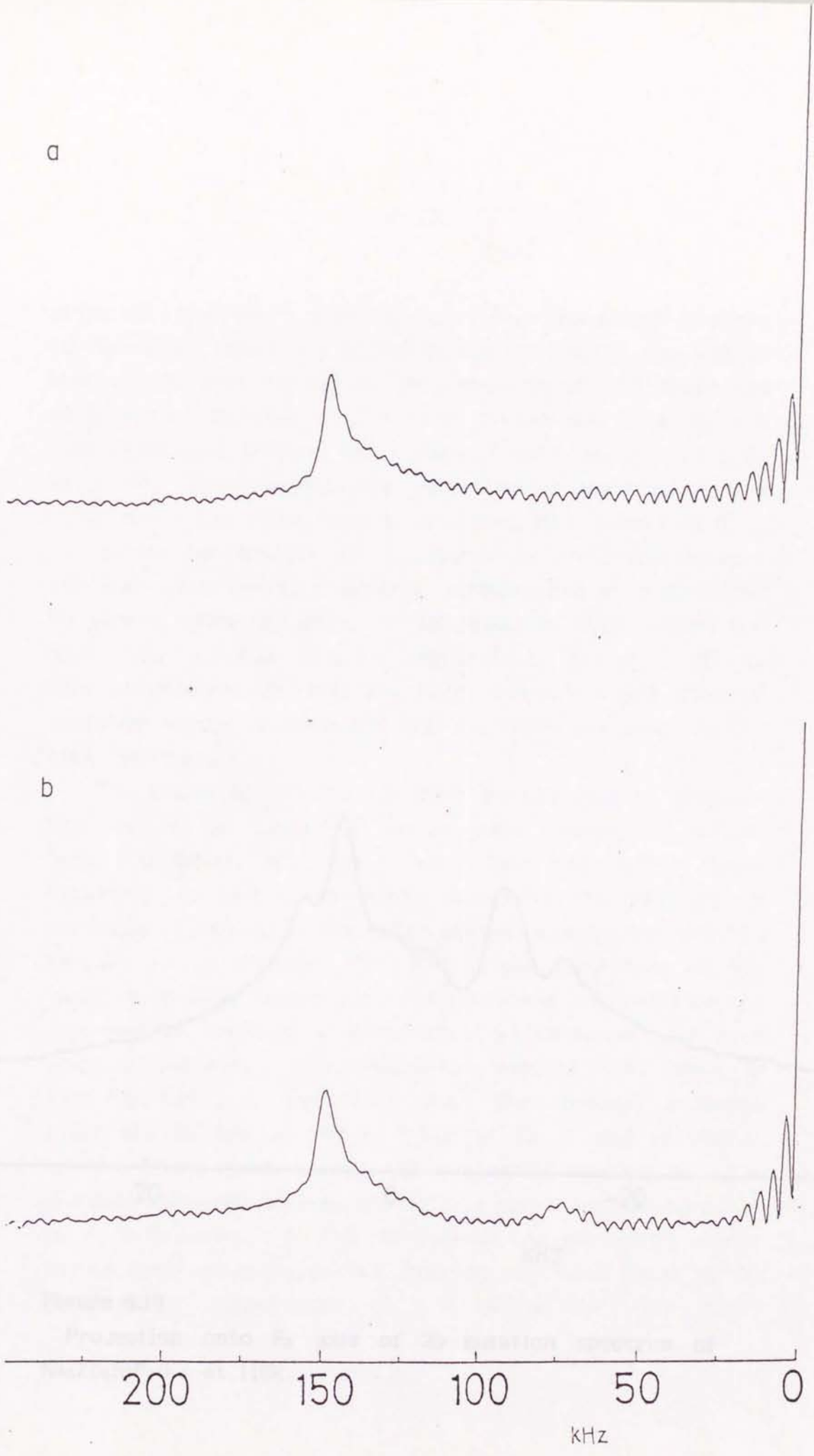

Figure 6.18

The slices at the positions marked by the arrows in Fig. 6.13.

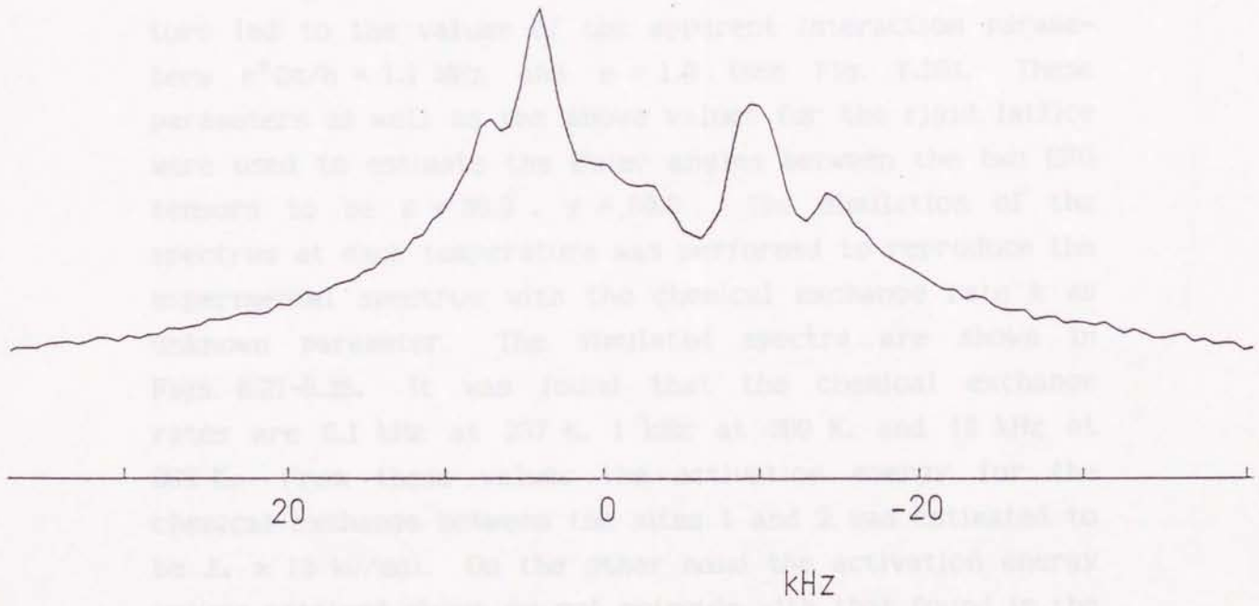

Figure 6.19

Projection onto F_2 axis of 2D nutation spectrum of $Na_3Zr_2SiP_2O_{12}$ at 116K.

appeared at around 0 frequency in the F_1 dimension) is shown in Fig. 6.19. Using the above values of e^2Qq/h the simulation of the best fitting to the experimental line shape was obtained by putting η = 0.0 (site 1) and 0.8 (site 2), and that difference between the chemical shifts at the two sites is 16 kHz. These results are supported by the crystal data : The site 1 has three fold symmetry and so η should be 0.

As the temperature was increased, the difference between the two sites became gradually unclear, and it disappeared to give a spectrum which corresponded to well defined one site case at the highest temperature (Fig. 6.17, 363 K). This phenomenon suggests strongly that the rapid chemical exchange occurs between the two nonequivalent sites at the high temperature.

The simulation of the spectrum at the highest temperature led to the values of the apparent interaction parameters e^2Qq/h = 1.1 MHz and η = 1.0 (see Fig. 6.20). These parameters as well as the above values for the rigid lattice were used to estimate the Euler angles between the two EFG tensors to be β = 30.0 , γ = 60.0 . The simulation of the spectrum at each temperature was performed to reproduce the experimental spectrum with the chemical exchange rate k as unknown parameter. The simulated spectra are shown in Figs. 6.21-6.25. It was found that the chemical exchange rates are 0.1 kHz at 237 K, 1 kHz at 300 K, and 10 kHz at 363 K. From these values the activation energy for the chemical exchange between the sites 1 and 2 was estimated to be $E_a \simeq$ 13 kJ/mol. On the other hand the activation energy values obtained above do not coincide with that found in the conductivity measurement ($E_a \simeq$ 31 kJ/mol) [2]. The large

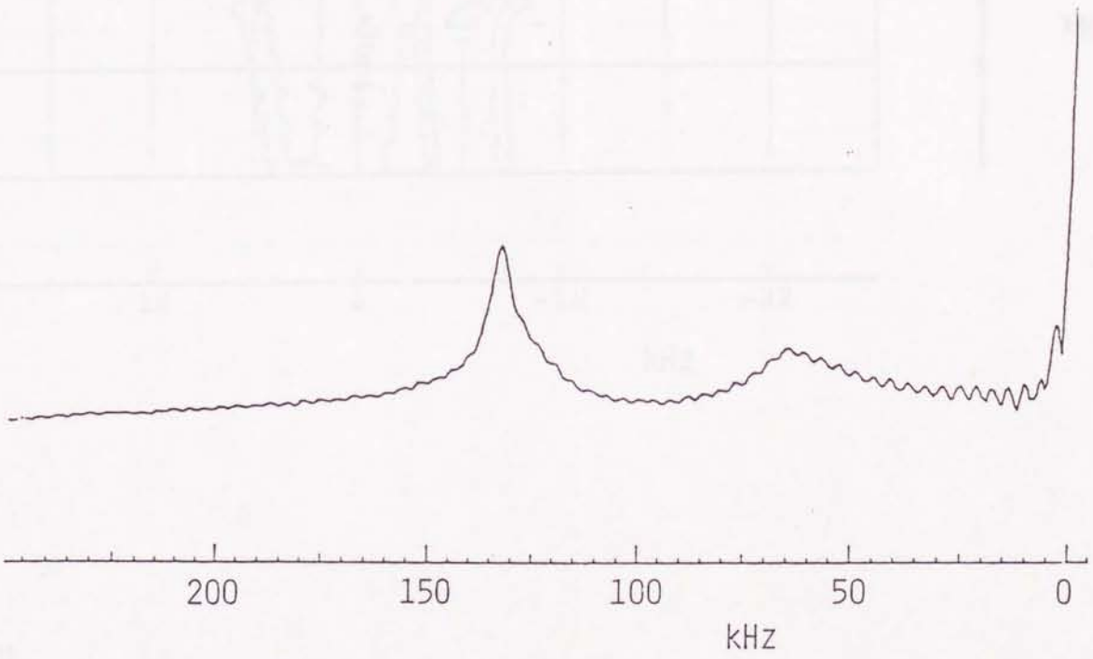

Figure 6.20

Projection onto F_1 axis of 2D nutation spectrum of $Na_3Zr_2SiP_2O_{12}$ at 363K.

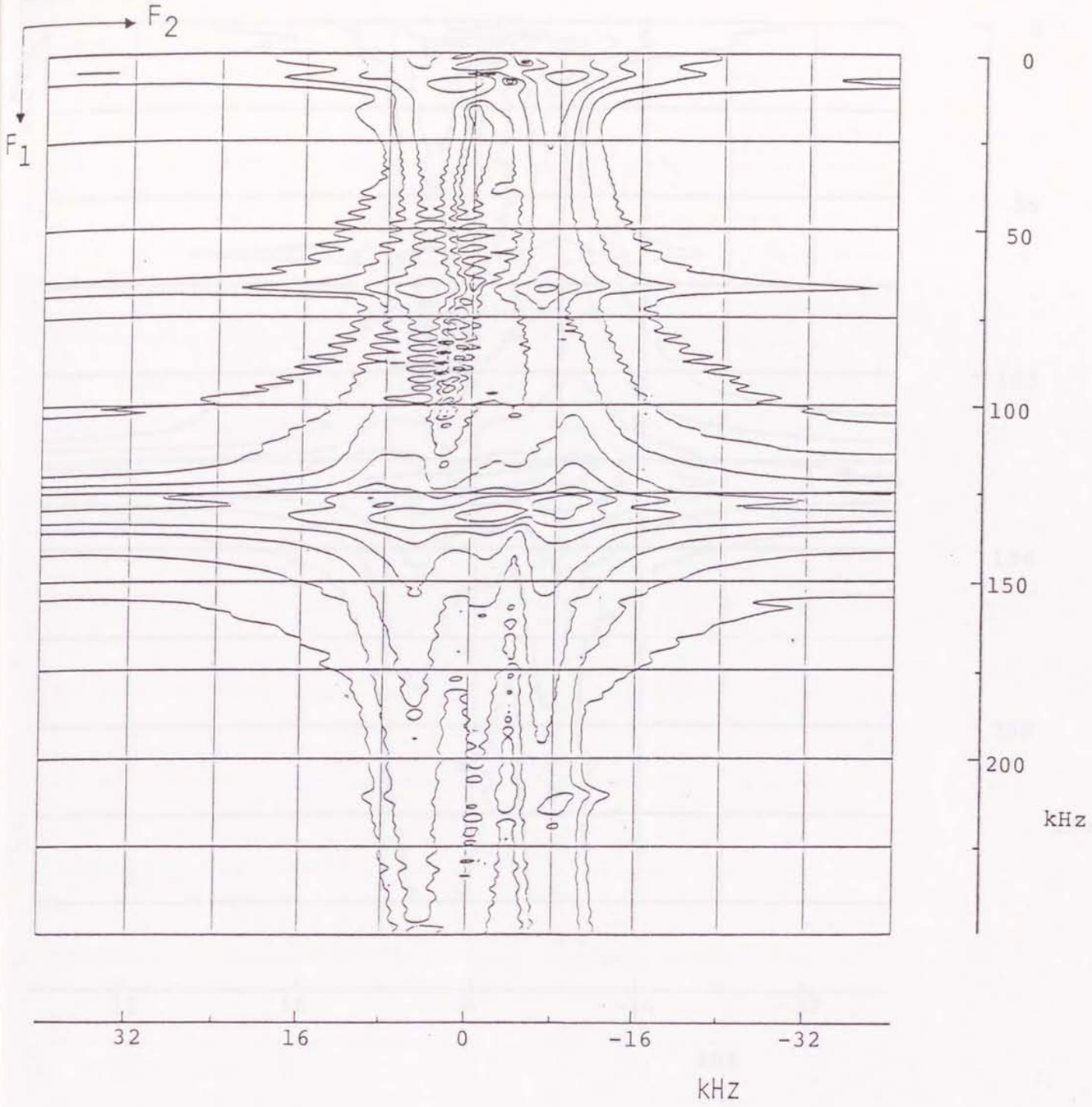

Figure 6.21

Contour plot of 2D nutation spectrum simulated with chemical exchange rate k = 0.001 kHz. Other parameters are described in the text.

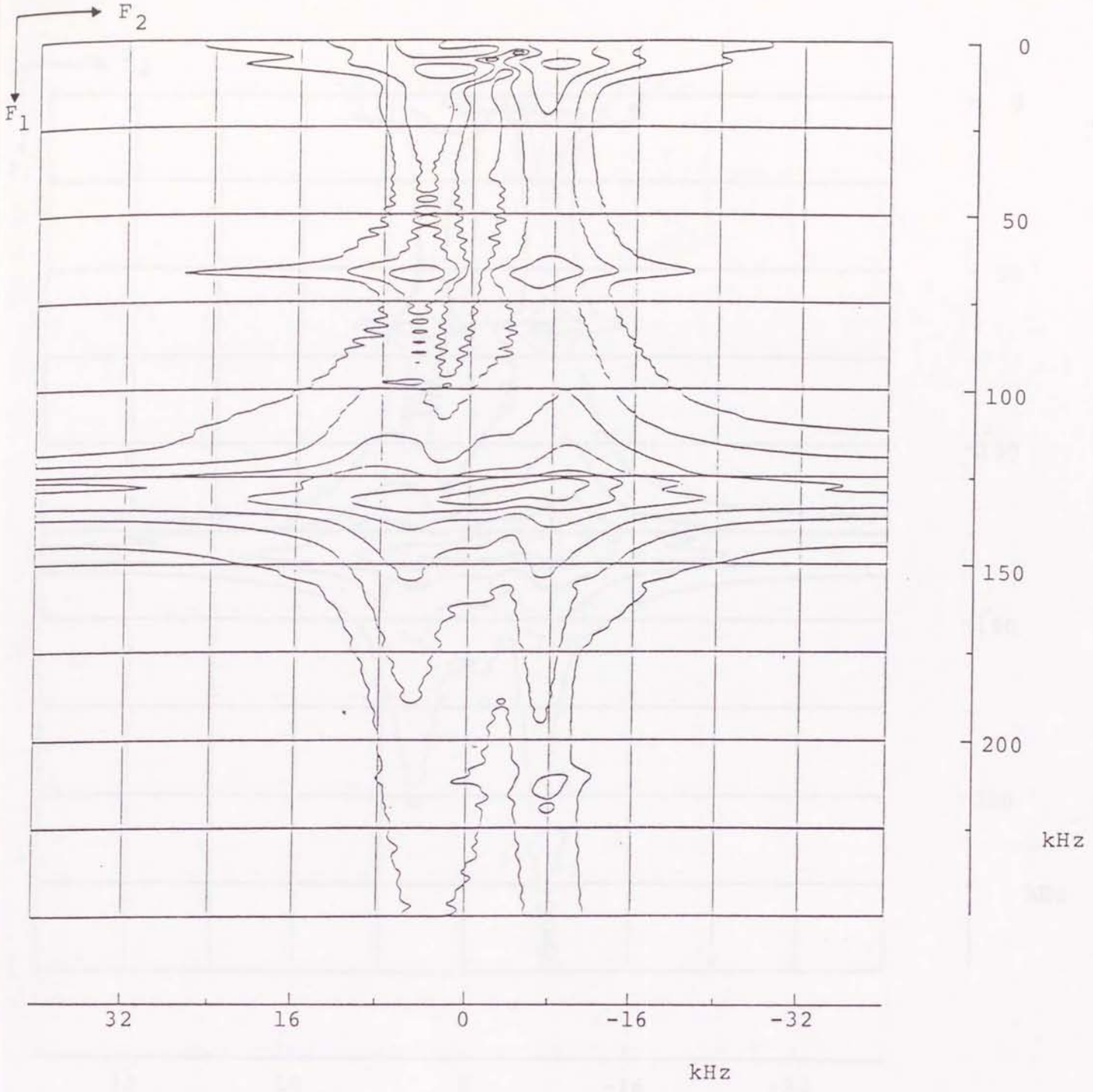

Figure 6.22

Contour plot of 2D nutation spectrum simulated with chemical exchange rate k = 0.01 kHz.

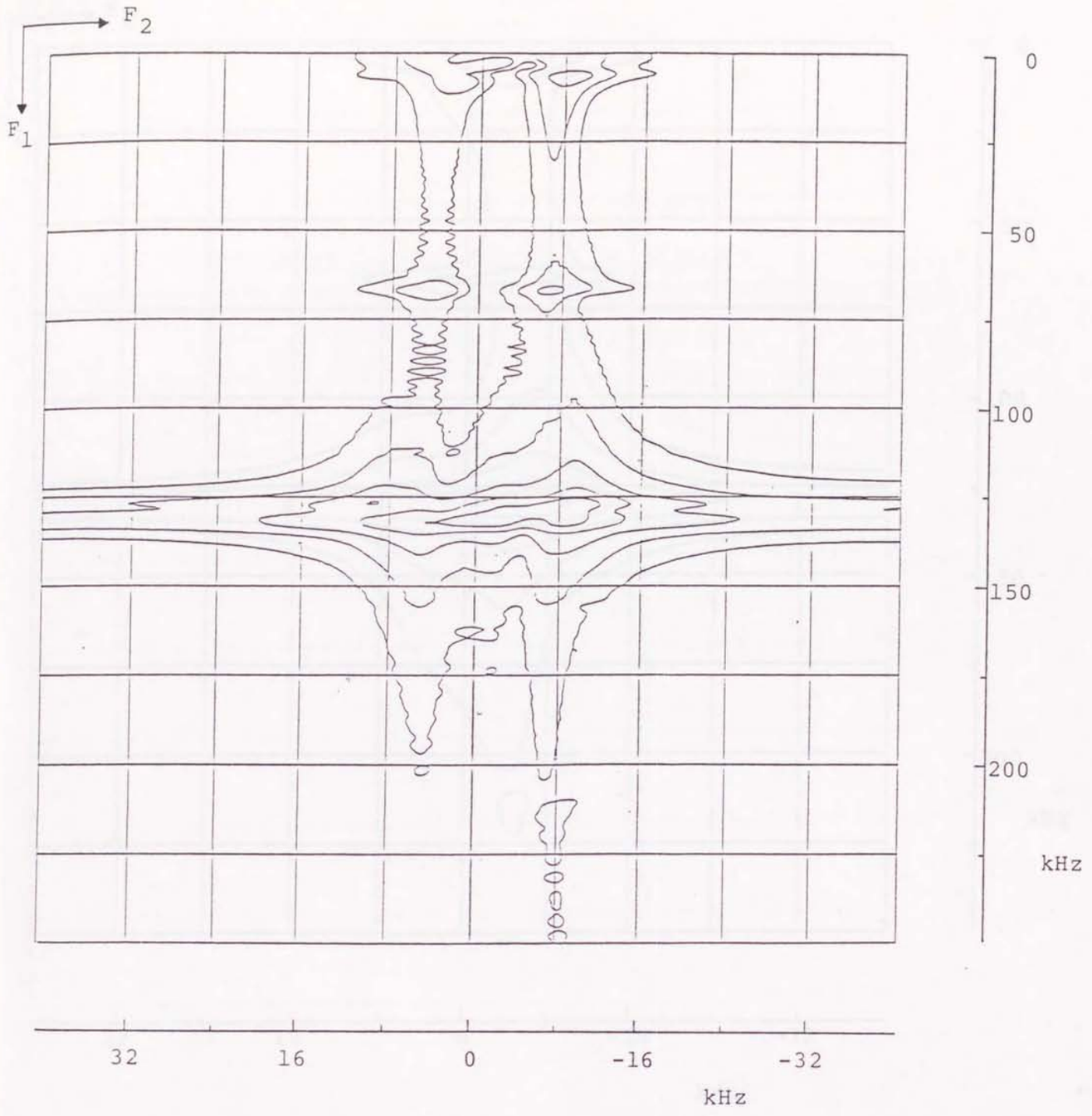

Figure 6.23

Contour plot of 2D nutation spectrum simulated with chemical exchange rate k = 0.1 kHz.

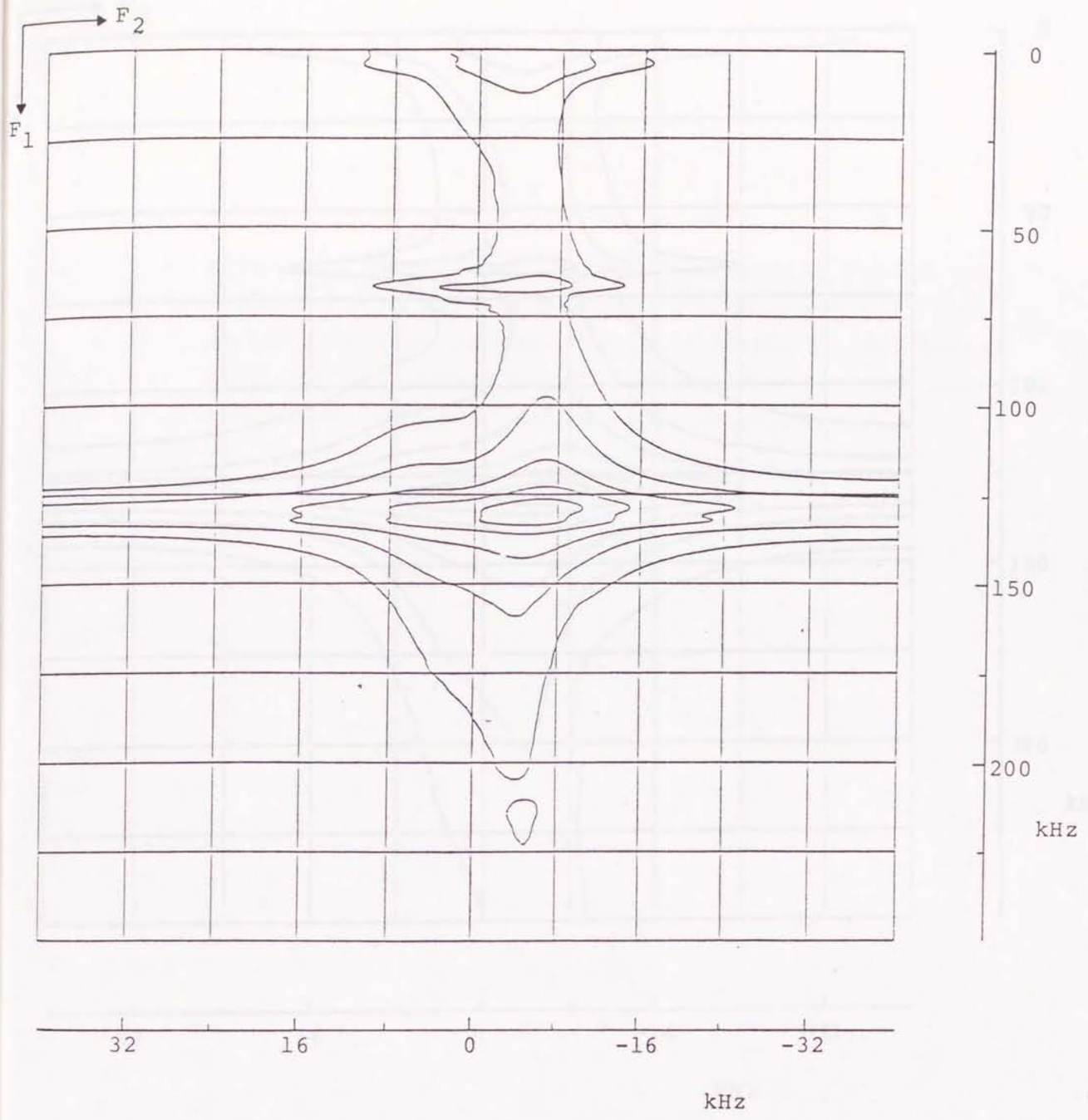

Figure 6.24

Contour plot of 2D nutation spectrum simulated with chemical exchange rate k = 1.0 kHz.

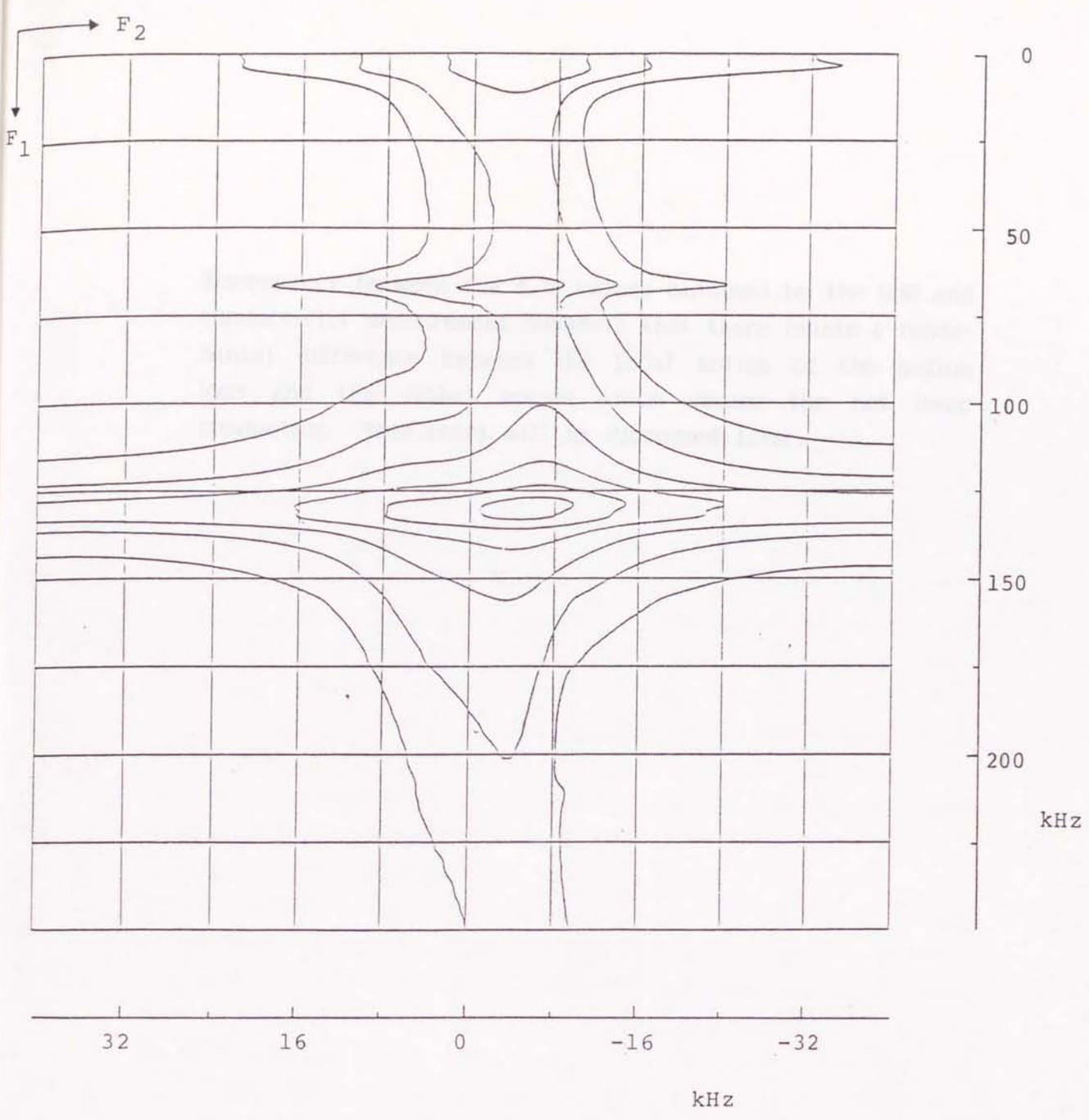

Figure 6.25

Contour plot of 2D nutation spectrum simulated with chemical exchange rate k = 10 kHz.

discrepancy between the E_a's values obtained by the NMR and conductivity measurement suggests that there exists a fundamental difference between the local motion of the sodium ions and the global motion which causes the net ionic conduction. This point will be discussed later.

References

[1] Landolt-Börnstein Tavellen, New Series, Group III, Vol 20a.

[2] J.B. Goodenough, H.Y-P. Hong, and J.A. Kafalas, *Mat. Res. Bull.*, 11, 203 (1976).

7. Discussion

7.1 Summary of the Present Work

So far in the previous Chapters a new theoretical method to describe the evolution of the quadrupolar spin system under the influence of strong rf field was established. This method is based on the Liouville representation and is superior in the following points to the other methods previously developed :

1. It is easy to construct the theoretical expression for the complex interaction between the spin system and the rf field and so can be easily extended to the system with spin higher than 3/2.
2. Although the dimension of the matrix to be determined is far larger than that based on other standard methods, the formalism with the Liouvillian can be coded by computer language(s) and therefore is much suitable for the computation by a big computer.
3. Liouville representation has a form which can incorporate effects other than spin interaction in a straightforward manner. This property makes it possible to apply the nutation method to chemically exchanging system.

The new method was coded by FORTRAN to prepare the general simulation program which is necessary for analyzing the experimental 2D nutation spectra. The program can be applied to quadrupolar nuclei with spin numbers 3/2 ~ 9/2 and to systems with and without chemical exchange.

The 2D nutation NMR experiments were conducted for ^{23}Na species involved in several compounds :

1. The ^{23}Na resonances in $NaNO_2$ and $NaHgCl_3.2H_2O$ were used to establish the optimal experimental conditions for the 2D

nutation spectra and to evaluate the sensitivity of the spectra to the quadrupole interaction parameters, e^2Qq/h and η.

2. The ^{23}Na nutation NMR was applied to Na_2SeO_3 to distinguish the three crystallographically nonequivalent Na sites in this compound. The value e^2Qq/h at the individual sites could be determined and also η was estimated for two of the three sites in this material.

3. The ^{23}Na 2D nutation NMR was used to examine the dynamic process of $Na_{1+x}Zr_2Si_xP_{3-x}O_{12}$. The spectrum was remarkably temperature dependent and by applying the new theoretical method for the chemically exchanging system to it the chemical exchange rate of Na ions between two nonequivalent sites was estimated at each temperature. It was found that the activation energy deduced from the nutation spectra differs significantly from that determined by a previous conductivity measurement.

In the course of this work a number of problems have been encountered concerning the practice of the 2D nutation NMR. In what follows I will discuss the applicability, advantage and/or disadvantage of the 2D nutation NMR newly developed in the present work.

7.2 2D Nutation NMR

Nuclear quadrupole interaction can provide a lot of useful information on the static and dynamic structures of crystalline materials. In the case that e^2Qq/h is larger than about 1 MHz, the pure quadrupole resonance can be applied to determine the quadrupole interaction parameters. When e^2Qq/h is much smaller than $\sim$ 100 kHz, the conventional NMR is used to detect the quadrupole-perturbed spectra either on single crystal or powdered specimen.

Many of chemically interesting nuclei such as ^{23}Na, ^{27}Al, ^{39}K, ^{59}Co , etc. give often e^2Qq/h of the magnitude between ca. 100 kHz and a few MHz region. In such a frequency region it is extremely difficult to apply the above two methods because of the limitation on the sensitivity and/or band width of the radio-frequency spectrometers. Moreover when a number of crystallographically nonequivalent sites exist for the nuclei of interest, it is usually almost impossible to analyze the complex spectra even if the second order quadrupole interaction could be detected.

It was shown in a preceding Chapter that the 2D nutation NMR can successfully be applied to such cases. Since the strength of the rf pulse usually available is 100 kHz at most, it means that this method can be applied to determine the quadrupole coupling constant $\Omega_Q/2\pi$ up to about 1 MHz.

Most remarkable feature of the nutation NMR method lies in the fact that if a strong rf field can be used and if the condition H_D, $H_{cs} \ll H_{rf}$ holds, undesirable line broadening effect due to H_D and H_{cs} along the F_1 axis is dramatically reduced. (In the usual 1D spectrum which corresponds to the F_2 direction, the line broadening due to other interactions

can not be eliminated.) In this way, detailed information on the quadrupole interaction can be derived from the nutation spectrum.

Another advantage of the nutation NMR is found in its simple setting of the experiment as having been demonstrated in Chap. 5.

A special use of the nutation method is, as pointed out [1], the determination of relative orientation between the EFG and the other interaction tensors. It is possible if the dominant interaction in the detection period, t_2, is other than the second order quadrupole interaction. For example, if the static magnetic field is considerably high the line width due to the chemical shift extends over wide frequency range and may dominate the second order quadrupole interaction. In such case, the spectra developed onto F_1 and F_2 axes contain the information mainly on the quadrupole and chemical shift interaction, respectively, and the correlation between them allows to determine the angles between tensors of both interactions.

However, several effects are found to deform the spectrum. These are discussed below.

a) Peak near 0 in F_1

When an off-resonant rf pulse is applied, i.e. when Larmor frequency in the absence of quadrupole interaction does not coincide with the rf frequency, there must appear a peak at zero frequency. This can be explained as follows in the case of $I = 1/2$ for simplicity. If the offset between the rf frequency and the Larmor frequency is $\Delta\omega$, the signal at the end of the pulse becomes

$$S(t) \propto [\alpha(1-\cos 2\Omega t)+i\beta \sin 2\Omega t)] \ , \qquad (7.2.1)$$

where

$$\Omega = \sqrt{\Delta\omega^2+\omega_1{}^2} \ ,$$
$$\alpha = \omega_1 \Delta\omega/\Omega^2 \ ,$$
$$\beta = \omega_1 /2\Omega \ . \qquad (7.2.2)$$

Since $\Delta\omega \neq 0$, α does not vanish and the term independent of time generates the peak at 0 frequency. Also the cosine term survives and this results in the phase modulation along F_1 which will cause the distortion of the spectrum. Then it is desirable to minimize the resonance offset as long as possible. But when the inhomogeneity of the external magnetic field and/or dipole interaction between the spins are significant, this effect cannot be eliminated perfectly.

Another cause of central peak is the effect of the second order quadrupole shift during the evolution period which has been neglected in the theoretical formulation. The nutation spectrum including these effects is shown in Fig. 7.1. The greater the quadrupole interaction, the greater the intensity of the central peak.

b) Line Broadening

Another undesirable effect in the nutation NMR is caused by the inhomogeneity of the rf field in space. This cannot be avoided in the use of the solenoid of the finite length : The rf magnetic field is strongest at the middle of the coil and decreases to some extent at the ends of it. [2] This brings about the distribution of the ratio Ω_0/ω_1 and it causes the line broadening in F_1 dimension. Also, if the shape of the rf pulse is not rectangular (although it is

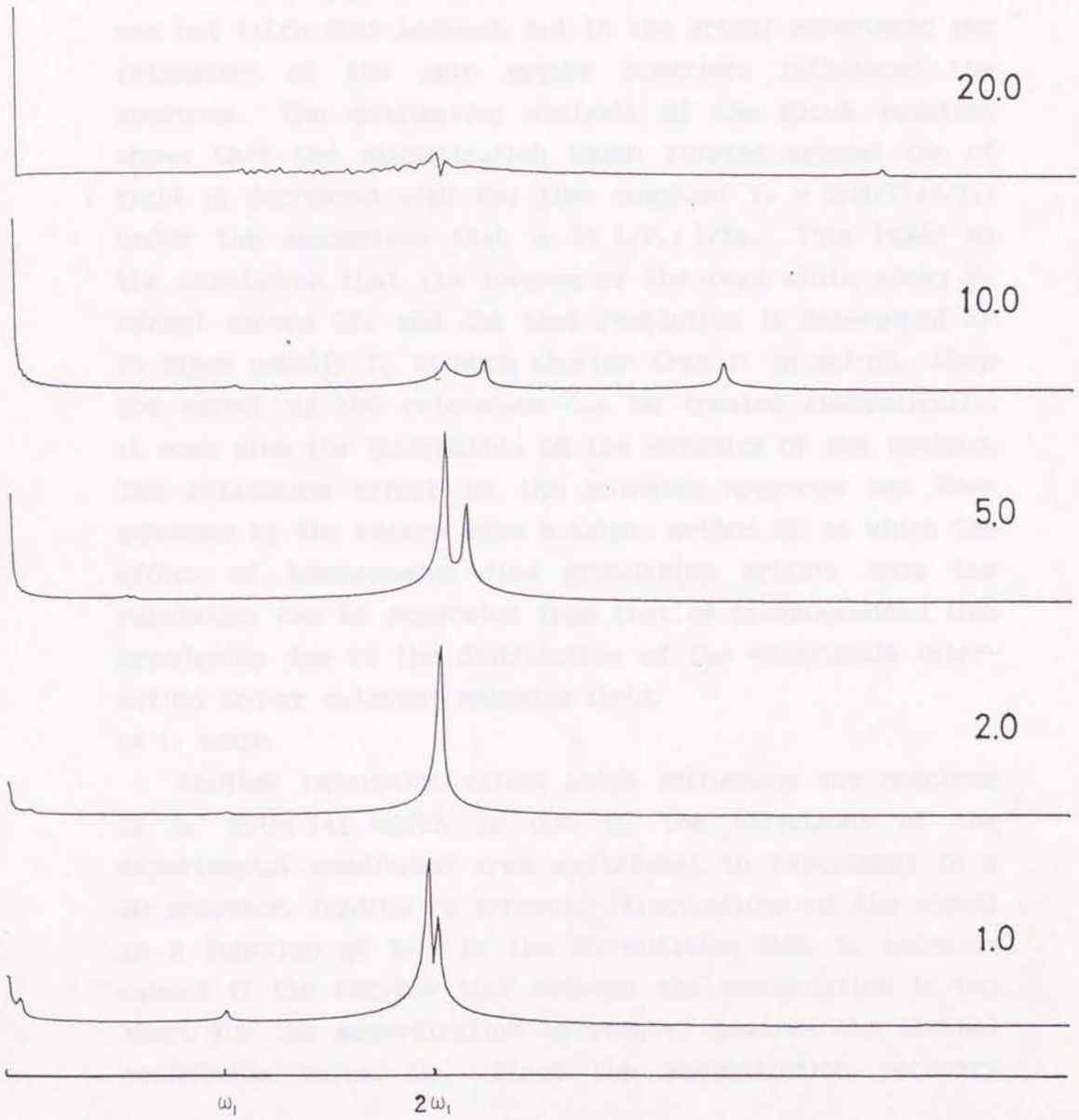

Figure 7.1

Dependence of nutation spectrum on the ratio Ω_Q/ω_1 including the second order quadrupole interaction as well as chemical shift.

assumed tacitly), it causes the spectrum to modify. The effect of the inhomogeneity in the rf field cannot be treated quantitatively.

In the discussions so far, the effect of the relaxation was not taken into account, but in the actual experiment the relaxation of the spin system sometimes influences the spectrum. The qualitative analysis of the Bloch equation shows that the magnetization which nutates around the rf field is decreased with the time constant $T_n = 2/(1/T_1+1/T_2)$ under the assumption that $\omega_1 \gg 1/T_1, 1/T_2$. This leads to the conclusion that the inverse of the peak width along F_1 cannot exceed $2T_2$ and the best resolution is determined by T_2 since usually T_2 is much shorter than T_1 in solids. When the effect of the relaxation can be treated theoretically, it must give the information on the dynamics of the nucleus. The relaxation effect on the nutation spectrum has been examined by the rotary echo nutation method [3] in which the effect of homogeneous line broadening arising from the relaxation can be separated from that of inhomogeneous line broadening due to the distribution of the quadrupole interaction and/or external magnetic field.

c) t_1 noise

Another relaxation effect which influences the spectrum is t_1 noise [4] which is due to the variations of the experimental conditions from experiment to experiment in a 2D sequence, leading to irregular fluctuations of the signal as a function of t_1. In the 2D nutation NMR, t_1 noise is caused if the recycle time between the accumulation is too short for the magnetization to recover towards the thermal equilibrium value, M_0. Since the magnetization recovery

depends on t_1 (and the recycle time) the peaks at $2\omega_1$, $3\omega_1$, $\cdots$ appears in the nutation spectrum.

7.3 Chemical Exchange Effect

As already demonstrated in a previous Chapter, the 2D nutation NMR gives its full ability in the situation where the spectrum arises from several nonequivalent sites. Often the signals corresponding to them overlap with each other and it is very difficult to decide which peak corresponds to each site. While by the use of 2D nutation NMR one can easily distinguish each site according to the difference of the strength of quadrupole interaction.

It was shown theoretically and experimentally that the nutation spectrum is drastically changed when the chemical exchange of the resonant nuclear species is excited. The detailed analysis of the spectrum brings about the quantitative information of the mechanism of the chemical exchange. Especially when slow and fast limits of the spectra can be obtained, one can determine the relative orientation of the EFG tensors as well as the rate constant of the exchange. Thus the method can be used to examine the mechanism of chemical exchange, ionic conduction, and/or solid state reaction from the microscopic point of view.

In Chap. 6 it was pointed out for $Na_{1+x}Zr_2Si_xP_{3-x}O_{12}$ that the activation energy for the sodium exchange was estimated from the 2D nutation NMR experiment to be 13 kJ/mol and that this value was very small compared with 31 kJ/mol deduced from a previous conductivity measurement. The most simple model for ionic conduction is based on the classical hopping mechanism through successive nearest-neighbor sites. In such a model conductivity measurement and NMR should give the same activation energy and jump rate. Serious discrepancies as was found above are often

encountered. [5] In the case that the ion transport occurs through the hopping between two or more nonequivalent ionic sites as was found in $Na_{1+x}Zr_2Si_xP_{3-x}O_{12}$, the discrepancy between the activation energies determined by different techniques can qualitatively interpreted. Consider an ion transport through a potential shown in Fig. 7.2. As the potentials at sites 1 and 2 are largely different one ion can jump easily from 'site 2' to 'site 1' but the opposite is much difficult. If the neighboring 'site 1' is initially occupied, the ion will hop back and forth between the nearest sites until one of the other 'site 1' happens to become empty. The repetition of such local motion does not contribute to the net conductivity whereas it affects the NMR spectrum. The exchange and conduction of the sodium ions in $Na_{1+x}Zr_2Si_xP_{3-x}O_{12}$ are considered to apply to such a model. The 2D nutation NMR mothod looks at the rapid local motion with an average activation energy while the ion transport experiment measures an energy which is the sum of the activation energy for the jump and the energy for the vacancy formation at the 'site 1'. This idea enables one also to interpret the experimental results that the activation energy obtained from conductivity measurement is independent of the composition (x) while that from NMR is strongly dependent on x. (When x = 2 the frequent jump between the sites 1 and 2 was observed as mentioned before but no sodium jump was recognized in the specimens with x = 0 and 2. In the latter two samples the activation energies for the sodium exchange appear to be infinity.)

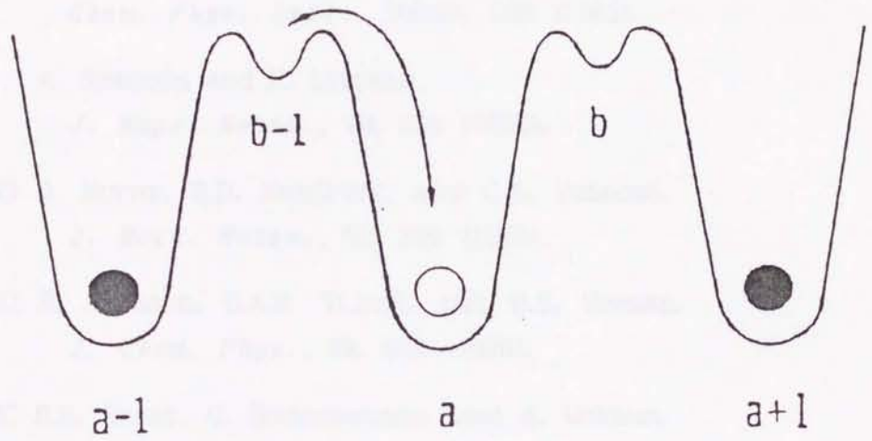

Figure 7.2
Nonequivalent site model with deep and shallow wells.

References

[1] A. Samoson and E. Lippmaa,
Chem. Phys. Lett., **100**(3), 205 (1983).

A. Samoson and E. Lippmaa,
J. Magn. Reson., **79**, 255 (1988).

[2] D. Horne, R.D. Kendrick, and C.S. Yannoni,
J. Magn. Reson., **52**, 299 (1983).

[3] R. Janssen, G.A.H. Tijink, and W.S. Veeman,
J. Chem. Phys., **88**, 518 (1988).

[4] R.R. Ernst, G. Bodenhausen, and A. Wokaun,
Principles of Nuclear Magnetic Resonance in One and Two Dimensions, Oxford Press, 1987.

[5] P.M. Richards,
Physics of Superionic Conductors, Chap. 6,
ed. by M.B. Salamon, Springer-Verlag, 1979.

Line# Source Line Microsoft FORTRAN Optimizing Compiler Version 4.01

```
    1  $NOTRUNCATE
    2  $DECLARE
    3        PROGRAM NUTATION
    4  C
    5        COMPLEX*16 ARYDAT(1,1024),H1(100),R1(100),RDR(100)
    6        COMPLEX*16 E1(10),EE(10),REC(10),ERC(10),W(10)
    7        REAL*8     THD(10),QCC,ETA,QC2,W1,Q1F(10),W1F(10)
    8        REAL*8     AI,W0,PI2,T1(2),CT1,CT2(20000),CP1(900),H1I(2,100),S,D
    9        INTEGER*4  DIM(2),MXD(2),NSP,NT,NP,MXT,I,J,K,L,N,ERS
   10        CHARACTER*15 RGF,TDF
   11  C
   12        EQUIVALENCE (H1,H1I),(CT2(901),CP1(1))
   13        COMMON /ARYDAT/ARYDAT,DIM
   14        COMMON /PARAMS/THD,QCC,ETA,QC2,Q1F,W1F
   15        COMMON /WRKVAR/RDR,EE,REC,ERC,W
   16  C     ------------------------------------------------------------------
   17  C       Declarations of Constants
   18  C     ------------------------------------------------------------------
   19        PARAMETER(PI2=6.283185307179586D+00)
   20        DATA MXD/1024,1/
   21  C     ------------------------------------------------------------------
   22  C       Spin Number
   23  C     ------------------------------------------------------------------
   24        WRITE(*,'(A11¥)') '0Spin *2 = '
   25        READ(*,'(I2)') NSP
   26        S=DBLE(NSP)/2.0D+00
   27        AI=S*S+S
   28  C     ------------------------------------------------------------------
   29  C       Lamor Frequency
   30  C     ------------------------------------------------------------------
   31        WRITE(*,'(A20¥)') '0Lamor Freq / MHz = '
   32        READ (*,'(F7.4)') W0
   33  C     ------------------------------------------------------------------
   34  C       Quadrupole Interaction Parameters
   35  C     ------------------------------------------------------------------
   36        WRITE(*,'(A17¥)') '0eqQ / MHz, η = '
   37        READ (*,'(2F10.6)') QCC,ETA
   38  C     ------------------------------------------------------------------
   39  C       RF Strength in Frequency Units
   40  C     ------------------------------------------------------------------
   41        WRITE(*,'(A27¥)') '0RF Field Strength / kHz = '
   42        READ (*,'(F6.3)') W1
   43  C     ------------------------------------------------------------------
   44  C       Sampling Points in each Dimension
   45  C     ------------------------------------------------------------------
   46        DO 300 I=1,2
   47          WRITE(*,'(A13,I1)') '0Dimension : ', I
   48          WRITE(*,'(A35,I4,A5¥)')
   49       &    '  Number of Sampling Points ( Max. ',MXD(I),' ) = '
   50          READ (*,'(I5)') DIM(I)
   51          WRITE(*,'(A25¥)') '  Time Increment / μs = '
   52          READ (*,'(F5.3)') T1(I)
   53    300 CONTINUE
```

Line# Source Line Microsoft FORTRAN Optimizing Compiler Version 4.01

```
C     ------------------------------------------------------------------
C       RGF : Stores Computational Condition
C       TDF : Saves FID Data
C     ------------------------------------------------------------------
      WRITE(*,'(A25¥)') '0Registry  File  Name  = '
      READ(*,'(A15)') RGF
      WRITE(*,'(A25¥)') ' Time Domain File Name = '
      READ(*,'(A15)') TDF
C     ------------------------------------------------------------------
C       Get the Number to be calculated
C     ------------------------------------------------------------------
      WRITE(*,'(A20)') ' Number of Division over θ '
      WRITE(*,'(A¥)') '   [ Max. : 20000 ( η  = 0)  900 ( η  > 0) ] = '
      READ(*,'(I5)') NT
      DO 400 I=1,NT
        CT1=DBLE(I)/DBLE(NT)
        CT2(I)=CT1*CT1
  400 CONTINUE
      IF (ETA .EQ. 0.0D+00) THEN
        NP=1
        CP1(1)=0.0D+00
      ELSE
        NP=NT
        DO 410 I=1,NP
          CP1(I)=ETA*DCOS(PI2*DBLE(I)/DBLE(NT))
  410   CONTINUE
      END IF
C     ------------------------------------------------------------------
C       Store the Parameters
C     ------------------------------------------------------------------
      OPEN (UNIT=50, FILE=RGF, ACCESS='SEQUENTIAL')
      WRITE(50,'(A40)') ' ------ Computational Conditions ------ '
      WRITE(50,'(A16)') '< Interactions >'
      WRITE(50,'(A10,I2,A4)')'   Spin = ',NSP,' / 2'
      WRITE(50,'(A22,F8.3)') '   Lamor Freq / MHz = ', W0
      WRITE(50,'(A22,F7.3)') '   RF  Field / kHz  = ', W1
      WRITE(50,'(A15,F10.6,A8,F10.6)')
     & '   QCC / MHz = ',QCC,'; ETA = ',ETA
      WRITE(50,'(A15)') '< Calculation >'
      WRITE(50,'(A44)') '   Dimension   Data Points   Time Increments'
      DO 500 I=1,2
        WRITE(50,'(7X,I1,10X,I4,9X,F10.5)') I,DIM(I),TI(I)
  500 CONTINUE
      WRITE(50,'(/A28, I5)') '   Total Division over  θ  = ',NT
      WRITE(50,'(/A18,A15)') '   Data Stored in ',TDF
      CLOSE (UNIT=50)
```

Line# Source Line Microsoft FORTRAN Optimizing Compiler Version 4.01

```
  100  C     ------------------------------------------------------------------
  101  C       Determine the Parameters suitable to Calculation
  102  C     ------------------------------------------------------------------
  103        QCC=QCC/DBLE(NSP*NSP-NSP)*2.5D-01
  104        QC2=QCC*QCC/W0*PI2*TI(2)*(AI-7.5D-01)
  105        QCC=QCC*PI2*TI(1)
  106        W1=W1*PI2*TI(1)*1.0D-03
  107        D=DBLE(NSP)/2.0D+00
  108        DO 600 I=1,NSP+1
  109          THD(I)=D
  110          Q1F(I)=D*D*3.0D+00-AI
  111          W1F(I)=W1*DSQRT(AI-D*(D-1.0D+00))/2.0D+00
  112          D=D-1.0D+00
  113     600 CONTINUE
  114        WRITE(*,'(A38,I5/)')
  115       & '     Total Division over THETA, PHI = ',NT*NP
  116  C     ------------------------------------------------------------------
  117  C       Powder Averaging Start here
  118  C     ------------------------------------------------------------------
  119        DO 710 I=1,NT
  120          WRITE(*,'(A30,I5)') '+      Powder Averaging Now : ',I*NP
  121          DO 700 J=1,NP
  122            CALL EVOLVE(NSP+1,H1,H11,R1,E1,CT2(I),CP1(J),ERS)
  123            IF (ERS .NE. 0) GOTO 20000
  124     700    CONTINUE
  125     710 CONTINUE
  126  C     ------------------------------------------------------------------
  127  C       Normalize and Store the Data
  128  C     ------------------------------------------------------------------
  129        OPEN (UNIT=10, FILE=TDF)
  130        D=1.0D+00/DBLE(NT*NP)
  131        DO 810 I=1,DIM(1)
  132          DO 800 J=1,DIM(2)
  133            ARYDAT(J,I)=ARYDAT(J,I)*D
  134            WRITE(10, FMT=9000, IOSTAT=ERS, ERR=10000) ARYDAT(J,I)
  135     800    CONTINUE
  136     810 CONTINUE
  137        CLOSE (UNIT=10)
  138    9000 FORMAT(D22.16,1X,D22.16)
  139  C     ------------------------------------------------------------------
  140  C       Normal End.
  141  C     ------------------------------------------------------------------
  142        GO TO 99999
  143  C     ------------------------------------------------------------------
  144  C       Error Exist in the Procedure.
  145  C     ------------------------------------------------------------------
  146  10000 WRITE(*,'(A18,I5)') ' File Write Error ',ERS
  147        GO TO 99999
  148  20000 WRITE(*,'(A23,I5)') ' Diagonalization Error ',ERS
  149  C
  150  99999 END
  151  $PAGE
```

Line# Source Line Microsoft FORTRAN Optimizing Compiler Version 4.01

```
152         SUBROUTINE EVOLVE(L,H1,H1I,R1,E1,CT2,CP1,ERR)
153   C     ------------------------------------------------------------------
154   C       Calculate the Evolution of the Density Vectors
155   C     ------------------------------------------------------------------
156         COMPLEX*16 ARYDAT(1,1024),H1(L,L),R1(L,L),E1(L),IC,Q2E
157         COMPLEX*16 RDR(10,10),EE(10),REC(10),ERC(10),W(10)
158         REAL*8     H1I(2,L,L),Q1,Q2,D,CT2,CT4,ST2,ST4,CP1,CP2,SP2
159         REAL*8     THD(10),QCC,ETA,QC2,Q1F(10),W1F(10)
160         INTEGER*4  DIM(2),N1,N2,I,J,K,ERR
161   C
162         COMMON /ARYDAT/ARYDAT,DIM
163         COMMON /PARAMS/THD,QCC,ETA,QC2,Q1F,W1F
164         COMMON /WRKVAR/RDR,EE,REC,ERC,W
165   C     ------------------------------------------------------------------
166   C       Transformation of Coordinate to Molecular Frame
167   C     ------------------------------------------------------------------
168         CT4=CT2*CT2
169         ST2=1.0D+00-CT2
170         ST4=ST2*ST2
171         CP2=CP1*CP1
172         SP2=ETA*ETA-CP2
173   C     ------------------------------------------------------------------
174   C       First Order Quadrupole Splitting
175   C     ------------------------------------------------------------------
176         Q1=QCC*(3.0D+00*CT2-1.0D+00+ST2*CP1)
177   C     ------------------------------------------------------------------
178   C       Second Order Quadrupole Shift for the Central Transition
179   C     ------------------------------------------------------------------
180   C     Q2=QC2*( ST4*9.0-(1.0-CT4)*CP1*6.0+(CT2*4.0+ST4)*CP2+CT2*SP2*4.0
181   C    &        -ST2*(CT2*(9.0+CP1*6.0+CP2)+SP2)*8.0 )
182         Q2E=DCMPLX(DCOS(Q2),DSIN(Q2))
183   C     ------------------------------------------------------------------
184   C       Set the Hamiltonian
185   C     ------------------------------------------------------------------
186         DO 30 I=1,L
187           DO 20 J=1,L
188             H1(J,I)=0.0D+00
189      20   CONTINUE
190           H1I(2,I,I)=Q1*Q1F(I)
191           IF (I .GT. 1) H1I(2,I-1,I)=W1F(I-1)
192           IF (I .LT. L) H1I(2,I+1,I)=W1F( I )
193      30 CONTINUE
```

Line# Source Line Microsoft FORTRAN Optimizing Compiler Version 4.01

```
194  C     ------------------------------------------------------------------
195  C       Get the Eigenvalues and Eigenvectors to Calculate Exponentials
196  C     ------------------------------------------------------------------
197         CALL CHEQRD(L,H1,E1,R1,ERR)
198         IF (ERR .NE. 0) RETURN
199         DO 100 I=1,L
200           EE(I)=CDEXP(E1(I))
201    100  CONTINUE
202         DO 110 J=1,L
203          DO 110 I=1,L
204            RDR(I,J)=0.0D+00
205            DO 110 K=1,L
206              RDR(I,J)=RDR(I,J)+R1(K,I)*THD(K)*R1(K,J)
207    110  CONTINUE
208         DO 120 I=1,L
209           REC(I)=R1(L/2,I)
210           ERC(I)=R1(L/2+1,I)
211    120  CONTINUE
212  C     ------------------------------------------------------------------
213  C       Calculate FID
214  C     ------------------------------------------------------------------
215         DO 300 N1=1,DIM(1)
216           DO 200 J=1,L
217             REC(J)=REC(J)*EE(J)
218             ERC(J)=ERC(J)*DCONJG(EE(J))
219    200    CONTINUE
220           DO 210 I=1,L
221             W(I)=0.0D+00
222             DO 210 J=1,L
223               W(I)=W(I)+REC(J)*RDR(J,I)
224    210    CONTINUE
225           DO 220 I=1,L
226             IC=0.0D+00
227             DO 220 J=1,L
228               IC=IC+W(J)*ERC(J)
229    220    CONTINUE
230           DO 300 N2=1,DIM(2)
231             ARYDAT(N2,N1)=ARYDAT(N2,N1)+IC
232             IC=IC*Q2E
233    300  CONTINUE
234  C
235         RETURN
236         END
237  C
238  $PAGE
```

Line# Source Line Microsoft FORTRAN Optimizing Compiler Version 4.01

```
      SUBROUTINE CHEQRD(N,LC,EC,VC,ERR)
C     ------------------------------------------------------------------
C       Calculate the Eigenvalues and Eigenvectors of Symmetric Matrix
C     ------------------------------------------------------------------
      COMPLEX*16 LC(N,N),VC(N,N),EC(N),ZX,ZY,ZZ,ZR,ZC,ZS
      REAL*8     CDABSP,DEL
      INTEGER*4  I,J,IP1,LL,LU,ITR,ITRMAX,ERR
C
      CDABSP(ZZ)=DABS(DREAL(ZZ))+DABS(DIMAG(ZZ))
      DATA DEL,ITRMAX/5.0D-15,30/
C     ------------------------------------------------------------------
C       Set the Eigenvectors to Unit Matrix
C     ------------------------------------------------------------------
      DO 110 I=1,N
        DO 100 J=1,N
          VC(J,I)=0.0D+00
  100   CONTINUE
        VC(I,I)=1.0D+00
  110 CONTINUE
C     ------------------------------------------------------------------
C        Search for a Small Sub-diagonal Element.
C     ------------------------------------------------------------------
      LU=N
  300 ITR=0
  310   LL=LU
  320   IF (CDABSP(LC(LL,LL-1)) .GT. DEL) THEN
          LL=LL-1
          IF (LL .GT. 1) GO TO 320
        END IF
        IF (LL .NE. LU) THEN
C     ------------------------------------------------------------------
C        If Convergence is not Attained within 30 Iterations,
C        Truncate the Computation.
C     ------------------------------------------------------------------
          IF (ITR .GT. ITRMAX) GO TO 10000
C     ------------------------------------------------------------------
C       Determine the Origin Shift as the Eigenvalue of the 2 by 2
C       Bottom Submatrix which is Nearer to the bottom Element.
C     ------------------------------------------------------------------
          ZX=(LC(LU-1,LU-1)+LC(LU,LU))*0.5D+00
          ZY=ZX-LC(LU,LU)
          ZZ=CDSQRT(LC(LU-1,LU)*LC(LU,LU-1)+ZY*ZY)
          ZZ=DSIGN(1.0D+00,CDABSP(ZY-ZZ)-CDABSP(ZY+ZZ))*ZZ+ZX
          LC(LL,LL)=LC(LL,LL)-ZZ
          ZC=1.0D+00
```

Line# Source Line Microsoft FORTRAN Optimizing Compiler Version 4.01

```
  284  C     ------------------------------------------------------------------
  285  C           Left- and Right-hand Transformation.
  286  C     ------------------------------------------------------------------
  287           DO 360 I=LL,LU-1
  288             IP1=I+1
  289             ZX=LC( I ,I)
  290             ZY=LC(IP1,I)
  291             ZR=CDSQRT(ZX*ZX+ZY*ZY)
  292             IF (CDABSP(ZR) .LT. DEL) GOTO 20000
  293             LC(I,I)=ZC*ZR
  294             IF (I .GT. LL) LC(I,I-1)=ZS*ZR
  295             LC(IP1,IP1)=LC(IP1,IP1)-ZZ
  296             ZC=ZX/ZR
  297             ZS=ZY/ZR
  298             DO 330 J=IP1,N
  299               ZY=LC(I,J)
  300               LC( I ,J)=ZY*ZC+LC(IP1,J)*ZS
  301               LC(IP1,J)=LC(IP1,J)*ZC-ZY*ZS
  302    330        CONTINUE
  303             DO 340 J=1,I
  304               ZY=LC(J,I)
  305               LC(J, I )=ZY*ZC+LC(J,IP1)*ZS
  306               LC(J,IP1)=LC(J,IP1)*ZC-ZY*ZS
  307    340        CONTINUE
  308             LC(I,I)=LC(I,I)+ZZ
  309             DO 350 J=1,N
  310               ZY=VC(J,I)
  311               VC(J, I )=ZY*ZC+VC(J,IP1)*ZS
  312               VC(J,IP1)=VC(J,IP1)*ZC-ZY*ZS
  313    350        CONTINUE
  314    360      CONTINUE
  315             LC(LU,LU-1)=LC(LU,LU)*ZS
  316             LC(LU, LU )=LC(LU,LU)*ZC+ZZ
  317             ITR=ITR+1
  318             GO TO 310
  319           END IF
  320           LU=LU-1
  321         IF (LU .GT. 1) GO TO 300
  322  C     ------------------------------------------------------------------
  323  C       QR-Transformation is Over.
  324  C       Eigenvalues are Given
  325  C        by the Diagonal Elements of the Resultant Matrix.
  326  C     ------------------------------------------------------------------
  327         DO 400 I=1,N
  328           EC(I)=LC(I,I)
  329    400 CONTINUE
```

Line# Source Line Microsoft FORTRAN Optimizing Compiler Version 4.01

```
  330  C     ------------------------------------------------------------------
  331  C       Normal Exit.
  332  C     ------------------------------------------------------------------
  333         ERR=0
  334         RETURN
  335  C     ------------------------------------------------------------------
  336  C       Error Exit.
  337  C        10000 : Not Converged.
  338  C        20000 : Devide by Zero.
  339  C     ------------------------------------------------------------------
  340  10000  ERR=10000
  341         RETURN
  342  20000  ERR=20000
  343         RETURN
  344         END
```

Line# Source Line Microsoft FORTRAN Optimizing Compiler Version 4.01

```
    1  $DECLARE
    2        PROGRAM EXCHANGE
    3  C     ------------------------------------------------------------------
    4  C       Simulation Program for 2D Nutation NMR with Chemical Exchange
    5  C     ------------------------------------------------------------------
    6        COMPLEX*8  ARD(256,128)
    7        REAL*8     QCC(2),ETA(2),QC2(2),ET2(2),CHS(2),RFS,EXC(2,2,2)
    8        REAL*8     ALP(2),BET(2),GAM(2),TDX(8),THD(4,2),R(4),P(2)
    9        REAL*8     X(-50:50,0:50),Y(-50:50,0:50),Z(-50:50)
   10        REAL*8     SA(2),CA(2),SB(2),CB(2),SG(2),CG(2),TI(2)
   11        REAL*8     W0,W1,D,PID,SNT,D2R,PI1,PI2,SQ3
   12        INTEGER*4  DIM(2),MXD(2),NSP,NSI,MXS,NN,MXT,I,J,N,ERS
   13        CHARACTER  CHA
   14        CHARACTER*15 RGF,TDF
   15  C
   16        EQUIVALENCE (TDX,THD),(CHA,RGF)
   17        COMMON /ARD/ARD,DIM,TDX,R,P
   18        COMMON /PAR/QCC,ETA,QC2,ET2,CHS,RFS,EXC
   19        COMMON /ARG/SA,CA,SB,CB,SG,CG
   20  C     ------------------------------------------------------------------
   21  C       Declarations of Constants
   22  C     ------------------------------------------------------------------
   23        PARAMETER(NSP=4,MXS=2,MXT=50)
   24        PARAMETER(D2R=1.745329251994329D-02,SQ3=8.660254037844385D-01)
   25        PARAMETER(PI1=3.141592653589793D+00,PI2=6.283185307179586D+00)
   26        DATA MXD/128,256/
   27  C     ------------------------------------------------------------------
   28  C       Lamor Frequency
   29  C     ------------------------------------------------------------------
   30        WRITE(*,'(A20¥)') '0Lamor Freq / MHz = '
   31        READ (*,'(F7.4)') W0
   32  C     ------------------------------------------------------------------
   33  C       Number of Sites to be Considered
   34  C     ------------------------------------------------------------------
   35      1 WRITE(*,'(A18¥)') '0Number of Site = '
   36        READ  (*,'(I1)') NSI
   37        IF (NSI .GT. MXS) GOTO 1
   38  C     ------------------------------------------------------------------
   39  C       Quadrupole Interaction Parameters and Chemical Shifts
   40  C     ------------------------------------------------------------------
   41        DO 100 I=1,NSI
   42          WRITE(*,'(A7,I1)') ' Site : ',I
   43          WRITE(*,'(A21¥)') '    eqQ / MHz, eta = '
   44          READ (*,'(2F10.6)') QCC(I),ETA(I)
   45          WRITE(*,'(A37¥)') '    Eular Angles of Principal Axis = '
   46          READ(*,'(3F10.6)') ALP(I),BET(I),GAM(I)
   47          D=ALP(I)*D2R
   48          SA(I)=DSIN(D)
   49          CA(I)=DCOS(D)
   50          D=BET(I)*D2R
   51          SB(I)=DSIN(D)
   52          CB(I)=DCOS(D)
   53          D=GAM(I)*D2R
   54          SG(I)=DSIN(D)
   55          CG(I)=DCOS(D)
   56          WRITE(*,'(A27¥)') '    Chemical Shift / kHz = '
   57          READ (*,'(F10.6)') CHS(I)
   58          CHS(I)=CHS(I)*1.0D-03
```

Line# Source Line Microsoft FORTRAN Optimizing Compiler Version 4.01

```
   59     100 CONTINUE
   60   C     ------------------------------------------------------------------
   61   C       Chemical Exchange
   62   C     ------------------------------------------------------------------
   63         WRITE(*,'(A60¥)')
   64        & '0Equilibrium Population of Each Site are Equal ( Y or N ) ? '
   65         READ (*,'(A1)') CHA
   66         IF ((ICHAR(CHA) .EQ. ICHAR('Y')) .OR.
   67        &    (ICHAR(CHA) .EQ. ICHAR('y'))) THEN
   68           D=DBLE(NSI)
   69           DO 200 I=1,NSI
   70             P(I)=1.0D+00/D
   71     200   CONTINUE
   72         ELSE
   73           D=0.0D+00
   74           DO 210 I=1,NSI
   75             WRITE(*,'(A30,I1,A3¥)')
   76        &             ' Relative Population of Site ',I,' = '
   77             READ (*,'(F6.4)') P(I)
   78             D=D+P(I)
   79     210   CONTINUE
   80           DO 220 I=1,NSI
   81             P(I)=P(I)/D
   82     220   CONTINUE
   83         END IF
   84         DO 230 I=1,NSI
   85           EXC(I,I,1)=0.0D+00
   86           DO 230 J=1,NSI
   87             IF (J .GT. I) THEN
   88               WRITE(*,'(A22,1X,I1,1X,A2,1X,I1,1X,A9¥)')
   89        &                '   Exchange Rate from',I,'to',J,' / MHz = '
   90               READ (*,'(F10.8)') EXC(J,I,1)
   91               EXC(I,J,1)=EXC(J,I,1)*P(I)/P(J)
   92             END IF
   93             IF (I .NE. J) EXC(I,I,1)=EXC(I,I,1)-EXC(J,I,1)
   94     230 CONTINUE
   95   C     ------------------------------------------------------------------
   96   C       RF Strength in Frequency Units
   97   C     ------------------------------------------------------------------
   98         WRITE(*,'(A27¥)') '0RF Field Strength / kHz = '
   99         READ (*,'(F6.3)') W1
  100   C     ------------------------------------------------------------------
  101   C       DIM(1),DIM(2) : Sampling Points in each Dimension
  102   C     ------------------------------------------------------------------
  103         DO 300 I=1,2
  104           WRITE(*,'(A13,I1)') '0Dimension : ', I
  105       2   WRITE(*,'(A30¥)') '  Number of Sampling Points = '
  106           READ (*,'(I5)') DIM(I)
  107           IF (DIM(I) .GT. MXD(I)) THEN
  108             WRITE(*,'(A14)') '0 Too Large !! '
  109             GO TO 2
  110           END IF
  111           WRITE(*,'(A35¥)') '  Time Increment ( in microsec ) = '
  112           READ (*,'(F5.3)') T1(I)
  113     300 CONTINUE
  114   C     ------------------------------------------------------------------
  115   C       RGF : Stores Computational Condition
  116   C       TDF : Saves FID Data
```

Line# Source Line Microsoft FORTRAN Optimizing Compiler Version 4.01

```
  117  C     ------------------------------------------------------------------
  118        WRITE(*,'(A25¥)') '0Registry  File  Name  = '
  119        READ(*,'(A15)') RGF
  120        WRITE(*,'(A25¥)') ' Time Domain File Name = '
  121        READ(*,'(A15)') TDF
  122  C     ------------------------------------------------------------------
  123  C       Get the Number to be calculated
  124  C     ------------------------------------------------------------------
  125      3 WRITE(*,'(A33¥)') '0Number of Division over THETA = '
  126        READ(*,'(I3)') N
  127        IF (N .GT. MXT) GOTO 3
  128        D=DBLE(N)
  129        PID=PI1/D
  130        DO 400 I=0,N
  131          Z( I)=DBLE(I)/D
  132          Z(-I)=-Z(I)
  133          SNT=DSQRT(1.0-Z(I)*Z(I))
  134          DO 400 J=0,N
  135            X( J,I)=SNT*DCOS(PID*DBLE(J))
  136            Y( J,I)=SNT*DSIN(PID*DBLE(J))
  137            X(-J,I)= X(J,I)
  138            Y(-J,I)=-Y(J,I)
  139    400 CONTINUE
  140        WRITE(*,'(A38,I5/)')
  141       & '     Total Division over THETA, PHI = ',N*N*4-N*2
  142  C     ------------------------------------------------------------------
  143  C       Store the Parameters
  144  C     ------------------------------------------------------------------
  145        OPEN (UNIT=50, FILE=RGF, ACCESS='SEQUENTIAL')
  146        WRITE(50,'(A40)') ' ------ Computational Conditions ------ '
  147        WRITE(50,'(/A17)') ' < Interactions >'
  148        WRITE(50,'(A22,F8.3)') '   Lamor Freq / MHz = ', W0
  149        WRITE(50,'(A22,F7.3)') '   RF  Field / kHz  = ', W1
  150        DO 500 I=1,NSI
  151          WRITE(50,'(/A10,I1,A16,F10.8,A2)')
  152       &   '   Site : ',I,' ( Population = ',P(I),' )'
  153          WRITE(50,'(A16,F6.4,A8,F6.4)')
  154       &   '    QCC / MHz = ',QCC(I),'; ETA = ',ETA(I)
  155          WRITE(50,'(A19,F5.2,A2,F5.2,A2,F5.2)')
  156       &   '    Euler Angles : ',ALP(I),', ',BET(I),', ',GAM(I)
  157          WRITE(50,'(A27,F6.2)')
  158       &   '    Chemical Shift / kHz = ',CHS(I)*1.0D+03
  159    500 CONTINUE
  160        WRITE(50,'(/A25)') ' < Exchange Rates / MHz >'
  161        DO 510 I=1,NSI
  162         DO 510 J=1,NSI
  163           WRITE(50,'(4X,I1,A5,I1,F16.12)') I,' --> ',J,EXC(I,J,1)
  164    510 CONTINUE
  165        WRITE(50,'(/A16)') ' < Calculation >'
  166        WRITE(50,'(A45)') '    Dimension   Data Points   Time Increments'
  167        DO 530 I=1,2
  168          WRITE(50,'(8X,I1,10X,I3,10X,F10.5)') I,DIM(I),TI(I)
  169    530 CONTINUE
  170        WRITE(50,'(/A21, I3)') '    Total Division = ',N*N*4-N*2
  171        WRITE(50,'(/A19,A15)') '    Data Stored in ',TDF
  172        CLOSE (UNIT=50)
  173  C     ------------------------------------------------------------------
  174  C       Symmetrize the Exchange Matrix
```

```
Line#  Source Line          Microsoft FORTRAN Optimizing Compiler Version 4.01

  175  C       and Set the Spin Density Vectors at Thermal Equilibrium
  176  C     -----------------------------------------------------------------
  177         DO 600 I=1,NSI
  178           P(I)=DSQRT(P(I))
  179           THD(1,I)= SQ3*P(I)
  180           THD(2,I)=    -P(I)
  181           THD(3,I)= 0.0D+00
  182           THD(4,I)=-SQ3*P(I)
  183     600 CONTINUE
  184         DO 610 I=1,NSI
  185          DO 610 J=1,NSI
  186            IF (J .NE. I) EXC(J,I,1)=EXC(J,I,1)*P(I)/P(J)
  187     610 CONTINUE
  188  C     -----------------------------------------------------------------
  189  C       Determine the Parameters suitable to Calculation
  190  C     -----------------------------------------------------------------
  191         DO 620 I=1,NSI
  192           QC2(I)=PI2*QCC(I)*QCC(I)/W0*TI(2)/9.6D+01
  193           QCC(I)=PI2*QCC(I)/8.0D+00*TI(1)
  194           ET2(I)=ETA(I)*ETA(I)
  195           CHS(I)=PI2*CHS(I)*TI(2)
  196           DO 620 J=1,NSI
  197             EXC(J,I,2)=EXC(J,I,1)*TI(2)
  198             EXC(J,I,1)=EXC(J,I,1)*TI(1)
  199     620 CONTINUE
  200         RFS=PI2*W1*TI(1)*1.0D-03
  201  C     -----------------------------------------------------------------
  202  C       Powder Averaging Start here
  203  C     -----------------------------------------------------------------
  204         NN=0
  205         DO 710 I=-N+1,N-1
  206           WRITE(*,'(A30,I5)')
  207        &       '+       Powder Averaging Now : ',NN+N*2
  208           DO 700 J=-N+1,N
  209             NN=NN+1
  210             CALL EVOLVE(NSP,NSI,X(J,IABS(I)),Y(J,IABS(I)),Z(I),ERS)
  211             IF (ERS .NE. 0) GOTO 20000
  212     700   CONTINUE
  213     710 CONTINUE
  214  C     -----------------------------------------------------------------
  215  C       Normalize and Store the Data
  216  C     -----------------------------------------------------------------
  217         OPEN(UNIT=10,FILE=TDF)
  218         D=1.0D+00/DBLE(NN)
  219         DO 800 I=1,DIM(1)
  220          DO 800 J=1,DIM(2)
  221            WRITE(10,'(E13.7,1X,E13.7)',IOSTAT=ERS,ERR=10000) ARD(J,I)*D
  222     800 CONTINUE
  223         CLOSE (UNIT=10)
  224  C     -----------------------------------------------------------------
  225  C       Normal End.
  226  C     -----------------------------------------------------------------
  227         GO TO 99999
  228  C     -----------------------------------------------------------------
  229  C       Error Exist in the Procedure.
  230  C     -----------------------------------------------------------------
  231  10000 WRITE(*,'(A18,I5)') ' File Write Error ',ERS
  232         GO TO 99999
```

Line# Source Line Microsoft FORTRAN Optimizing Compiler Version 4.01

```
20000 WRITE(*,'(A23,I5)') ' Diagonalization Error ',ERS
C
99999 END
C
      BLOCK DATA IXTOIZ
      COMPLEX*8 ARD(256,128)
      REAL*8     TDX(8),R(4),P(2)
      INTEGER*4  DIM(2)
      COMMON /ARD/ARD,DIM,TDX,R,P
C     ------------------------------------------------------------------
C       Transformation Laws in Ix to Iz basis
C     ------------------------------------------------------------------
      DATA R/ 6.123724356957945D-01,
     &        3.535533905932738D-01,
     &       -1.060660171779821D+00,
     &       -6.123724356957945D-01/
      END
$PAGE
```

Line# Source Line Microsoft FORTRAN Optimizing Compiler Version 4.01

```
      SUBROUTINE EVOLVE(L,M,X,Y,Z,ERR)
C     ------------------------------------------------------------------
C       Calculate the Evolution of the Density Vectors
C     ------------------------------------------------------------------
      COMPLEX*8  ARD(256,128)
      COMPLEX*16 L1(8,8),H1(4,2,4,2),Q1(8,8),E1(8),L2(2,2),Q2(2,2),E2(2)
      COMPLEX*16 DZ1(2,128),RQ1(2,8),PQ2(2,2),C
      REAL*8     QCC(2),ETA(2),QC2(2),ET2(2),CHS(2),RFS,EXC(2,2,2)
      REAL*8     X,Y,Z,SA(2),CA(2),SB(2),CB(2),SG(2),CG(2)
      REAL*8     XC(4,4,2),WQ1,WQ2,WQ3,SQ3,X2,Y2,Z2,CT2,ST2,CP1
      REAL*8     TDX(8),R(4),P(2),CDABSP,EPS
      INTEGER*4  DIM(2),I,J,K,S,S1,S2,SS,LM,ERR
C
      EQUIVALENCE (L1,H1)
      PARAMETER(SQ3=8.660254037844385D-01)
      COMMON /PAR/QCC,ETA,QC2,ET2,CHS,RFS,EXC
      COMMON /ARG/SA,CA,SB,CB,SG,CG /ARD/ARD,DIM,TDX,R,P
      CDABSP(C)=DABS(DREAL(C))+DABS(DIMAG(C))
      DATA EPS/1.0D-18/
C     ------------------------------------------------------------------
C       Set the Liouvillians correspond to F1 and F2 axis
C     ------------------------------------------------------------------
      DO 100 S=1,M
C     ------------------------------------------------------------------
C       Transformation of Coordinate to Molecular Frame
C     ------------------------------------------------------------------
        Z2=SB(S)*CG(S)*X+SB(S)*SG(S)*Y+CB(S)*Z
        X2= (CA(S)*CB(S)*CG(S)-SA(S)*SG(S))*X
     &     +(CA(S)*CB(S)*SG(S)+SA(S)*CG(S))*Y-CA(S)*SB(S)*Z
        Y2=-(SA(S)*CB(S)*CG(S)+CA(S)*SG(S))*X
     &     -(SA(S)*CB(S)*SG(S)-CA(S)*CG(S))*Y+SA(S)*SB(S)*Z
        CT2=Z2*Z2
        ST2=1.0D+00-CT2
        CP1=(X2*X2-Y2*Y2)*ETA(S)
C     ------------------------------------------------------------------
C       First Order Quadrupole Splitting
C     ------------------------------------------------------------------
        WQ1=QCC(S)*(CT2*3.0+CP1-1.0)
C     ------------------------------------------------------------------
C       Second Order Quadrupole Shift + Chemical Shift
C     ------------------------------------------------------------------
        WQ2=CHS(S)+QC2(S)
     &               *( ST2*ST2*9.-(1.+CT2)*CP1*6.+CP1*CP1+ET2(S)*CT2*4.
     &                 -(ST2*CT2*9.+CT2*CP1*6.0-CP1*CP1+ET2(S)*ST2)*8.0 )
        L2(S,S)=DCMPLX(EXC(S,S,2),WQ2)
C     ------------------------------------------------------------------
C       Set the Hamiltonian in the basis Ix
C     ------------------------------------------------------------------
        WQ3=WQ1*SQ3
        XC(1,1,S)= WQ1+RFS
        XC(1,2,S)= WQ3
        XC(1,3,S)= WQ3
        XC(1,4,S)= 0.0
        XC(2,2,S)=    -RFS
        XC(2,3,S)= 0.0
        XC(2,4,S)= WQ3
        XC(3,3,S)=     RFS*3.0D+00
        XC(3,4,S)= WQ3
```

```
309           XC(4,4,S)=-WQ1+RES
310       100 CONTINUE
311     C     ------------------------------------------------------------------
312     C       Set the Liouvillan
313     C     ------------------------------------------------------------------
314           DO 220 S=1,M
315            DO 200 I=1,L
316             H1(I,S,I,S)=DCMPLX(EXC(S,S,1),XC(I,I,S))
317             DO 200 J=I+1,L
318               H1(I,S,J,S)=DCMPLX(0.0D+00,XC(I,J,S))
319               H1(J,S,I,S)=H1(I,S,J,S)
320       200   CONTINUE
321             DO 210 SS=S+1,M
322              DO 210 I=1,L
323               DO 210 J=1,L
324                 IF (I .EQ. J) THEN
325                   H1(I,S,I,SS)=EXC(S,SS,1)
326                   H1(I,SS,I,S)=EXC(S,SS,1)
327                 ELSE
328                   H1(I,S,J,SS)=0.0D+00
329                   H1(J,S,I,SS)=0.0D+00
330                   H1(I,SS,J,S)=0.0D+00
331                   H1(J,SS,I,S)=0.0D+00
332                 END IF
333       210   CONTINUE
334       220 CONTINUE
335     C
336           DO 300 S=1,M
337            DO 300 SS=S+1,M
338              L2(S,SS)=EXC(S,SS,2)
339              L2(SS,S)=EXC(S,SS,2)
340       300 CONTINUE
341     C     ------------------------------------------------------------------
342     C       Get the Eigenvalues and Eigenvectors to Calculate Exponentials
343     C     ------------------------------------------------------------------
344           LM=L*M
345           CALL CHEQRD(LM,L1,4,E1,Q1,ERR)
346           IF (ERR .NE. 0) RETURN
347           DO 400 I=1,LM
348             E1(I)=CDEXP(E1(I))
349       400 CONTINUE
350           SS=0
351           DO 420 S=1,2
352             DO 410 K=1,LM
353               RQ1(S,K)=0.0D+00
354               DO 410 J=1,L
355                DO 410 I=1,LM
356                 RQ1(S,K)=RQ1(S,K)+R(J)*Q1(J+SS,K)*Q1(I,K)*TDX(I)
357       410   CONTINUE
358             SS=SS+L
359       420 CONTINUE
360           CALL CHEQRD(M,L2,1,E2,Q2,ERR)
361           IF (ERR .NE. 0) RETURN
362           DO 500 I=1,M
363             E2(I)=CDEXP(E2(I))
364       500 CONTINUE
365           DO 510 S2=1,M
366            DO 510 S1=1,M
```

Line# Source Line Microsoft FORTRAN Optimizing Compiler Version 4.01

```
367             PQ2(S1,S2)=0.0D+00
368             DO 510 S=1,M
369               PQ2(S1,S2)=PQ2(S1,S2)+P(S1)*Q2(S1,S2)*Q2(S,S2)
370       510 CONTINUE
371   C     ------------------------------------------------------------------
372   C       Calculate Density Vectors at the end of rf Pulse
373   C     ------------------------------------------------------------------
374           DO 600 I=1,DIM(1)
375            DO 600 S=1,M
376              DZ1(S,I)=0.0D+00
377              DO 600 J=1,LM
378                RQ1(S,J)=RQ1(S,J)*E1(J)
379                DZ1(S,I)=DZ1(S,I)+(RQ1(S,J)-DCONJG(RQ1(S,J)))
380       600 CONTINUE
381   C     ------------------------------------------------------------------
382   C       Calculate FID's
383   C     ------------------------------------------------------------------
384           DO 710 J=1,DIM(2)
385             DO 700 I=1,DIM(1)
386               DO 700 S1=1,M
387                 DO 700 S2=1,M
388                   ARD(J,I)=ARD(J,I)+PQ2(S1,S2)*DZ1(S2,I)
389       700   CONTINUE
390             DO 710 S2=1,M
391              DO 710 S1=1,M
392                PQ2(S1,S2)=PQ2(S1,S2)*E2(S2)
393       710 CONTINUE
394   C
395           RETURN
396           END
397   C
398   $PAGE
```

Line# Source Line Microsoft FORTRAN Optimizing Compiler Version 4.01

```
      SUBROUTINE CHEQRD(N,LC,NBW,EC,VC,ERR)
C     ------------------------------------------------------------------
C       Calculate the Eigenvalues and Eigenvectors of Symmetric Matrix
C     ------------------------------------------------------------------
      COMPLEX*16 LC(N,N),VC(N,N),EC(N),ZX,ZY,ZZ,ZR,ZQ,ZC,ZS
      REAL*8     CDABSP,DEL
      INTEGER*4  I,J,K,IP1,IPM,IM1,JPM,JM1,LL,LU,M,ITR,ITRMAX,ERR
C
      CDABSP(ZZ)=DABS(DREAL(ZZ))+DABS(DIMAG(ZZ))
      DATA DEL,ITRMAX/1.0D-15,30/
C     ------------------------------------------------------------------
C       Parameter Error Check
C     ------------------------------------------------------------------
      IF ((N .LE. 1) .OR. (NBW .GT. N)) GO TO 20000
C     ------------------------------------------------------------------
C       Set the Eigenvectors to Unit Matrix
C       and Determines the Band Width of the Matrix under Treatment.
C     ------------------------------------------------------------------
      DO 110 I=1,N
        DO 100 J=1,N
          VC(J,I)=0.0D+00
  100   CONTINUE
        VC(I,I)=1.0D+00
  110 CONTINUE
      IF (NBW .LE. 0) THEN
        DO 130 I=1,N
          DO 120 J=I+1,N
            IF (CDABSP(LC(J,I)) .GT. DEL) K=J-I
  120     CONTINUE
          NBW=MAX0(NBW,K)
  130   CONTINUE
      END IF
C     ------------------------------------------------------------------
C       Reduction of Band Width to Tridiagonal Matrix
C        by Jacobi Rotations.
C     ------------------------------------------------------------------
      DO 270 M=NBW,2,-1
       DO 270 I=1,N-M
         IPM=I+M
         IM1=IPM-1
         IF (CDABSP(LC(I,IPM)) .GT. DEL) THEN
           ZR=-LC(I,IM1)/LC(I,IPM)
           ZQ=CDSQRT(1.0D+00+ZR*ZR)
           IF (CDABSP(ZQ) .LT. DEL) GOTO 30000
           ZS=1.0D0/ZQ
           ZC=-ZS*ZR
           DO 200 J=1,N
             ZZ=LC(IM1,J)
             LC(IM1,J)=ZZ*ZC+LC(IPM,J)*ZS
             LC(IPM,J)=LC(IPM,J)*ZC-ZZ*ZS
  200      CONTINUE
           DO 210 J=1,N
             ZZ=LC(J,IM1)
             LC(J,IM1)=ZZ*ZC+LC(J,IPM)*ZS
             LC(J,IPM)=LC(J,IPM)*ZC-ZZ*ZS
  210      CONTINUE
           DO 220 J=1,N
             ZZ=VC(J,IM1)
```

Line# Source Line Microsoft FORTRAN Optimizing Compiler Version 4.01

```
                  VC(J,IM1)=ZZ*ZC+VC(J,IPM)*ZS
                  VC(J,IPM)=VC(J,IPM)*ZC-ZZ*ZS
  220           CONTINUE
                DO 260 J=IM1,N-M-1,M
                  JPM=J+M
                  JM1=JPM+1
                  IF (CDABSP(LC(J,JM1)) .GT. DEL) THEN
                    ZR=-LC(J,JPM)/LC(J,JM1)
                    ZQ=CDSQRT(1.0D0+ZR*ZR)
                    IF (CDABSP(ZQ) .LT. DEL) GOTO 30000
                    ZS=1.0D0/ZQ
                    ZC=-ZS*ZR
                    DO 230 K=1,N
                      ZZ=LC(JPM,K)
                      LC(JPM,K)=ZZ*ZC+LC(JM1,K)*ZS
                      LC(JM1,K)=LC(JM1,K)*ZC-ZZ*ZS
  230               CONTINUE
                    DO 240 K=1,N
                      ZZ=LC(K,JPM)
                      LC(K,JPM)=ZZ*ZC+LC(K,JM1)*ZS
                      LC(K,JM1)=LC(K,JM1)*ZC-ZZ*ZS
  240               CONTINUE
                    DO 250 K=1,N
                      ZZ=VC(K,J+M)
                      VC(K,JPM)=ZZ*ZC+VC(K,JM1)*ZS
                      VC(K,JM1)=VC(K,JM1)*ZC-ZZ*ZS
  250               CONTINUE
                  END IF
  260           CONTINUE
              END IF
  270       CONTINUE
C     ------------------------------------------------------------------
C        Search for a Small Sub-diagonal Element.
C     ------------------------------------------------------------------
          LU=N
  300     ITR=0
  310       LL=LU
  320       IF (CDABSP(LC(LL,LL-1)) .GT. DEL) THEN
              LL=LL-1
              IF (LL .GT. 1) GO TO 320
            END IF
            IF (LL .NE. LU) THEN
C     ------------------------------------------------------------------
C        If Convergence is not Attained within 30 Iterations,
C        Truncate the Computation.
C     ------------------------------------------------------------------
              IF (ITR .GT. ITRMAX) GO TO 10000
C     ------------------------------------------------------------------
C        Determine the Origin Shift as the Eigenvalue of the 2 by 2
C        Bottom Submatrix which is Nearer to the bottom Element.
C     ------------------------------------------------------------------
              ZX=(LC(LU-1,LU-1)+LC(LU,LU))*0.5D+00
              ZY=ZX-LC(LU,LU)
              ZZ=CDSQRT(LC(LU-1,LU)*LC(LU,LU-1)+ZY*ZY)
              ZZ=DSIGN(1.0D+00,CDABSP(ZY-ZZ)-CDABSP(ZY+ZZ))*ZZ+ZX
              LC(LL,LL)=LC(LL,LL)-ZZ
              ZC=1.0D+00
              DO 360 I=LL,LU-1
```

Line# Source Line Microsoft FORTRAN Optimizing Compiler Version 4.01

```
  515                IP1=I+1
  516  C     ------------------------------------------------------------------
  517  C               Left- and Right-hand Transformation.
  518  C     ------------------------------------------------------------------
  519                ZX=LC( I ,I)
  520                ZY=LC(IP1,I)
  521                ZR=CDSQRT(ZX*ZX+ZY*ZY)
  522                IF (CDABSP(ZR) .LT. DEL) GOTO 30000
  523                LC(I,I)=ZC*ZR
  524                IF (I .GT. LL) LC(I,I-1)=ZS*ZR
  525                LC(IP1,IP1)=LC(IP1,IP1)-ZZ
  526                ZC=ZX/ZR
  527                ZS=ZY/ZR
  528                DO 330 J=IP1,N
  529                  ZY=LC(I,J)
  530                  LC( I ,J)=ZY*ZC+LC(IP1,J)*ZS
  531                  LC(IP1,J)=LC(IP1,J)*ZC-ZY*ZS
  532     330        CONTINUE
  533                DO 340 J=1,I
  534                  ZY=LC(J,I)
  535                  LC(J, I )=ZY*ZC+LC(J,IP1)*ZS
  536                  LC(J,IP1)=LC(J,IP1)*ZC-ZY*ZS
  537     340        CONTINUE
  538                LC(I,I)=LC(I,I)+ZZ
  539                DO 350 J=1,N
  540                  ZY=VC(J,I)
  541                  VC(J, I )=ZY*ZC+VC(J,IP1)*ZS
  542                  VC(J,IP1)=VC(J,IP1)*ZC-ZY*ZS
  543     350        CONTINUE
  544     360      CONTINUE
  545              LC(LU,LU-1)=LC(LU,LU)*ZS
  546              LC(LU, LU )=LC(LU,LU)*ZC+ZZ
  547              ITR=ITR+1
  548              GO TO 310
  549            END IF
  550            LU=LU-1
  551          IF (LU .GT. 1) GO TO 300
  552  C     ------------------------------------------------------------------
  553  C       QR-Transformation is Over.
  554  C       Eigenvalues are Given
  555  C         by the Diagonal Elements of the Resultant Matrix.
  556  C     ------------------------------------------------------------------
  557          DO 400 I=1,N
  558            EC(I)=LC(I,I)
  559     400  CONTINUE
  560  C     ------------------------------------------------------------------
  561  C       Normal Exit.
  562  C     ------------------------------------------------------------------
  563          ERR=0
  564          RETURN
  565  C     ------------------------------------------------------------------
  566  C       Error Exit.
  567  C         10000 : Not Converged.
  568  C         20000 : Parameter Error.
  569  C         30000 : Devide by Zero.
  570  C     ------------------------------------------------------------------
  571  10000 ERR=10000
  572          RETURN
```

Line# Source Line Microsoft FORTRAN Optimizing Compiler Version 4.01

```
   573  20000 ERR=20000
   574        RETURN
   575  30000 ERR=30000
   576        RETURN
   577        END
```

Global Symbols

Name	Class	Type	Size	Offset

```
Code size = 0000 (0)
Data size = 0000 (0)
Bss size  = 0000 (0)

No errors detected
```